

1
2
3
4
5
6
7
8
9
10
11
12
13
14
15
16
17
18
19
20
21
22
23
24
25
26
27
28
29
30
31
32
33
34
35
36
37
38
39
40
41

Geochemical and planetary dynamical views on the origin of Earth's atmosphere and oceans

Nicolas Dauphas^{1,*} & Alessandro Morbidelli²

¹Origins Laboratory, Department of the Geophysical Sciences and Enrico Fermi Institute, The University of Chicago, 5734 South Ellis Avenue, Chicago IL 60637, USA (dauphas@uchicago.edu)

²Université de Nice Sophia Antipolis, CNRS, Observatoire de la Côte d'Azur, Laboratoire Cassiopée, Boulevard de l'Observatoire, B.P. 4229, 06304 Nice Cedex 4, France (Alessandro.MORBIDELLI@obs-nice.fr)

*Visiting scientist at UJF-Grenoble 1/CNRS-INSU, Institut de Planétologie et d'Astrophysique de Grenoble (IPAG), UMR 5274, Grenoble, F-38041, France

Submitted to "Volume 13 of Treatise on Geochemistry" April 19, 2011
Revised November 29, 2011
19,321 words, 20 figures, and 4 tables

42 **Abstract.** Earth's volatile elements (H, C, and N) are essential to maintaining
43 habitable conditions for metazoans and simpler life forms. However, identifying the
44 sources (comets, meteorites, and trapped nebular gas) that supplied volatiles to
45 Earth is not straightforward because secondary processes like mantle degassing,
46 crustal recycling, and escape to space modified the composition of the atmosphere.
47 Here, we review two complementary approaches to investigate the origin of Earth's
48 atmosphere and oceans. The geochemical approach uses volatile element
49 abundances and isotopic compositions to identify the possible contributors to the
50 atmosphere and to disentangle the processes that shaped it. In that respect, noble
51 gases (He, Ne, Ar, Kr, and Xe), elements that are chemically inert and possess several
52 isotopes produced by radioactivity, play a critical role. The dynamical approach uses
53 our knowledge of planetary dynamics to track volatile delivery to the Earth, starting
54 with dust transport in the disk to planet-building processes. The main conclusion is
55 that Earth acquired most of its major volatile elements by accretion of planetesimals
56 or embryos akin to volatile-rich meteorites. At the same time, solar/meteoritic
57 noble gases were captured by embryos and some gases were lost to space, by
58 hydrodynamic escape and large impacts. Comets did not contribute much H, C, and
59 N but may have delivered significant noble gases, which could represent the only
60 fingerprints of the bombardment of our planet with icy bodies. The processes that
61 governed the delivery of volatile elements to the Earth are thought to be relatively
62 common and it is likely that Earth-like planets covered with oceans exist in extra-
63 solar systems.

64 65 66 **1. Introduction**

67
68 The oldest water-laid chemical sediments identified in the geologic record are
69 found in southern West Greenland and Northern Québec and are dated at ~ 3.8 Ga*,
70 indicating that liquid water was present at that time (CATES and MOJZSIS, 2007;
71 DAUPHAS et al., 2007; DAUPHAS et al., 2004b; MOORBATH et al., 1973; NUTMAN et al.,
72 1997; O'NEIL et al., 2007). This age corresponds to the transition between the
73 Hadean and the Archean and marks the time when the rock record starts. The
74 Hadean has also been referred to as the dark age of the Earth because, for lack of
75 samples, very little is known about that period. However, there are direct witnesses
76 of the Hadean in the form of zircons (ZrSiO_4), which are tiny minerals resistant to
77 chemical alteration and abrasion that are readily datable by the U-Pb method
78 (HARRISON, 2009). The oldest zircons are found in detrital sediments at Jacks Hill
79 (Australia) and some of these have been dated at 4.3 Ga. Oxygen isotope ratios
80 indicate that the zircons were crystallized from a magma that was produced by
81 melting of a clay-rich sediment produced by water-rock interaction at Earth's
82 surface (MOJZSIS et al., 2001; WILDE et al., 2001). This suggests that liquid water was
83 present on Earth as early as 4.3 Ga.

84 In undifferentiated meteorites (*i.e.*, chondrites), water is present in the structure
85 of hydrated minerals as well as in fluid inclusions. In comets, water is in the form of

*We use annum (as in Ga) for absolute time relative to present and year (as in Gyr) for relative time and duration.

86 ice. However, largely anhydrous bodies also exist. Isotopically, the meteorites that
87 best match the composition of the Earth are enstatite chondrites (*i.e.*, they have
88 identical O, Ti, Cr, and Mo isotopic ratios to terrestrial rocks, CLAYTON, 1993; DAUPHAS
89 et al., 2002; TRINQUIER et al., 2007; TRINQUIER et al., 2009; Fig. 1), leading some to
90 suggest that the Earth formed from these meteorites (JAVOY et al., 2010). A notable
91 difficulty with this idea is that enstatite chondrites have a high Si/Mg ratio, so that
92 unrealistic amounts of Si in the core would be needed to explain the lower Si/Mg
93 ratio of Earth's mantle. Javoy et al. (2010) solved this conundrum by proposing that
94 the Earth was made of material isotopically similar to enstatite chondrites, yet
95 chemically distinct from these meteorites. There is no reason why any of the
96 surviving meteorite groups should match the main source population for Earth. A
97 planet formed solely from such highly reduced bodies would undoubtedly be sterile,
98 posing the question of how and when Earth acquired its water.

99 Any model that attempts to explain the origin of the oceans and atmosphere also
100 must be able to explain the elemental and isotopic compositions of noble gases in
101 air. These are trace gases that play no biological role but their inertness makes them
102 particularly powerful to unravel the sources and processes that have shaped the
103 atmosphere (OZIMA and PODOSEK, 2001). In addition, some noble gas isotopes are
104 part of radioactive decay schemes (*e.g.*, ^{40}K - ^{40}Ar , ^{129}I - ^{129}Xe) that can be used to date
105 processes like mantle degassing or atmosphere loss to space.

106 In this contribution, we examine how geochemical and planetary dynamical
107 considerations can provide constraints on the formation of Earth's atmosphere.
108 Marty & Yokochi (2006), and Pepin (2006) presented detailed reviews on that topic.
109 The question of the origin of Earth's atmosphere covers two aspects: how volatile
110 elements were delivered to the Earth and how secondary processes modified the
111 chemical and isotopic compositions of the atmosphere. This history must be
112 understood in the framework of the formation of the Earth itself, which is discussed
113 in Sect. 2 (reviewed by DAUPHAS and CHAUSSIDON, 2011; RAYMOND, 2010).

114 115 116 **2. Making terrestrial planets**

117
118 We start this review by discussing the process of terrestrial planet formation
119 from the astrophysical point of view. The purpose is to build a framework that can
120 be useful to interpret the volatile record on the Earth. Terrestrial planet formation is
121 thought to proceed in three steps. In step I, the first planetesimals are formed, from
122 a disk of gas and dust. In step II, the collision evolution of the planetesimal
123 population gives birth to a new class of objects, called planetary embryos, which
124 represent an intermediate stage between planetesimals and planets. At the same
125 time, giant planets are formed. In step III, after the disappearance of gas from the
126 proto-planetary disk, the embryos become unstable, and their mutual collisions give
127 birth to a small number of massive objects, known as the terrestrial planets.

128 129 **Step I: from dust to planetesimals.**

131 In the proto-planetary disk, the most refractory materials condense first,
132 gradually followed (while the local temperature drops) by more and more volatile
133 elements. Coexisting with the condensate grains thus formed are dust particles
134 inherited from circumstellar/interstellar chemistry that escaped vaporization in the
135 solar nebula. Collisions helped by electrostatic and magnetic forces stick the grains
136 together, forming fractal aggregates. Other collisions then rearrange the aggregates,
137 and compact them. When the grains reach a size of about a millimeter to a
138 centimeter, they begin to rapidly sediment onto the median plane of the disk in a
139 time of the order of 10^3 yr. This timescale, however, can be longer if the nebula is
140 strongly turbulent.

141 The growth from these grains to kilometer-size planetesimals is still quite a
142 mystery. In principle, one could expect that grains stick to each other to form
143 progressively bigger and bigger objects, in an ordered-growth process. However,
144 particles of cm-size are too small for gravity to be effective in particle-particle
145 collisions, but they are too big to stick through electrostatic forces (although sticking
146 may be possible for particles with large size ratios). Moreover, grains are subject to
147 gas drag, which makes them drift towards the central star (Weideschilling, 1977).
148 The drift speed is size dependent; thus, particles of different sizes must collide with
149 non-negligible relative velocities (of the order m/s). At these velocities particles
150 should break, rather than coagulate (Blum and Wurm, 2008). Because the drift
151 speed towards the central star is maximal for meter-size boulders, this issue is
152 known as the “meter-size barrier problem”, but it is likely that this bottleneck for
153 accretion starts already at much smaller sizes (cm or dm).

154 A new alternative to this ordered-growth process is that planetesimals form
155 thanks to the collective gravity of massive swarms of small particles, concentrated
156 at some locations (vortices or inter-vortex regions, depending on particle sizes) by
157 the turbulence of the disk (Johansen et al., 2007; Cuzzi et al., 2008). This model can
158 explain the formation of large planetesimals (100 km or larger) without passing
159 through intermediate small sizes, so that the meter-size barrier problem is
160 circumvented. Thus, in these gravito-turbulent models, planetesimals form big. The
161 size distribution of objects in the asteroid belt and in the Kuiper belt, where most of
162 the mass is concentrated in 100 km objects, supports this scenario (Morbidelli et al.,
163 2009). The existence and the properties of Kuiper belt binary objects also are best
164 explained by the gravitational collapse of massive swarms of small particles that
165 have too large angular momentum to form a single object (Nesvorny et al., 2010).
166 This new view of planetesimal formation is rapidly gaining support. Although more
167 work is needed to explore all its facets we can start to discuss, in a broad sense, its
168 implications.

169 Once enough small particles are concentrated at some location, the formation
170 of a planetesimal is extremely rapid (Johansen et al., 2007; Cuzzi et al., 2008).
171 However, the formation of self-gravitating clumps of small particles is sporadic
172 (Cuzzi et al., 2010; Chambers, 2010). Therefore, planetesimal formation can proceed
173 over a long time interval. The planetesimals that form first are rich in the short-lived
174 radionuclide ^{26}Al and therefore they can melt and differentiate in a core-mantle-
175 crust structure. Those that form after a couple of millions of years probably can
176 escape differentiation because the majority of short-lived radioactive elements have

177 already decayed. This can explain the co-existence of differentiated and
178 undifferentiated planetesimals that we deduce from the meteorite collections (iron
179 and basaltic meteorites being fragments of differentiated objects and chondritic
180 meteorites being representative of undifferentiated ones). However, it is not
181 necessarily true that each region of the proto-planetary disk had to form both
182 differentiated and undifferentiated planetesimals. The reason is that sufficient
183 clumping of small particles to form planetesimals is possible only if the solid/gas
184 density ratio is larger than some threshold value (Johansen et al., 2009). For
185 instance in the innermost part of the disk, this condition might have been met very
186 early, thus leading to a first generation of planetesimals rich enough in radioactive
187 elements to melt. But in other regions of the disk, this condition might have been
188 met only later, after the removal by photo-evaporation of a substantial fraction of
189 the gas, or the diffusion into the considered region of debris from elsewhere in the
190 disk. Thus, in these regions, all planetesimals formed would remain
191 undifferentiated. This might have been the case of the asteroid belt, in which the
192 solid/gas ratio might have become large enough only after the formation of
193 chondrules (Scott, 2006).

194 At a given time, the temperature in the disk decreases with the distance from
195 the Sun. Thus, close to the Sun only refractory elements can be in solid form,
196 whereas further away more volatile elements are locked up in solids, following the
197 classical condensation sequence. Thus, if all planetesimals had formed at the same
198 time, we would expect two basic properties to be manifested: (a) the planetesimal
199 disk should be characterized by a clear radial gradient of chemical properties; (b)
200 the abundance pattern in each planetesimal should be characterized by a very sharp
201 transition between elements that were refractory enough to condense and those
202 that were too volatile and stayed in the gas. However, this is not the pattern of
203 abundance that is observed in chondrites, which show instead a relatively smooth
204 pattern of depletion as a function of element volatility. Moreover, asteroid belt
205 objects of different compositions have partially overlapping distributions in orbital
206 semi major axis (Gradie and Tedesco, 1982). Why neither (a) nor (b) are true can be
207 understood by the following reasons:

208 (i) According to the gravito-turbulent models, planetesimals form
209 sporadically so that, even at the same location they do not form at the same time
210 (Johansen et al., 2007; Cuzzi et al., 2008). This is consistent with existing
211 chronological constraints on meteorite formation, showing that it spanned ~3-4
212 Myr. With time passing, the temperature decreases and more volatile elements can
213 condense in solids. Thus, this can explain why (a) is not true.

214 (ii) Dynamical evolution after planetesimal formation can partially mix
215 planetesimals originally born at distinct locations (see below). This also can explain
216 why (a) is not true.

217 (iii) Dust transport in the disk partially obliterated the strong heliocentric
218 gradient in temperature. The most blatant evidence for that is the presence of highly
219 refractory dust (*i.e.*, calcium-aluminum-rich inclusion) formed at a temperature of
220 1500 K in comet Wild 2 that coexists with water ice condensed at a temperature of
221 presumably less than ~70 K. This is also seen in meteorites where CAIs coexist with
222 carbonaceous material formed by cold chemistry in the interstellar medium or in

223 outer regions of the disk. This mechanism can explain why (b) is not true (Cassen,
224 2001 and references herein).

225

226 In the absence of clear predictions from the formation models, we can turn to
227 observational constraints to deduce properties of the planetesimal disk. There are
228 basically three classes of chondritic meteorites: enstatite, ordinary and
229 carbonaceous. Their chemistry and mineralogy suggest that they formed at overall
230 decreasing temperatures. For instance, water is essentially absent on enstatite
231 meteorites, and quite abundant in (some subclasses of) carbonaceous chondrites,
232 while the water-content in ordinary chondrites is between the two (Robert, 2003).
233 Spectroscopic observations link these three classes of meteorites to asteroids of
234 different taxonomic type: enstatite chondrites can be linked with E-type asteroids
235 (Fornasier et al., 2008), which are predominant in the Hungaria region at 1.8
236 astronomical units (AU; 1 AU is the mean Sun-Earth distance); ordinary chondrites
237 are linked to S-type asteroids (Binzel et al., 1996; Nakamura et al., 2011), which are
238 predominant in the inner belt (2.1-2.8 AU); carbonaceous chondrites are linked to C-
239 type asteroids (Burbine, 2000), which are predominant in the outer belt (beyond 2.8
240 AU).

241 Comets are representative of the planetesimal disk that formed at larger
242 distances than the asteroid belt, *i.e.* in between the giant planet orbits and beyond.
243 The classical view is that, while the parent bodies of carbonaceous chondrites are
244 rich in hydrated minerals, comets are rich in water ice, presumably because they
245 formed in a colder environment. The difference between carbonaceous chondrites
246 (or C-type asteroids) and comets, though, is becoming less well defined, with new
247 discoveries. The close flyby images of comets (*e.g.*, comet Borrelly) show very little
248 surface ice and small active regions (Sunshine et al., 2006). The Stardust samples
249 turned out to be quite similar to meteoritic samples (Zolensky et al., 2006).
250 Modeling work on the origin of the dust that produces the zodiacal light (Nesvorny
251 et al., 2010) predicts that at least 50 % of the micro-meteorites collected on Earth
252 are cometary; however, we see no clear separation of micro-meteorites into two
253 categories, which could be traced to asteroidal and cometary dust (Levison et al.,
254 2009). Water-ice has been found on the C-type asteroid Themis (Campins et al.,
255 2010; Rivkin et al., 2010) and some C-type asteroids in the main belt show cometary
256 activity (Hsieh and Jewitt, 2006). The possibility of a continuum in physical and
257 chemical properties between carbonaceous asteroids and comets is well described
258 in Gounelle et al. (2008). The Rosetta encounter with comet 67P/Churyumov-
259 Gerasimenko may shed some light on the question of the relationship between
260 cometary dust and carbonaceous chondrites.

261 Putting all this information together in a coherent picture is not a simple
262 task. However at the very least we can say that there is evidence that a radial
263 gradient in temperature existed in the disk at the time(s) when planetesimals
264 formed, although this gradient has probably been smeared by the processes (i) and
265 (ii) described above. In particular, planetesimals in the inner disk (in the inner
266 asteroid belt region and presumably also in the terrestrial planet region) appear dry
267 and volatile poor. As proposed by Albarède (2009), probably the gas was removed

268 from the system before that the temperature decreased enough to allow the
269 condensation of the volatiles in the inner solar system and hence primitive objects
270 (*i.e.*, objects with near-solar compositions for moderately volatile elements) could
271 not form there.

272 **Step II: from planetesimals to planetary embryos**

273 Once the proto-planetary disk contains a substantial population of
274 planetesimals, the second stage of planet formation can start. The dynamics of
275 accretion is initially dominated by the effect of the gravitational attraction between
276 pairs of planetesimals. A *runaway growth* phase starts, during which the big bodies
277 grow faster than the small ones, hence increasing their relative difference in mass
278 (Greenberg et al, 1978). This process can be summarized by the equation:

$$279 \quad d/dt (M_1/M_2) > 0, \quad (1)$$

281 where M_1 and M_2 are respectively the characteristic masses of the “big” and of the
282 “small” bodies. The reasons for runaway growth can be explained as follows. At the
283 beginning of the growth phase, the largest planetesimals represent only a small
284 fraction of the total mass. Hence the dynamics is governed by the small bodies, in
285 the sense that the relative velocities among the bodies is of order of the escape
286 velocity of the small bodies $V_{\text{esc}(2)}$. This velocity is independent of the mass M_1 of the
287 big bodies and is smaller than the escape velocity of the large bodies $V_{\text{esc}(1)}$. For a
288 given body, the collisional cross-section is enhanced with respect to the geometrical
289 cross-section by the so-called *gravitational focusing* factor F_g , so that:

$$291 \quad dM/dt \sim R^2 F_g \quad (2)$$

293 The gravitational focussing factor is given by (Greenzweig and Lissauer, 1992):
294

$$295 \quad F_g = 1 + V_{\text{esc}}^2/V_{\text{rel}}^2 \quad (3)$$

297 where V_{esc} is the body's escape velocity and V_{rel} is the relative velocity of the other
298 particles in its environment. Because $V_{\text{rel}} \sim V_{\text{esc}(2)}$, the gravitational focusing factor
299 of the small bodies ($V_{\text{esc}}=V_{\text{esc}(2)}$) is ~ 2 , while that of the large bodies
300 ($V_{\text{esc}}=V_{\text{esc}(1)} \gg V_{\text{esc}(2)}$) is much larger, of order $V_{\text{esc}(1)}^2/V_{\text{rel}}^2$. In this situation,
301 remembering that both $V_{\text{esc}(1)}$ and the geometrical cross section are proportional to
302 $M_1^{2/3}$, the mass growth of a big body is described by the equation

$$303 \quad 1/M_1 dM_1/dt \sim M_1^{1/3} V_{\text{rel}}^{-2} \quad (4)$$

307 (Ida and Makino, 1993). Therefore, the relative growth rate is an increasing function
308 of the body's mass, which is the condition for the runaway growth (Fig. 2). Runaway
309 growth stops when the masses of the large bodies become important (Ida and
310

311 Makino, 1993) and the latter start to govern the dynamics. The condition for this to
312 occur is:

313
314
$$n_1 M_1^2 > n_2 M_2^2, \quad (5)$$

315

316 where n_1 (resp. n_2) is the number of big bodies (resp. small bodies). In this case, V_{rel}
317 $\sim V_{\text{esc}(1)}$, so that $F_g \sim 2$; hence $(1/M_1)(dM_1/dt) \sim M_1^{-1/3}$. The growth rate of the
318 embryos gets slower and slower as the bodies grow and the relative differences in
319 mass among the embryos also slowly decreases. In principle, one could expect that
320 the small bodies catch up, narrowing their mass difference with the embryos. But in
321 reality, the now large relative velocities prevent the small bodies from accreting
322 with each other due to collisional fragmentation. The small bodies can only
323 participate to the growth of the embryos. This phase is called ‘oligarchic growth’.

324 The runaway growth phase happens with timescales that depend on the local
325 dynamical time (keplerian time) and on the local density of available solid material.
326 The density also determine the maximum size of the embryos when the runaway
327 growth ends (Lissauer, 1987). Assuming a reasonable surface density of solid
328 materials, the runaway growth process forms planetary embryos of lunar to
329 martian mass at 1 AU in 10^5 - 10^6 y, separated by a few 10^{-2} AU (Kokubo and Ida,
330 1998). Thus, the planetary embryos are not yet the final terrestrial planets. They are
331 not massive enough, they are too numerous and they are closely packed relative to
332 the terrestrial planets that we know. Moreover they form too quickly, compared to
333 the timescale of several 10^7 y suggested for the Earth by radioactive chronometers
334 (Kleine et al., 2010).

335 Because runaway growth is a local process, the embryos form essentially
336 from the local planetesimals in their neighbourhoods. Little radial mixing is
337 expected at this stage. Thus, if the planetesimal disk is characterized by a radial
338 gradient of chemical properties, such a gradient is expected to be reflected in the
339 embryos distribution. Nevertheless, embryos can undergo internal physical
340 modifications. In view of their large mass and their rapid formation timescale, they
341 can undergo differentiation. We stress, though, that embryo formation cannot be
342 faster than planetesimal formation, because a massive planetesimal population is
343 needed to trigger the runaway growth of the embryos. [It is not correct to say that
344 planetesimals formed late. Iron meteorites formed very rapidly and the meteorite
345 collections could give us a biased sampling of the objects that were present when
346 embryos formed] Embryos formed early would have incorporated enough ^{26}Al to
347 melt (Dauphas and Pourmand 2011) while embryos formed late could have escaped
348 global differentiation, similarly to what is invoked for Callisto (Canup and Ward,
349 2002) or Titan (Sotin et al., 2010). The lack of differentiation could have helped the
350 embryos formed in the outer asteroid belt to preserve the water inherited from the
351 local carbonaceous chondrite-like planetesimals. Nevertheless, even if
352 differentiation occurred, water would not have been necessarily lost; water ice
353 could have formed a mantle around a rocky interior, possibly differentiated itself
354 into a metallic core and a silicate outer layer, like on Europa and Ganymede.

355 The formation of the giant planets is intimately related to the
356 runaway/oligarchic growth of embryos. Beyond the so-called *snow line* at about 4

357 AU, where condensation of water ice occurred thanks to the low temperature,
358 enhancing the surface density of solid material, the embryos would have been
359 bigger, probably approaching an Earth mass. The formation of the massive cores of
360 the giant planets (of about 10 Earth masses each) is still not well understood. It has
361 been proposed that convergent migration processes would have brought these
362 embryos together, favoring their rapid mutual accretion (Morbidelli et al., 2008;
363 Lyra et al., 2009; Zandor et al., 2010). Once formed, the cores started to accrete
364 massive atmospheres of hydrogen and helium from the proto-planetary disk, thus
365 becoming the giant planets that we know.

366 **Step III: from embryos to terrestrial planets**

367 At the disappearance of the gas from the proto-planetary disk, the solar
368 system should have had the following structure: a disk of planetesimals and
369 planetary embryos, roughly of equal total masses, in the inner part; the system of
370 the giant planets already fully formed, in the central part; another disk of
371 planetesimals beyond the orbits of the giant planets. The orbits of the giant planets
372 were inherited from their previous dynamical evolution, dominated by their
373 gravitational interactions with the gas disk. They were therefore likely different
374 from the current ones. We will come back to this important issue below.

375 Nebular gas was present in the inner part of the disk probably for 3-5 Myr
376 after solar system birth (Dauphas and Chaussidon 2011). The gas has a stabilizing
377 effect on the system of embryos and planetesimals because it continuously damps
378 their orbital eccentricities, through tidal and drag effects, respectively. Thus, when
379 the gas is removed by accretion onto the central star and by photoevaporative loss
380 (Alexander 2008, Hollenbach et al. 2000), the embryos rapidly become unstable and
381 their orbits begin to intersect; collisions can take place (Chambers and Wetherill,
382 1998). Numerical simulations (Chambers and Wetherill, 2001; Raymond et al., 2004,
383 2005; O'brien et al., 2006) show that the dynamical evolution is very different in the
384 terrestrial planet region and in the asteroid belt. In the terrestrial planet region,
385 where the perturbations exerted by Jupiter are weak, the embryos' eccentricities
386 remain relatively small, and the embryos can accrete each other in low velocity
387 collisions. Instead, the asteroid belt is crossed by several powerful resonances with
388 Jupiter, which excite the eccentricities of the resonant objects. The orbits of embryos
389 and planetesimals change continuously due to mutual encounters; every time that
390 one of them temporarily falls into a resonance, its eccentricity is rapidly enhanced.
391 Thus, most of the original population eventually leaves the asteroid belt region by
392 acquiring orbits that are so eccentric to cross the terrestrial planet region.
393 Ultimately, the majority of the population originally in the asteroid belt is
394 dynamically removed by collisions with the Sun or ejections on hyperbolic orbits,
395 but a fraction of it can also be accreted by the growing planets inside of 2 AU (see
396 Fig. 3 for an illustration of this process). The typical result of this highly chaotic
397 phase --simulated with several numerical N-body integrations-- is the elimination of
398 all the embryos originally situated in the asteroid belt and the formation a small
399 number of terrestrial planets on stable orbits in the 0.5--2 AU region in a timescale

400 of several tens of millions of years (Chambers and Wetherill, 2001; O'Brien et al.,
401 2006).

402 This scenario has several strong points:

403 (i) Typically, 2 to 4 planets are formed on well-separated and stable orbits. If
404 the initial disk of embryos and planetesimals contains about 4-5 Earth masses of
405 solid material, typically the two largest planets are about one Earth mass each.
406 Moreover, in the most modern simulations, accounting for the dynamical interaction
407 between embryos and planetesimals (O'Brien et al., 2006), the final eccentricities
408 and inclinations of the synthetic terrestrial planets are comparable or even smaller
409 than those of the real planets.

410 (ii) Quasi-tangent collisions of Mars-mass embryos onto the proto-planets
411 are quite frequent (Agnor et al., 1999; Morishima et al., 2009). These collisions are
412 expected to generate a disk of ejecta around the proto-planets (Canup and Asphaug,
413 2002), from which a satellite is likely to accrete (Canup and Esposito, 1996). This is
414 the standard, generally accepted, scenario for the formation of the Moon.

415 (iii) The accretion timescale of the terrestrial planets in the simulations is
416 ~30-100 Myr. This is in gross agreement with the timescale of Earth accretion
417 deduced from radioactive chronometers (whose estimates change from one study to
418 another over a comparable range; Yin et al., 2002; Touboul et al., 2007; Kleine et al.
419 2009; Allègre et al. 1995).

420 (iv) No embryos and only a small fraction of the original planetesimals
421 typically remain in the asteroid belt on stable orbits at the end of the process of
422 terrestrial planet formation (Petit et al, 2001; O'Brien et al., 2007). This explains
423 well the current mass deficit of the asteroid belt. The orbital eccentricities and
424 inclinations of these surviving particles compare relatively well with those of the
425 largest asteroids in the current belt. Moreover, because of the scattering suffered
426 from the embryos, the surviving particles are randomly displaced in semi major
427 axis, relative to their original position, by about half of an AU. This can explain the
428 partial mixing of asteroids of different taxonomic types, discussed above.

429

430 There is a clear dependence of the final outcomes of the simulations on the
431 orbital architecture assumed for the giant planets. As said above, the giant planets
432 should be fully formed by the time the gas is removed from the disk, *i.e.* well before
433 the formation of the terrestrial planets. The simulations with larger orbital
434 eccentricities of the giant planets (up to 2 times the current eccentricities) form
435 terrestrial planets on a shorter timescale and on more circular final orbits than
436 those with more circular giant planets; moreover, the terrestrial planets accrete
437 fewer material from the asteroid belt and the synthetic planet produced at the place
438 of Mars is smaller (Raymond et al., 2009). All these properties are related to each
439 other. In fact, eccentric giant planets deplete more violently the asteroid belt:
440 embryos and planetesimals originally in the belt are removed by collisions with the
441 Sun or ejection on hyperbolic orbit before they have a significant chance to interact
442 with the growing terrestrial planets inside of 2 AU. Thus, terrestrial planet
443 formation proceeds as in a "close" system, with little material (or none) coming into
444 the game from outside of 1.5-2.0 AU. Accretion proceeds faster because the material

445 that builds the planets is more radially confined. On the other hand, faster accretion
446 timescales imply that more planetesimals are still in the system at the end of the
447 terrestrial planet accretion process, so that the orbital eccentricities of the
448 terrestrial planets can be damped more efficiently by planet-planetesimal
449 interactions. Finally, Mars forms smaller because it is close to the edge of the radial
450 distribution of the mass that participates to the construction of the terrestrial
451 planets (Raymond et al., 2009).

452 To understand which giant planet orbital architecture was more likely at the
453 time of terrestrial planet formation, one has to examine the dynamical evolution
454 that the giant planets should have had in the disk of gas in which they formed. It is
455 well known that, by interacting gravitationally with the gas-disk, the orbits of the
456 giant planets migrate (see Ward, 1997, for a review). Eventually the planets tend to
457 achieve a multi-resonance configuration, in which the period of each object is in
458 integer ratio with that of its neighbour (Morbidelli et al., 2007). The interaction
459 with the disk also damps the planets' orbital eccentricities. Thus, at the
460 disappearance of the gas disk, the giant planets should have been closer to each
461 other, on resonant and quasi-circular orbits (the giant planets could have achieved
462 the current orbits at a much later time, corresponding to the so-called Late Heavy
463 Bombardment; see Morbidelli, 2011 and Sect. 7). Unfortunately, this kind of orbital
464 configuration of the giant planets systematically leads to synthetic planets at ~ 1.5
465 AU that are much more massive than the real Mars (Raymond et al., 2009).

466 Hansen (2009) convincingly showed that the key parameter for obtaining a
467 small Mars is the radial distribution of the solid material in the disk. If the outer
468 edge of the disk of embryos and planetesimals is at about 1 AU, with no solid
469 material outside of this distance, even simulations with giant planets on circular
470 orbits achieve systematically a small Mars (together with a big Earth). This scenario
471 would also imply a short accretion timescale for Mars, of the order of a few My,
472 consistent with estimates obtained from Hf-W systematics (Dauphas and Pourmand
473 2011). The issue is then how to justify the existence of such an outer edge and how
474 to explain its compatibility with the existence of the asteroid belt, between 2 and 4
475 AU. The asteroid belt as a whole has a small mass (about 6×10^{-4} Earth masses;
476 Krasinsky et al., 2002), but it is well known that it had to contain at least a thousand
477 times more solid material when the asteroids formed (Wetherill, 1989).

478 The result by Hansen motivated Walsh et al. (2011) to look in more details at
479 the possible orbital history of the giant planets and their ability to sculpt the disk in
480 the inner solar system. For the first time, the giant planets were not assumed to be
481 on static orbits (even if different from the current ones); instead Walsh et al. studied
482 the co-evolution of the orbits of the giant planets and of the precursors of the
483 terrestrial planets. Walsh et al. built their model on previous hydro-dynamical
484 simulations showing that the migration of Jupiter can be in two regimes: when
485 Jupiter is the only giant planet in the disk, it migrates inwards (Lin and Papaloizou,
486 1986); when it is neighbored by Saturn, both planets typically migrate outward,
487 locked in a 2:3 mean motion resonance (where the orbital period of Saturn is $3/2$ of
488 that of Jupiter; Masset and Snellgrove, 2001; Morbidelli and Crida, 2007). Thus,
489 assuming that Saturn formed later than Jupiter, Walsh et al. envisioned the following
490 scenario: first, Jupiter migrated inwards while Saturn was still growing; then, when

491 Saturn reached a mass close to its current one, it started to migrate inwards more
492 rapidly than Jupiter, until it captured Jupiter in the 3/2 resonance (Masset and
493 Snellgrove, 2001; Pierens and Nelson, 2008) when the latter was at ~1.5 AU; finally
494 the two planets migrated outwards until Jupiter reached ~5.5 AU at the complete
495 disappearance of the disk of gas. The reversal of Jupiter's migration at 1.5 AU
496 provides a natural explanation for the existence of the outer edge at 1 AU of the
497 inner disk of embryos and planetesimals, required to produce a small Mars (Fig.
498 4,5). Because of the prominent inward-then-outward migration of Jupiter that it
499 assumes, Walsh et al. scenario is nicknamed "Grand Tack".

500 Several giant extra-solar planets have been discovered orbiting their star at a
501 distance of 1-2 AU, so the idea that Jupiter was sometime in the past at 1.5 AU from
502 the Sun is not shocking by itself. A crucial diagnostic of this scenario, though, is the
503 survival of the asteroid belt. Given that Jupiter should have migrated through the
504 asteroid belt region twice, first inwards, then outwards, one could expect that the
505 asteroid belt should now be totally empty. However, the numerical simulations by
506 Walsh et al. show that the asteroid belt is first fully depleted by the passage of the
507 giant planets, but then, while Jupiter leaves the region for the last time, it is re-
508 populated by a small fraction of the planetesimals scattered by the giant planets
509 during their migration. In particular, the inner asteroid belt is dominantly
510 repopulated by planetesimals that were originally inside the orbit on which Jupiter
511 formed, while the outer part of the asteroid belt is dominantly repopulated by
512 planetesimals originally in between and beyond the orbits of the giant planets.
513 Assuming that Jupiter accreted at the location of the snow line, it is then tempting to
514 identify the planetesimals originally closer to the Sun with the largely anhydrous
515 asteroids of E- and S-type and those originally in between and beyond the orbits of
516 the giant planets with the "primitive" C-type asteroids. With this assumption, the
517 Grand Tack scenario explains the physical structure of the asteroid belt (see above),
518 its small mass of the asteroid belt and its eccentricity and inclination distribution.

519

520 **3. Inventories and isotopic compositions of volatiles in** 521 **terrestrial planets, meteorites, and comets**

522

523 Major volatile elements are constantly recycled into Earth's mantle at
524 subduction zones and are degassed into the atmosphere in volcanic regions. We
525 review here the inventory of volatile elements in terrestrial and extraterrestrial
526 reservoirs (Tables 1-3). Earth's core is absent from this discussion because it is not
527 accessible and its volatile element content is unknown. This section describes how
528 volatile inventories are estimated from various measurements; it can be skipped
529 entirely without affecting readability.

530

531 3.1. Earth

532 The Earth is an active planet where volatile elements can exchange between the
533 atmosphere, ocean, crust, and mantle. These exchanges have played a major role in
534 maintaining habitable conditions at the surface of our planet. This is best
535 exemplified by the carbon cycle, where CO₂ degassing, rock alteration, carbonate

536 deposition, and recycling into the mantle must have regulated surface temperatures
537 through weathering of silicate rocks (written here as CaSiO_3) by CO_2 from the
538 atmosphere (dissolved in water as carbonic acid), to make carbonate (CaCO_3) and
539 silica (SiO_2) that precipitate in the ocean: $\text{CaSiO}_3 + \text{CO}_2 \rightarrow \text{CaCO}_3 + \text{SiO}_2$ (*i.e.*, the Urey
540 reaction). When some forcing acts to increase the temperature (*e.g.*, increase of the
541 solar luminosity with time), the rate of chemical weathering increases, more
542 carbonates are formed and the CO_2 is drawn down, which creates a negative
543 greenhouse feedback. It is therefore important to assess where major volatile
544 elements reside in the solid Earth, as the atmosphere is not an isolated reservoir.
545 We review hereafter the terrestrial inventories of H, N, C, and noble gases. For
546 Earth's outer portion ("surface reservoirs" in Table 1), we consider the following
547 reservoirs: the atmosphere, the hydrosphere (oceans, porewater, ice, lakes, rivers,
548 and groundwater), the biosphere (marine and land biota), and crust (oceanic crust,
549 continental crust including soils, sediments, igneous and metamorphic rocks).

550 Mantle volatile budgets are notoriously difficult to establish. For that
551 purpose, we compare volatile elements to other elements that have similar
552 behaviors during mantle melting and magma differentiation. Thus, H (as H_2O) is
553 normalized to Ce (MICHAEL, 1995), N (as N_2) is normalized to ^{40}Ar (produced by
554 decay of ^{40}K) (MARTY, 1995), C (as CO_2) is normalized to Nb (SAAL et al., 2002). We
555 use two approaches that provide lower and upper limits on the budgets of the major
556 volatile elements:

557 i) We use H/Ce, N/ ^{40}Ar , and C/Nb atomic ratios of mid-ocean ridge basalts
558 (MORBs) with estimates of the Ce, ^{40}Ar , and Nb concentrations of the depleted
559 mantle to calculate the volatile content of the mantle by considering that the MORB
560 source extends all the way to the core-mantle boundary. This represents a very
561 conservative lower-limit on the volatile budget of the mantle as it neglects the
562 presence of a volatile-rich reservoir in the mantle source of plume-related magmas.

563 ii) We calculate the H/Ce, N/ ^{40}Ar , and C/Nb ratios in the crust-hydrosphere-
564 biosphere-atmosphere system. Assuming that H, C, and N were derived from mantle
565 melting and that they were not decoupled from Ce, ^{40}Ar , and Nb during magma
566 generation and recycling, this approach would give good estimates of bulk silicate
567 Earth (BSE) H/Ce, N/ ^{40}Ar , and C/Nb ratios. However, during subduction, H and C
568 could have been less efficiently recycled than Ce and Nb. Therefore, H/Ce and C/Nb
569 ratios of surface reservoirs represent upper-limits on the BSE ratios. Similarly, N
570 might have been degassed from the mantle before significant decay of ^{40}K , so the
571 N/ ^{40}Ar ratio of surface reservoirs represents an upper-limit on the N/ ^{40}Ar ratio of
572 the BSE. In Table 1, we only compile abundance data derived from this second
573 approach, as we believe that it provides a better estimate of the mantle volatile
574 budget.

575

576 The noble gas data for Earth are from a compilation by Ozima & Podosek (2001).
577 While approximately half of ^{40}Ar is in the solid Earth (ALLÈGRE et al., 1996), most of
578 the inventory of other noble gases except helium is in the atmosphere. For example,
579 the $^{40}\text{Ar}/^{36}\text{Ar}$ ratio of the silicate Earth is at least a factor of 10 higher than that of
580 the atmosphere (*i.e.*, >3,000 in the mantle vs. 295.5 in air), so the atmosphere must
581 contain >90 % of the global inventory of ^{36}Ar (MARTY et al., 1998; VALBRACHT et al.,

582 1997a). This crude estimate assumes a negligible volume for volatile-rich, low
583 $^{40}\text{Ar}/^{36}\text{Ar}$ (<3,000) mantle reservoirs.

584

585

586 3.1.1 Hydrogen

587 The water content of Earth's atmosphere is small and is spatially and temporally
588 variable. Lécuyer et al. (1998) and Mottl et al. (2007) reviewed the water
589 inventories and D/H ratios of Earth's surface reservoirs (see Table 3 of MOTTL et al.,
590 2007). The hydrosphere contains 1.80×10^{23} mol H, 85 % of which is in the oceans
591 ($M_{\text{ocean}} = 1.37 \times 10^{21}$ kg). The δD value of the hydrosphere is slightly negative (-6 ‰),
592 due to a small contribution of water from ice that is characterized by $\delta\text{D} \sim -400$ ‰.
593 The biosphere contains only 1.51×10^{20} mol H (0.001 M_{ocean}) with a δD value of -100
594 ‰. The crust contains 3.43×10^{22} mol H (0.22 M_{ocean}) with a δD value of -75 ‰. Most
595 of that inventory is in shales. Unsurprisingly, the hydrosphere represents the largest
596 reservoir of water at Earth's surface.

597 The water content of Earth's mantle has been the focus of considerable work
598 as it affects the viscosity of the mantle (HIRTH and KOHLSTEDT, 1996), which has
599 important implications for the dynamical evolution of our planet. Lack of water in
600 the Venusian mantle may explain the absence of plate tectonics on that planet (*e.g.*,
601 RICHARDS et al., 2001). The Ce concentration of the depleted mantle is 3.93×10^{-9}
602 mol/g (WORKMAN and HART, 2005a). The H/Ce atomic ratio of MORBs is $\sim 3.1 \times 10^3$
603 (200 ppm H₂O ppm Ce, MICHAEL, 1995), which translates into a H-concentration of
604 the source of MORBs of 1.2×10^{-5} mol/g (~ 110 ppm H₂O). A lower limit on the H
605 content of the mantle is therefore 4.9×10^{22} mol (0.4×10^{21} kg H₂O; 0.3 M_{ocean}).

606 The masses of the continental and oceanic crusts are 21.3×10^{21} kg and
607 6.4×10^{21} kg, respectively (MURAMATSU and WEDEPOHL, 1998). The Ce concentration in
608 the continental crust is $\sim 3.1 \times 10^{-7}$ mol/g (43 ppm Ce, RUDNICK and GAO, 2003) while
609 that of the oceanic crust is $\sim 1.1 \times 10^{-7}$ mol/g (15 ppm Ce, STRACKE et al., 2003). We
610 thus estimate that the bulk crust contains 7.2×10^{18} mol of Ce. Using the H data from
611 Table 1, we calculate an H/Ce atomic ratio for surface reservoirs of 3.0×10^4 . The Ce
612 concentration of the BSE is 4.37×10^{-9} mol/g (0.613 ppm Ce, McDONOUGH and SUN,
613 1995a), which corresponds to a total Ce content of 1.75×10^{19} mol. This translates
614 into a H-content of 5.2×10^{23} mol H in the BSE (3.4 M_{ocean}). Subtracting the H amount
615 in surface reservoirs, we calculate that the mantle must contain at most 3.05×10^{23}
616 mol H (2.0 M_{ocean} ; 2.7×10^{21} kg H₂O, corresponding to a concentration of ~ 690 ppm).
617 The δD value of the mantle is ~ -80 ‰ (LECUYER et al., 1998).

618

619 3.1.2. Carbon

620 Earth's surface carbon cycle has been the subject of much attention due to the
621 societal importance of that element as a fuel and a greenhouse gas. MacKenzie &
622 Lerman (2006) and Sundquist & Visser (2003) reviewed the carbon budget of
623 Earth's surface. The C isotopic compositions are from Heimann & Maier-Reimer
624 (1996). The atmosphere contains 6.6×10^{16} mol C with a $\delta^{13}\text{C}$ of ~ -8 ‰. The land and
625 ocean biota contain 6×10^{16} and 0.025×10^{16} mol C, respectively with a $\delta^{13}\text{C}$ of ~ -25

626 ‰. The hydrosphere contains $\sim 320 \times 10^{16}$ mol C (most as dissolved inorganic
627 carbon) with a $\delta^{13}\text{C}$ value of ~ 0 ‰. In the crust, soils contain 24×10^{16} mol C,
628 methane hydrates contain 83×10^{16} mol C, coal, oil and natural gas contain 42×10^{16}
629 mol C, sedimentary organic matter contains $105,000 \times 10^{16}$ mol C, sedimentary
630 carbonates contain $544,000 \times 10^{16}$ mol C, the igneous oceanic crust contains
631 $7,660 \times 10^{16}$ mol C, and the igneous-metamorphic continental crust contains
632 $21,400 \times 10^{16}$ mol C. The $\delta^{13}\text{C}$ values of sedimentary organic matter and carbonates,
633 which dominate the crustal budget, are ~ -25 ‰ and ~ 0 ‰, respectively.

634 The C/Nb atomic ratio of MORBs is $\sim 1,120$ (*i.e.*, $\text{CO}_2/\text{Nb} \sim 530$ ppm/ppm, Saal et
635 al. 2002; CARTIGNY et al., 2008). The Nb concentration of the MORB source is
636 1.60×10^{-9} mol/g (0.1485 ppm Nb, WORKMAN and HART, 2005a), which translates into
637 a C concentration of 1.79×10^{-6} mol/g (~ 79 ppm CO_2). This corresponds to a lower
638 limit on the C content of the mantle of 7.2×10^{21} mol (0.3×10^{21} kg CO_2 , 75 ppm CO_2).

639 The Nb concentration in the continental crust is $\sim 9 \times 10^{-8}$ mol/g (8 ppm Nb,
640 RUDNICK and GAO, 2003), while that of the oceanic crust is $\sim 2.7 \times 10^{-8}$ mol/g (2.5 ppm
641 Nb, STRACKE et al., 2003). We thus estimate that the bulk crust contains 2.01×10^{18}
642 mol of Nb. Using the C data from Table 1, we calculate a C/Nb atomic ratio for
643 surface reservoirs of 3.4×10^3 . The Nb concentration of the bulk silicate Earth (BSE)
644 is $\sim 2.6 \times 10^{-9}$ mol/g (0.240 ppm Nb, McDONOUGH and SUN, 1995a), the mass of the BSE
645 (mantle+crust) is 4.03×10^{24} kg, the BSE must contain 1.0×10^{19} mol Nb. Using a C/Nb
646 ratio of 3.4×10^3 , we calculate a C content of the BSE of 33.8×10^{21} mol. Subtracting
647 the amount of C in surface reservoirs, we estimate that the mantle must contain at
648 most 27×10^{21} mol C (1.2×10^{21} kg CO_2 , corresponding to a CO_2 concentration of 300
649 ppm). The carbon isotopic compositions of samples from the mantle are variable
650 with an average value of $\delta^{13}\text{C} = -5$ ‰ (Deines 1980; Pineau and Javoy 1983; MARTY
651 and ZIMMERMAN, 1999; CARTIGNY et al., 2001).

652

653 3.1.3. Nitrogen

654 Galloway (2003) reviewed the global geochemical cycle of nitrogen. Boyd
655 (2001) estimated the N isotopic compositions of the various reservoirs involved in
656 that cycle. Houtlon and Bai (2009) focused on the $\delta^{15}\text{N}$ value of the biosphere. The
657 atmosphere contains 2.82×10^{20} mol N with a $\delta^{15}\text{N}$ of 0 ‰ (by definition). The
658 oceans contain 1.47×10^{18} mol N (1.43×10^{18} mol N as dissolved N_2 and 4.1×10^{16} mol
659 N as dissolved NO_3^-) with a positive $\delta^{15}\text{N}$ value of $+6$ ‰ imparted by denitrification.
660 The biosphere contains 7.50×10^{14} mol N (7.14×10^{14} and 3.6×10^{13} mol N in land and
661 marine biota, respectively) with a $\delta^{15}\text{N}$ of ~ 0 ‰ for the vegetation. The crust
662 contains 7.14×10^{19} mol N (mostly as sedimentary rocks and 1.4×10^{16} as soil
663 organics). The $\delta^{15}\text{N}$ of sediments is $\sim +6$ ‰.

664 The nitrogen content of the mantle is fairly well known from N_2 - ^{40}Ar
665 systematics. MORBs have an $\text{N}/^{40}\text{Ar}$ ratio of 248 and the depleted mantle has a ^{40}Ar
666 concentration of 2.8×10^{-11} mol/g (MARTY and DAUPHAS, 2003, updated with the ^4He
667 degassing rate of Bianchi et al. 2010). We can thus calculate a lower-limit on the N
668 content of the mantle of 0.3×10^{20} mol (0.1 ppm N_2).

669 In magmatic systems, N₂ and Ar tend to have similar chemical behaviors. The
670 amount of radiogenic ⁴⁰Ar in the whole Earth can be calculated using the amount of
671 ⁴⁰K in the mantle and crust, the half-life of that nuclide, and the known branching
672 ratio between ⁴⁰K and ⁴⁰Ca (ALLÈGRE et al., 1996). We thus estimate that the Earth
673 contains 3.6×10¹⁸ mol ⁴⁰Ar. The ⁴⁰Ar content of the atmosphere-crust is 1.9×10¹⁸
674 mol (1.65×10¹⁸ mol in the atmosphere and 0.25×10¹⁸ mol in the crust). The N/⁴⁰Ar
675 ratio of Earth's surface reservoir is therefore 187. Using the amount of ⁴⁰Ar in the
676 whole Earth, this would translate into a total N content of 6.7×10²⁰ mol. Subtracting
677 the amount of N in surface reservoirs, we calculate an upper-limit on the mantle N
678 content of 3.15×10²⁰ mol (1.1 ppm N₂). This upper-limit is probably close to the
679 actual N content of the mantle because the N/⁴⁰Ar ratio is approximately constant
680 between surficial (atmosphere-crust) and mantle reservoirs (MARTY and DAUPHAS,
681 2003).

682 The nitrogen isotopic composition of the mantle is uncertain. The source of
683 MORBs has a δ¹⁵N of ~-5 ‰ while the source of plume-related magmas has a δ¹⁵N of
684 ~+3 ‰ (Dauphas et al. 1999; MARTY and DAUPHAS, 2003). Plume-related sources
685 may dominate the nitrogen inventory of the mantle, so we ascribe a δ¹⁵N value of +3
686 ‰ to the whole mantle.

687

688 3.2 Solar, Mars, Venus, meteorites, and comets

689 3.2.1 Solar composition

690 The H, C, N and noble gas concentrations are from a compilation by Lodders
691 (2010). Early on, the sun experienced deuterium burning and the present-day solar
692 wind D/H ratio is not representative of that of the protosolar nebula. The solar D/H
693 ratio pre-deuterium burning is estimated to be 25×10⁻⁶ (ROBERT et al., 2000). The
694 current best estimate of the solar carbon isotopic composition is from a
695 spectroscopic determination, which gave ¹³C/¹²C=0.01152 (SCOTT et al., 2006). The
696 solar wind nitrogen isotopic was recently measured in collector material recovered
697 from the Genesis mission, yielding a ¹⁵N/¹⁴N ratio of 0.002178 (δ¹⁵N=-407 ‰,
698 MARTY et al., 2011). The solar ²⁰Ne/²²Ne, ²¹Ne/²²Ne, and ³⁸Ar/³⁶Ar ratios are from
699 measurements of Genesis collector material (HEBER et al., 2009). The solar ⁴⁰Ar/³⁶Ar
700 ratio is from Lodders (2010). Lunar samples provide the best estimates of the solar
701 Kr and Xe isotopic compositions (PEPIN et al., 1995; WIELER, 2002).

702

703 3.2.2 Venus and Mars

704 The inventories of major volatile elements in Venus and Mars are difficult to
705 establish as a significant fraction of those elements may be residing in crustal and
706 mantle reservoirs (*e.g.*, see Sect. 3.1 for Earth, illustrating how complex such
707 estimates can be).

708 On Venus, C and N are two major atmospheric constituents and their
709 abundances are well known (VON ZAHN et al., 1983). Hydrogen is present as a trace
710 gas in the venusian atmosphere (~30 ppm H₂O) and is characterized by a D/H ratio
711 ~157×SMOW (DE BERGH et al., 2006). Noble gas abundances and isotopic
712 compositions in the venusian atmosphere are from Donahue & Russell (1997).

713 Mars missions and studies of SNC meteorites have given us a better insight into
714 the cycles of major volatile elements on that planet. Most of the water at the surface
715 of Mars is locked up in the cryosphere. Christensen (2006) estimated that it
716 represents $\sim 5 \times 10^{18}$ kg of water. This corresponds to an H concentration of 9×10^{-7}
717 mol/g-planet. The D/H ratio was only measured in the atmosphere and it is unsure
718 whether this is representative of the bulk surface composition, which is dominated
719 by ice. For example, Montmessin et al. (2005) proposed a D/H value of $6.5 \times \text{SMOW}$
720 for martian surface water, which is higher than that measured in the atmosphere
721 ($5.6 \times \text{SMOW}$). SNC meteorites have also revealed the presence of a component
722 enriched in deuterium in the martian crust (Leshin Watson 1994; Leshin et al.
723 1996). The martian atmosphere contains 95.32 % CO_2 (OWEN et al., 1977),
724 corresponding to a C concentration of 8.6×10^{-10} mol/g-planet. Carbonates have been
725 found at the surface of Mars and in martian meteorites (BOYNTON et al., 2009;
726 BRIDGES et al., 2001; EHLMANN et al., 2008; MORRIS et al., 2010). However, the amount
727 of C trapped as carbonate in the martian crust is currently unknown. Pollack et al.
728 (1987) showed that in order to have liquid water stable during the early history of
729 Mars a PCO_2 of 0.75 to 5 bar would be needed. For reference, a PCO_2 of 1 bar would
730 correspond to a C concentration of 1.4×10^{-7} mol/g-planet. Niles et al. (2010)
731 recently measured the C isotopic composition of atmospheric CO_2 with good
732 precision ($\delta^{13}\text{C} = -2.5 \pm 4.3$ ‰). The martian atmosphere contains 2.7 % N_2 (OWEN
733 et al., 1977), which correspond to a N concentration of 4.8×10^{-11} mol/g-planet.
734 Manning et al. (2008) suggested that as much 1.2×10^{19} mol N as nitrate might be
735 present in the martian regolith. However, no direct evidence for the presence of
736 such a large reservoir has been found yet. The N isotopic composition of the martian
737 atmosphere is from a compilation by Bogard et al. (2001). The noble gas
738 composition of the martian atmosphere is well known from measurements of gases
739 trapped SNC meteorites. Bogard et al. (2001) reviewed all constraints on the
740 martian noble gas compositions. The $^{20}\text{Ne}/^{22}\text{Ne}$ ratio of the martian atmosphere is
741 uncertain and values between 7 and 10 have been proposed. The higher values may
742 reflect contamination with terrestrial air ($^{20}\text{Ne}/^{22}\text{Ne} = 9.8$, GARRISON and BOGARD,
743 1998). For that reason, we adopt a value of 7 for the martian atmosphere, keeping in
744 mind that the actual value may be different. The martian $^{21}\text{Ne}/^{22}\text{Ne}$ is unknown as
745 ^{21}Ne is affected by cosmogenic effects during exposure of SNC meteorites to cosmic
746 rays in space. The Ar isotopic composition is that recommended by Bogard et al.
747 (2001). The Kr isotopic composition is from Garrison and Bogard (1998). Note that
748 ^{78}Kr is not reported in Table 3 as the value given by Garrison and Bogard (1998) is
749 unusually high and these authors concluded that this could be due to an analytical
750 artifact (*e.g.*, an isobaric interference of hydrocarbon). Approximately 9 % of ^{80}Kr in
751 the atmosphere was produced by neutron capture on ^{79}Br in the martian regolith
752 (RAO et al., 2002). The martian Xe isotopic composition is from Swindle et al. (1986).

753

754 3.2.3. CI1 meteorites and comets

755 The H, C, and N concentrations and isotopic compositions of CI1 chondrites are
756 from Kerridge (1985), noble gas abundances as well as Ne and Ar isotopic ratios are
757 from Mazor et al. (1970), Kr isotopic ratios are from Eugster et al. (1967), and Xe

758 isotopic ratios are from Pepin (2000b). In chondrites, ^{21}Ne is affected by cosmogenic
759 effects and ^{40}Ar is affected by ^{40}K decay. In Table 3, we list the $^{21}\text{Ne}/^{22}\text{Ne}$ and
760 $^{40}\text{Ar}/^{36}\text{Ar}$ ratios of the dominant trapped components present in primitive
761 chondrites (OTT, 2002).

762 The H, C, and N concentrations of comets are from Marty & Dauphas (2002),
763 based on estimates of the dust and gas compositions reported by Jessberger et al.
764 (1988) and Delsemme (1988). Jehin et al. (2009) compiled and discussed measured
765 D/H, $^{13}\text{C}/^{12}\text{C}$, and $^{15}\text{N}/^{14}\text{N}$ isotopic ratios measured in comets. The water D/H ratios
766 of the 6 Oort-cloud comets analyzed thus far are higher than the terrestrial ratio by
767 a factor of ~ 2 . Given that water is the dominant H-bearing species, its D/H ratio is
768 representative of the bulk cometary composition, yielding an average of 0.00034.
769 Note that HCN has a high D/H ratio but its contribution to the bulk composition is
770 minor. The $^{13}\text{C}/^{12}\text{C}$ ratios measured in CN, HCN, and C_2 are close to the chondritic
771 ratio. A significant fraction of C may be present in refractory dust, which has the
772 same C isotopic composition as the volatile component so this adds no
773 uncertainty. However, the C isotopic composition of important molecules like CO is
774 presently unknown. The $^{15}\text{N}/^{14}\text{N}$ ratio was measured in CN and HCN. The main N-
775 bearing species in comets is NH_3 so one should bear in mind that the measurements
776 done so far may not be representative of the bulk cometary composition. Jewitt et al.
777 (1997) had found a $^{15}\text{N}/^{14}\text{N}$ ratio in HCN of Hale-Bopp that was similar to the
778 terrestrial ratio. However, subsequent measurements did not confirm that result
779 (BOCKELEEE-MORVAN et al., 2008) but found instead that the $^{15}\text{N}/^{14}\text{N}$ ratio in both HCN
780 and CN of comets was approximately twice the terrestrial ratio (i.e., 0.0068).
781 Recently, the D/H ratio of a Kuiper-belt comet (103P/Hartley 2) was analyzed and
782 against all expectations, was found to be identical to Earth (Hartogh et al. 2011).
783 Meech et al. (2011) reported a $^{13}\text{C}/^{12}\text{C}$ ratio of 0.0105 ± 0.0017 for the CN molecules
784 in that comet, consistent with the terrestrial ratio (~ 0.11). However, the $^{15}\text{N}/^{14}\text{N}$
785 ratio of CN (0.00645 ± 0.00104) was found to be significantly higher than the
786 terrestrial ratio (0.00367). Further work on Kuiper belt comets is needed to
787 documents their volatile element isotopic compositions. The noble gas
788 concentrations in comets are unknown. In Table 2, we list the noble gas
789 concentration data derived from trapping experiments in amorphous ice (BAR-NUN
790 et al., 1988; BAR-NUN and OWEN, 1998; DAUPHAS, 2003). Trapping experiments have
791 shown limited isotopic fractionation for Ar, Kr, and Xe, so their isotopic
792 compositions in comets might be solar (NOTESCO et al., 1999).

793
794

795 **4. Modeling the origin of noble gases in the terrestrial** 796 **atmosphere**

797
798
799
800
801
802

Noble gases are chemically inert and as such they can provide an unparalleled record of the origin and evolution of the atmosphere. They are relatively easy to extract from rocks, show large abundance and isotopic variations, and were the focus of numerous studies since the dawn of geochemistry. For instance, the first radiometric age was reported by Rutherford in 1905 by measuring α -particles

803 produced by U-decay in some pitchblende. However, there is still no consensus on
804 the origin of noble gases in the atmospheres of Earth and other terrestrial planets. A
805 complete model of the origin of terrestrial noble gases must account for the
806 following observations (Tables 2, 3; Fig. 6):

- 807 • When normalized to solar composition, noble gases –with the exception of Xe–
808 show a pattern of elemental depletion of light versus heavy noble gases (*e.g.*, the
809 air Ne/Ar ratio is lower than the solar Ne/Ar ratio).
- 810 • This depletion is accompanied by larger isotopic fractionation for the lighter
811 noble gases Ne, Ar, and Kr (*e.g.*, the isotopic fractionation in ‰/amu relative to
812 solar is higher for Ne than for Ar).
- 813 • Xenon is an exception to the rules outlined above. Despite being heavier, Xe is
814 more depleted than Kr (*i.e.*, the Xe/Kr in air is lower than solar) and it is more
815 isotopically fractionated than Kr (*i.e.*, 38 ‰/amu for Xe vs 8 ‰/amu for Kr).
816 This is known as the missing Xe problem and the peculiarities of all the models
817 proposed thus far are related to solving this issue.

818 More constraints on the origin and timing of the formation of the atmosphere can be
819 derived from noble gas isotopes of radiogenic origin. These can be examined
820 independently of the stable non-radiogenic isotopes and are discussed in more
821 detail in Sect. 5 of this chapter, as well as Chapter 2 (Zhang, 2012) of the present
822 volume. Most models proposed so far involve an episode of hydrodynamic escape to
823 space, which is presented in more detail below. This is followed by a presentation of
824 the three main models that can explain the characteristics of Earth’s atmosphere,
825 underlining their strengths and weaknesses.

826 4.1. Hydrodynamic escape and Earth’s missing Xe problem

827 Noble gases like Xe are too heavy to escape from a planet such as Earth by
828 thermal escape following Jean’s theory. Instead, they can escape Earth’s atmosphere
829 by hydrodynamic escape (ZAHNLE and KASTING, 1986; HUNTEN et al., 1987; SASAKI and
830 NAKAZAWA, 1988; PEPIN, 1991; DAUPHAS, 2003). Individual H₂ molecules moving
831 upwards can drag along heavy noble gas atoms that would otherwise not be able to
832 escape Earth’s gravity. For such hydrodynamic escape to proceed, a significant
833 inventory of H₂ must be present on the protoplanet. Possible origins for H₂ include
834 trapped nebular gases or redox reaction between H₂O and a reductant like metallic
835 iron (*i.e.*, H₂O+Fe⁰->H₂+Fe²⁺+O). The energy required to sustain an outward flux of H₂
836 could be provided by EUV radiation from the young active T-Tauri sun or by
837 gravitational energy released upon impact with large extraterrestrial bodies.
838 Extrasolar planets that are close to their central star can be subject to such
839 hydrodynamic escape (BALLESTER et al., 2007; TIAN et al., 2005; VIDAL-MADJAR et al.,
840 2003). Following Hunten et al. (1987), the single most important quantity that
841 determines whether an isotope *i* can be lost by hydrodynamic escape is the cross-
842 over mass,

$$843 \quad m_{ci} = m + \frac{kT\Phi}{b^i g X}, \quad (6)$$

844 where *k* is the Boltzmann constant, *g* is the standard gravity, *T* is the temperature,
845 *m*, Φ and *X* are the mass, the escape flux and mole fractions of the major light
846 constituent (*i.e.*, H₂), *bⁱ* is the diffusion parameter of *i* (*e.g.*, $b^{\text{Xe}} \approx 14.4 \times 10^{18}$,

847 $b^{\text{Kr}} \approx 16.3 \times 10^{18}$, $b^{\text{Ar}} \approx 18.8 \times 10^{18}$, and $b^{\text{Ne}} \approx 26.1 \times 10^{18} \text{ cm}^{-1}\text{s}^{-1}$ for diffusion in H_2 at 270 K;
 848 ZAHNLE and KASTING, 1986; PEPIN, 1991) . If the crossover mass is known for one
 849 isotope, it is straightforward to derive it for any another isotope j,

$$850 \quad m_{cj} = m + (m_{ci} - m) \frac{b^i}{b^j}. \quad (7)$$

851 When $m_i > m_{ci}$, the escape flux is null and the mixing ratio of the trace constituent
 852 follows a diffusive equilibrium profile with the scale height augmented by a term
 853 corresponding to the flux of H_2 . When $m_i < m_{ci}$, the trace constituent can escape to
 854 space. It is assumed that X remains constant through time at 1 (*i.e.*, the atmosphere
 855 is dominated by H_2) and that the escape flux evolved as a function of time following
 856 the functional form $\Phi = \Phi_0 \Psi(t)$, where Ψ is a function that starts at $\Psi(0) = 1$ and
 857 decreases with time. If we write N and N_i the column densities of the major (H_2) and
 858 minor constituents, we can relate the flux of the minor constituent to that of H_2
 859 through,

$$860 \quad \Phi_i = \frac{N_i}{N} \left(\frac{m_{ci} - m_i}{m_{ci} - m} \right) \Phi. \quad (8)$$

861 Let us introduce $\mu_i = (m_i - m) / (m_{ci}^0 - m)$. Note that in this expression, the cross-over
 862 mass m_{ci}^0 is taken at time $t=0$. Using Eq. 1, we have $(m_{ci} - m) = (m_{ci0} - m) \Psi(t)$. Taking Φ_0
 863 positive for a net escape flux, the previous equation can be rewritten as,

$$864 \quad \frac{dN_i}{N_i} = - \frac{\Phi_0}{N} [\Psi(t) - \mu_i] dt. \quad (9)$$

865 Integration of this equation is only meaningful until the time when the atmosphere
 866 becomes retentive for that constituent. This happens at a closure time, $t_{ci} = \Psi^{-1}(\mu_i)$.
 867 Therefore, the general equation that should be used to calculate the evolution of a
 868 trace constituent during hydrodynamic escape is (DAUPHAS, 2003; HUNTEN et al.,
 869 1987; PEPIN, 1991),

$$870 \quad \ln \frac{N_i}{N_i^0} = - \int_0^{\Psi^{-1}(\mu_i)} \frac{\Phi_0}{N} [\Psi(t) - \mu_i] dt. \quad (10)$$

871 To integrate this equation, one has to specify N as well as the functional form of Ψ .
 872 For example, one can assume that N is constant at a value N_0 (H_2 is constantly
 873 replenished) and that the escape flux decreases with time following an exponential
 874 $\Psi(t) = \exp(-t/\tau)$. Under these assumptions, the number of free parameters is reduced
 875 to 2 (*i.e.*, $\tau \Phi_0 / N_0$ and $m_{c, Xe}^0$ if Xe is chosen as the reference noble gas) and the
 876 abundance of an isotope in the atmosphere has a simple analytical expression,

$$877 \quad \ln \frac{N_i}{N_{i0}} = \frac{\Phi_0 \tau}{N_0} (\mu_i - 1 - \mu_i \ln \mu_i). \quad (11)$$

878 The degree of curvature in $\ln N$ vs m space in hydrodynamic escape is set by Ψ ,
 879 which directly influences the evolution of the cross-over mass with time. Thus,
 880 changing the parameterization of the escape flux offers additional freedom in
 881 hydrodynamic escape models to reproduce measured data.

882 One may wonder what it means to reproduce elemental and isotopic data.
 883 Are the two constraints independent? Expressing isotopic fractionation in ‰/amu,
 884 we have,

885
$$F = \left(\frac{N_{i2}/N_{i1}}{N_{i2}^0/N_{i1}^0} - 1 \right) \times \frac{1000}{m_{i2} - m_{i1}}. \quad (12)$$

886 We now introduce an alternative quantity to express isotopic fractionation that is
887 sometimes used in isotope geochemistry (δ' notation; Criss and Farquhar 2008),

888
$$F' = \ln \left(\frac{N_{i2}/N_{i1}}{N_{i2}^0/N_{i1}^0} \right) \times \frac{1000}{m_{i2} - m_{i1}}. \quad (13)$$

889 The general relationship between these two functions is,

890
$$F = \left[e^{F'(m_{i2} - m_{i1})/1000} - 1 \right] \times \frac{1000}{m_{i2} - m_{i1}}. \quad (14)$$

891 When isotopic fractionation is small and the isotopes cover a narrow mass range, F'
892 is almost identical to F . Because isotopic variations are small and affect isotopes of
893 similar masses, $\ln(N/N^0)$ in Eq. 13 can be expanded in m through a Taylor series
894 truncated at the second order,

895
$$F' \approx 1000 \times \frac{d \ln(N_i/N_i^0)}{dm_i}. \quad (15)$$

896 We recognize the derivative in mass of Eq. 10. Therefore, reproducing the
897 abundance and isotopic composition of the terrestrial atmosphere is mathematically
898 equivalent to fitting a curve in $\ln N$ vs m that has the right position and the right
899 derivatives at each mass corresponding to the four noble gases. The general
900 equation to calculate the isotopic composition of a trace constituent during
901 hydrodynamic escape is (this is a new development of the present work),

902
$$F' \approx 1000 \times \frac{\Phi_0}{m_{ci}^0 - m} \int_0^{\Psi^{-1}(u_i)} \frac{1}{N} dt. \quad (16)$$

903 Note that this formula is strictly valid in the limit that the isotopic fractionation is
904 small, that the relative mass difference between isotopes is small, so that Eq. 15 can
905 approximate Eq. 13. Even for light noble gases with large relative mass difference
906 and large isotopic fractionation such as Ne, we have found that this formula gives a
907 good estimate of the isotopic fractionation produced by hydrodynamic escape. Using
908 the model presented previously where $N = N_0$ and $\Psi(t) = \exp(-t/\tau)$ we have,

909
$$F' \approx -1000 \times \frac{\Phi_0}{(m_{ci}^0 - m)N_0} \ln(u_i). \quad (17)$$

910 Expectedly, this equation has the same free parameters as before, i.e., $\tau \Phi_0/N_0$ and
911 $m_{c,Xe}^0$. Using $\tau \Phi_0/N_0 = 16.04$ and $m_{c,Xe}^0 = 345$ (Hunten et al. 1987; Dauphas 2003), the
912 exact calculation from Eq. 11 gives $F_{Xe} = 48.7$, $F_{Kr} = 72.0$, $F_{Ar} = 109.1$, and $F_{Ne} = 161.4$
913 while the approximate calculation using Eq. 15 and 12c gives $F_{Xe} = 48.3$, $F_{Kr} = 71.6$,
914 $F_{Ar} = 110.5$, and $F_{Ne} = 164.4$

915 For hydrodynamic escape, we expect the abundance curve to increase with
916 mass (heavier noble gases are more efficiently retained, Eq. 10). This is what is
917 observed for Ne, which is more depleted than Ar, which is in turn more depleted
918 than Kr. However, Xe is more depleted than Kr, which cannot be explained by
919 hydrodynamic escape alone. We also expect light noble gases to be more isotopically
920 fractionated than heavier ones (Eq. 16). This is true for Ne-Ar-Kr, with Ne more
921 isotopically fractionated than Ar, which is in turn more isotopically fractionated
922 than Kr. However, Xe is more isotopically fractionated than Kr, which cannot be

923 explained by hydrodynamic escape alone. Below, we discuss the three models than
924 can account for these puzzling observations, *i.e.*, the missing Xe problem.

925 4.2. Hydrodynamic escape and preferential Xe retention (PEPIN, 1991, 1997).

926 As will be reviewed in Sect. 5, Earth has lost most of radiogenic ^{129}Xe
927 produced by decay of ^{129}I . Such loss was possibly driven by hydrodynamic escape
928 and could have been accompanied by elemental and isotopic fractionation of noble
929 gases. An important idea behind the model proposed by Pepin (1991, 1997) is that
930 during core formation, mantle melting, and degassing, Xe can be preferentially
931 retained in the Earth. This idea is partially backed by laboratory experiments as well
932 as ab initio studies showing that under pressure; Xe could be retained in the mantle
933 (BROCK and SCHROBILGEN, 2010; JEPHCOAT, 1998; LEE and STEINLE-NEUMANN, 2006;
934 SANLOUP et al., 2005). In the original 1991 version, Pepin assumed that
935 hydrodynamic escape was powered primarily by EUV radiation from the active
936 young T-Tauri Sun (ZAHNLE and WALKER, 1982). This model was subsequently
937 revised in 1995 to account for the possibility that the Moon-forming giant impact
938 powered noble gas escape to space. The different steps involved in this later model
939 are outlined below (Fig. 7).

940 In Pepin's model, the initial atmosphere starts with a noble gas abundance
941 pattern that is close to solar except for a significant depletion in Ne. No reason is
942 provided for this depletion other than the same feature is required to explain the
943 composition of the venusian atmosphere. The assumed isotopic compositions are
944 solar for all noble gases. Collision between the proto-Earth and a planetary embryo
945 leads to an episode of hydrodynamic escape. Noble gases are lost to space according
946 to the prescriptions outlined in Sect. 4.1. The lighter noble gases are more depleted
947 and isotopically fractionated than heavier ones. Subsequently, noble gases are
948 degassed from Earth but Xe is preferentially retained in the mantle (or core).
949 Therefore, all Xe in the atmosphere at that time is from the first escape episode and
950 its isotopic composition is highly fractionated. Krypton on the other hand is derived
951 from mantle degassing of juvenile noble gases and it shows limited isotopic
952 fractionation. By adjusting the proportions of leftover gases from the escape episode
953 and juvenile gases from mantle degassing, Pepin (1997) was able to reproduce the
954 near-solar Xe/Kr ratio of the atmosphere. Argon is mainly derived from the escape
955 episode. In a late escape episode driven by EUV radiation, some Ne is lost and is
956 fractionated isotopically. Heavier noble gases are not affected by this episode.

957 This model can reproduce most of the features of Earth's atmosphere.
958 However, an important difficulty is that no mantle reservoir has been documented
959 yet that could host the missing Xe, which Pepin (1991; 1997) argued was retained in
960 the Earth. High-pressure experiments have shown that the core or deep mantle
961 could serve as a possible repository for the missing Xe. However, Mars possess the
962 same missing Xe problem as Earth despite the fact that its internal pressure is much
963 lower (*e.g.*, ~ 23 GPa at the core-mantle boundary on Mars vs ~ 135 GPa on Earth)
964 and the mineral physics involved would presumably be different. Finally, the model
965 predicts that Kr in Earth's mantle should be less isotopically fractionated compared
966 to the atmosphere, which is inconsistent with the measured Kr isotopic composition
967 of CO_2 well gases (HOLLAND et al., 2009).
968

969

970 4.3. Hydrodynamic escape and solubility-controlled Xe degassing (Tolstikhin
971 and O’Nions 1994).

972 Of all noble gases, Xe has the lowest solubility in silicate melts (Lux, 1987);
973 $S(\text{Ar}) = 5 \times 10^{-5} \text{ cm}^3 \text{ STP} / (\text{g atm})$, $S(\text{He})/S(\text{Ar}) = 10$, $S(\text{Ne})/S(\text{Ar}) = 4$, $S(\text{Kr})/S(\text{Ar}) =$
974 0.55 and $S(\text{Xe})/S(\text{Ar}) = 0.3$. During mantle degassing, it is conceivable that Xe would
975 be preferentially degassed relative to Ne, Ar, and Kr. Tolstikhin and O’Nions (1994)
976 followed in the footsteps of Pepin (1991) and proposed a model to solve the missing
977 Xe problem that relies on this idea of solubility controlled degassing during Earth’s
978 accretion (Fig. 8). Ideal gas behaviour, equilibrium partitioning between melt and
979 gas phases, and infinitesimal small gas/melt ratio were assumed. In this scenario,
980 the starting composition of Earth’s heavy noble gases is chondritic. During mantle
981 degassing, insoluble Xe is preferentially degassed into the atmosphere, where it is
982 lost and isotopically fractionated by hydrodynamic escape. In subsequent stages,
983 remaining mantle noble gases are degassed and lost to space. This model can
984 account for the elemental and isotopic characteristics of noble gases in Earth’s
985 atmosphere. Tolstikhin and Kramers (2008) have shown that the conditions of
986 solubility controlled ingassing/degassing and weakening hydrodynamic escape can
987 be achieved in the context of a realistic model of post-giant impact magma ocean
988 evolution on the early Earth. The model cannot explain the heavy Kr isotopic
989 composition of Earth’s mantle relative to the atmosphere (HOLLAND et al., 2009).

990

991

992 4.4. Hydrodynamic escape and cometary input (Dauphas 2003).

993 Except for measurements of dust returned from comet 81P/Wild 2 by the
994 Stardust spacecraft (MARTY et al., 2008), the noble gas composition of comets is
995 completely unknown (BOCKELEEE-MORVAN et al., 2004). The only indirect information
996 on the composition of cometary ice is from laboratory trapping experiments in
997 amorphous ice (BAR-NUN et al., 1988; Owen and Bar-Nun 1992; BAR-NUN and OWEN,
998 1998; NOTESCO et al., 2003). These experiments revealed that at a certain
999 temperature, Xe is less efficiently trapped than Kr. No satisfactory microphysical
1000 explanation has been provided for this depletion and further experimental work will
1001 be required to understand this aspect of noble gas trapping experiments in
1002 amorphous ice. Owen and Bar-Nun (1992) showed that this could explain one
1003 important aspect of Earth’s missing Xe, namely why the Xe/Kr ratio in Earth’s
1004 atmosphere is lower than the solar ratio. Dauphas (2003) showed that such a
1005 cometary input could explain all the abundance and isotopic characteristics of noble
1006 gases in Earth’s atmosphere (Fig. 9). In this model, atmospheric noble gases start
1007 with solar isotopic compositions and relative abundances (actually, some of the
1008 noble gases may have been derived from a chondritic source but this was not
1009 considered in the model to avoid unnecessary complication). The noble gases are
1010 then lost to space by hydrodynamic escape powered by EUV radiation from the
1011 young T-Tauri Sun. Following this escape episode; lighter noble gases are more
1012 depleted and isotopically fractionated than heavier ones. In a second stage, comets
1013 deliver noble gases with near-solar isotopic compositions but with an abundance
1014 pattern corresponding to that measured in trapping experiments at ~50 K (or ~25

1015 K based on experiments performed at lower deposition rates; Notesco and Bar-Nun,
1016 2003). As Xe trapped in amorphous ice is possibly deficient relative to Kr, comets
1017 could have delivered isotopically solar Kr without disturbing the Xe isotopic
1018 signature produced by the hydrodynamic escape episode. This model can also
1019 explain the abundances and isotopic compositions of other noble gases. In the
1020 model of Dauphas (2003), the isotopic composition of Xe was assumed to be solar
1021 but low temperature condensation is prone to creating measurable isotopic
1022 fractionation. The Hertz-Knudsen equation derived from the kinetic theory of gases
1023 gives the flux of molecules impinging on a surface $F = P/\sqrt{2\pi mkT}$ (molecule $\text{m}^{-2} \text{s}^{-1}$).
1024 Only a fraction γ (sticking coefficient) of the impacting molecules will be able to
1025 adhere permanently to the surface. So the fractionation of two isotopes 1 and 2
1026 upon trapping is simply $\alpha_{2/1} = (\gamma_2/\gamma_1)\sqrt{m_1/m_2}$. Assuming a sticking coefficient that does
1027 not depend on mass, the isotopic fractionation for trapped vs gas-phase Xe is -3.8
1028 ‰/amu. This is opposite in sign and is much smaller than what is measured in
1029 Earth's atmosphere of $\sim +38$ ‰/amu, meaning that comets did not deliver already
1030 fractionated Xe or that more complex ice trapping mechanisms must be considered.
1031 For example, it remains to be seen if trapping or processing of Xe in ice under UV (in
1032 the interstellar or outer solar system) can fractionate Xe isotopes and abundance
1033 relative to other noble gases. While lighter noble gases have ionization energies
1034 higher than hydrogen (Ne=21.56 eV, Ar=15.76 eV, Kr=14.00 eV vs. H=13.60 eV),
1035 xenon has an ionization energy (12.13 eV) that is lower than hydrogen, which could
1036 have affected its trapping efficiency in conditions relevant to cometary ice
1037 formation. Laboratory experiments have shown that ionized Xe could be
1038 fractionated isotopically during trapping in refractory solids (Dziczkaniec et al.
1039 1981; Bernatowicz and Hagee 1987; Ponganic et al. 1997; Hohenberg et al. 2002;
1040 Marrocchi et al. 2011) but the effects are small in regard of the large Xe isotopic
1041 fractionation measured in air. Experiments of noble gas trapping in ice under
1042 ionizing radiation remain to be performed. In the different context of hydrodynamic
1043 escape from Earth's atmosphere, the low ionization energy of Xe had been identified
1044 as a feature that could potentially explain its fractionation relative to lighter noble
1045 gases (Zahnle 2000; Pujol et al. 2011). Indeed, this increases the cross-section of Xe
1046 for collisions with hydrogen and facilitates its escape to space.

1047 The composition of Jupiter can provide some clues on the noble gas
1048 composition of comets. Indeed, the Galileo probe measured noble gas abundances in
1049 Jupiter and found that these were enriched by a factor of 2 to 3 relative to hydrogen
1050 and solar composition (except for Ne that can be sequestered in the planet's
1051 interior). Such enrichments can be explained if these noble gases were delivered to
1052 Jupiter in the form of comets (Owen et al. 1999). The enrichment is uniform for Ar,
1053 Kr, and Xe (Ar/Kr/Xe are in solar proportions) suggesting that the planetesimals
1054 that formed Jupiter trapped volatiles at low temperature, *i.e.* <30 K. To explain the
1055 missing Xe in Earth's atmosphere, heavy noble gases have to be fractionated relative
1056 to each other, which would require higher trapping temperatures. Although
1057 Jupiter's atmosphere can inform us on the composition of icy planetesimals in the
1058 giant-planet forming region, these comets may not be relevant to the icy
1059 planetesimals that delivered noble gases to Earth's atmosphere.

1060 One difficulty with the model proposed by Dauphas (2003) is that it relies on
1061 the composition of hypothetical comets based on trapping experiments that are not
1062 fully understood. Like the other two models, the similarity between the terrestrial
1063 and martian atmospheres must be taken as a coincidence. However, this model can
1064 explain why mantle Kr is enriched in the heavy isotopes relative to the atmosphere
1065 (HOLLAND et al., 2009) because it predicts that mantle Kr should have been
1066 fractionated in the early Earth while atmospheric Kr was delivered later by the
1067 accretion of cometary material with near-solar isotopic composition. Following a
1068 similar line of reasoning, Marty and Meibom (2007) argued that accretion of
1069 extraterrestrial material by Earth during the late heavy bombardment at ~3.9 Ga
1070 could have modified the noble gas composition of Earth's atmosphere.

1071

1072 4.5. Standing issues

1073 While several models can explain all the elemental and isotopic
1074 characteristics of Earth's atmosphere, there are a number of standing issues that
1075 will need to be addressed to make progress in our understanding of the origin of
1076 Earth's atmosphere. One of those is to understand why Mars and Earth both present
1077 the same missing Xe problem. The similarity can be taken as a coincidence but this is
1078 not very satisfactory as Earth and Mars have very different masses and should have
1079 followed different evolutionary tracks. In particular, all of the three models
1080 discussed above (Sect. 4.2, 4.3, and 4.4) invoke hydrodynamic escape to fractionate
1081 Xe isotopes, the efficiency of which should depend on the planet's gravity. One
1082 possible solution is that Earth inherited its missing Xe problem from one or several
1083 Mars-size embryos that collided to form our planet during the stage of chaotic
1084 growth (Dauphas and Pourmand 2011). Indeed, Mars accreted in a few million
1085 years, while Earth's accretion was not completed until >30 Myr after solar system
1086 birth. Thus, it is conceivable that Earth formed from Mars-like embryos and that
1087 some of the features measured in the terrestrial atmosphere reflect evolution on
1088 these embryos. The Xe composition of the Venusian atmosphere is completely
1089 unknown. This is unfortunate, as this would provide important constraints on the
1090 origin of the terrestrial planet atmospheres. If Venus has the same Xe isotopic
1091 composition as Earth and Mars, resorting to coincidental conditions to explain this
1092 similarity will be even less tenable. The single most important data that is needed at
1093 present is an estimate of the noble gas composition of cometary ice. Indeed, it is the
1094 only major noble gas planetary reservoir that has not been measured; yet laboratory
1095 experiments seem to indicate that they could have played a major role in
1096 establishing the noble gas composition of the atmospheres of terrestrial planets.
1097 This is an issue that the Rosina instrument on board the Rosetta mission (Balsiger et
1098 al. 2007) may be able to settle by measuring the composition of gases emanating
1099 from the surface of comet 67P/Churyumov-Gerasimenko.

1100 Pujol et al. (2011) recently reported the discovery of xenon with isotopic
1101 composition intermediate between modern air and chondritic/solar in fluid
1102 inclusions in ~3.5 Ga quartz and barite. These measurements suggest that the
1103 fractionated Xe isotopic composition of the modern atmosphere was established
1104 over an extended period of several billions of years. If correct, this may call for a
1105 revision of the evolution of the atmosphere. Pujol et al. (2011) suggested that the

1106 isotopic fractionation of Xe was related to its low ionization potential compared to
1107 other noble gases. Ionized Xe has a much larger size than the neutral form, which
1108 could have promoted its atmospheric loss (Zahnle 2000). In this scenario, noble
1109 gases Ne, Ar, and Kr would have been derived from mixing between solar and
1110 meteoritic components (Marty 2012). A proper mechanism/setting to selectively
1111 lose ionized Xe remains to be identified. Given that Mars shows the same missing Xe
1112 problem, fractionating Xe on precursors of planets (*e.g.*, embryos or comets) may be
1113 more appealing.

1114
1115

1116 **5. Nature and timing of noble gas degassing and escape**

1117 Several noble gases possess parent radioactive isotopes, which can be used to
1118 establish the timing of mantle degassing and escape to space. ^{40}K decays into ^{40}Ar
1119 with a half-life of 1.248 Gy. ^{129}I is an extinct nuclide that decays into ^{129}Xe with a
1120 half-life of 15.7 My. ^{244}Pu is another extinct radionuclide that can produce
1121 fissionogenic Xe isotopes (^{131}Xe - ^{136}Xe) with a half-life of 80.0 My and a branching ratio
1122 of 0.012, 5.6 % of which goes to ^{136}Xe . Finally, fissionogenic Xe isotopes can also be
1123 produced by decay of ^{238}U ($t_{1/2}$ =4.468 Gy) with a spontaneous fission branching of
1124 5.45×10^{-7} , 6.3 % of which goes to ^{136}Xe . Both ^{232}Th and ^{235}U have very low
1125 spontaneous fission probabilities (1.1×10^{-11} and 7.0×10^{-11} , respectively), so they did
1126 not contribute significantly to fissionogenic Xe isotopes on Earth. SHUKOLYUKOV et al.
1127 (1994) and MESHNIK et al. (2000) argued that some of Xe isotopes might have been
1128 contributed by neutron-induced fission of ^{235}U in the form of CFF-Xe (Chemical
1129 Fractionation of Fission Xe) if Oklo-type natural reactor were abundant on early
1130 Earth. However, Ballentine et al. (2002) presented mass balance arguments against
1131 a significant contribution of CFF-Xe to Earth's atmosphere. At large scales and over
1132 long periods of time, it is unlikely that CFF-Xe would be preferentially released into
1133 the atmosphere relative to the complementary enriched ^{136}Xe component.

1134

1135 5.1. Mantle noble gases

1136 Several reviews have discussed this topic at length (BALLENTINE and HOLLAND,
1137 2008; FARLEY and NERODA, 1998; LUPTON, 1983; Ozima and Podosek 2001; Graham
1138 2002) and a brief summary is provided below (the depleted upper-mantle
1139 composition is compiled in Table 4). This section (5.1) describes how mantle
1140 volatile inventories can be inferred from measurements of mantle-derived samples;
1141 it can be skipped entirely without affecting readability.

1142

1143 5.1.1. MORBs and CO_2 well gases

1144 The elemental and isotopic compositions of the depleted upper-mantle are
1145 known from measurements of mid-ocean ridge basalts (MORBs). The noble gas that
1146 has been most extensively studied is helium (Fig. 10). MORBs have a near-constant
1147 $^3\text{He}/^4\text{He}$ ratio ($R/R_A \sim 8$, where R is the $^3\text{He}/^4\text{He}$ ratio of a sample and R_A is the
1148 $^3\text{He}/^4\text{He}$ ratio in air, *i.e.* 1.38×10^{-6}), which is more radiogenic than that of most
1149 plume-related sources (KURZ et al., 1982). This indicates that MORBs are from a
1150 relatively well-homogenized mantle source that has been extensively degassed (*i.e.*,

1151 the depleted convective upper-mantle). Because He is constantly lost to space by
1152 thermal escape and its concentration is low in the atmosphere (its residence is only
1153 ~ 1 Myr), the ^3He flux from MORBs can be detected in the form of a plume in the
1154 ocean above ridges (CRAIG et al., 1975; LUPTON and CRAIG, 1981). This can be used in
1155 turn to infer a ^3He flux at ridges of 527 ± 102 mol/year (BIANCHI et al. 2010). Using a
1156 global ridge production rate of $21 \text{ km}^3/\text{year}$ (with a density of 3 g/cm^3) and a
1157 degree of partial melting of 10 % for MORBs, it is possible to calculate the ^3He
1158 content of their mantle source of $(8.4 \pm 1.6) \times 10^{-16}$ mol/g. For a $^3\text{He}/^4\text{He}$ ratio of 7.3
1159 R_A (Fig. 10), this gives a ^4He concentration of $(8.3 \pm 1.6) \times 10^{-11}$ mol/g. Using Th and U
1160 concentrations of 7.9 and 3.2 ppb respectively for the depleted MORB mantle
1161 (WORKMAN and HART, 2005b), this amount of ^4He corresponds to ~ 2.5 Gyr of
1162 accumulation.

1163 Noble gases heavier than He are abundant in the atmosphere, and MORB samples
1164 are prone to contamination by air. In that respect, the gas-rich samples known as
1165 popping-rocks have played a tremendous role in establishing the composition of the
1166 upper-mantle for noble gases. These rocks are named after the noise that they make
1167 on the ship deck when the vesicles burst due to decompression. Equally important
1168 are CO_2 well gases, which sample a mixture between crustal and mantle-derived
1169 gases (BALLENTINE and HOLLAND, 2008). Neon isotope systematics reveals interesting
1170 facts about Earth (Fig. 11). The $^{20}\text{Ne}/^{22}\text{Ne}$ ratio can only vary due to mass
1171 fractionation. Sarda et al. (1988), Marty (1989) and Honda et al. (1991) showed that
1172 the mantle $^{20}\text{Ne}/^{22}\text{Ne}$ ratio was higher than the air ratio (9.8). In plume-derived
1173 samples from the Kola peninsula (Russia), the $^{20}\text{Ne}/^{22}\text{Ne}$ ratio is higher ($\geq 13.0 \pm 0.2$)
1174 and approaches the solar ratio of 13.7 (YOKOCHI and MARTY, 2004). Other parts of the
1175 mantle, including the source of MORBs, may be characterized by a lower $^{20}\text{Ne}/^{22}\text{Ne}$
1176 ratio of ~ 12.5 (BALLENTINE et al., 2005; TRIELOFF et al., 2000). Regardless of these
1177 complications, the large difference in Ne isotopic composition between the silicate
1178 Earth and air is the strongest evidence that atmospheric noble gases could not have
1179 been derived solely from degassing of the mantle without further processing. The
1180 $^{21}\text{Ne}/^{22}\text{Ne}$ ratio can vary due to nucleogenic production in the mantle through the
1181 Wetherill reactions, in particular $^{18}\text{O}(\alpha, n)^{21}\text{Ne}$, where α particles are from decay of
1182 U and Th (YATSEVICH and HONDA, 1997). The $^{21}\text{Ne}/^{22}\text{Ne}$ therefore reflects the long-
1183 term evolution of the U/ ^{22}Ne ratio and like the $^3\text{He}/^4\text{He}$ ratio can inform us on the
1184 degree of degassing of mantle reservoirs. At a $^{20}\text{Ne}/^{22}\text{Ne}$ ratio of 12.5-13.7, the
1185 $^{21}\text{Ne}/^{22}\text{Ne}$ ratio of MORBs is higher than the solar ratio and is also higher than that
1186 seen in some plume-related magmas. This confirms the view that the source of
1187 MORBs is a degassed reservoir. The $^{40}\text{Ar}/^{36}\text{Ar}$ ratio of the MORB source is much
1188 higher than air (295.5) and is probably around 25,000-40,000 (BURNARD et al., 1997;
1189 MOREIRA et al., 1998, Fig. 12). The stable isotope ratio $^{38}\text{Ar}/^{36}\text{Ar}$ is indistinguishable
1190 from the atmospheric ratio (Ballentine and Holland 2008; RAQUIN and MOREIRA,
1191 2009). Krypton isotopes in MORBs show indistinguishable isotopic composition
1192 from air. However, more recent work has shown, through high-precision
1193 measurements of CO_2 well gases, that the Kr isotopic composition of Earth's mantle
1194 was probably different compared to that of the atmosphere (HOLLAND et al., 2009,
1195 Fig. 13). The atmosphere is slightly enriched in the heavy isotopes of Kr by ~ 8

1196 ‰/amu relative to solar. Holland et al. (2009) found that mantle Kr was even more
1197 fractionated isotopically, which is consistent with a meteoritic or fractionated solar
1198 origin and addition of solar-type Kr by late cometary accretion, as was suggested by
1199 Dauphas (2003). Xenon isotopes have been the focus of much work, as they
1200 comprise several decay systems that can be used as chronometers of mantle
1201 degassing and atmospheric loss. Xenon non-radiogenic isotopes in MORBs are
1202 indistinguishable from air. However, higher precision measurements of CO₂ well-
1203 gases have revealed that mantle Xe has a different isotopic composition relative to
1204 the atmosphere (CAFFEE et al., 1999; HOLLAND and BALLENTINE, 2006, Fig. 13).
1205 Because solar and meteoritic reservoirs have similar Xe isotopic compositions, it is
1206 not possible to tell one end-member from the other using non-radiogenic Xe
1207 isotopes alone. MORBs show excess ¹²⁹Xe from decay of ¹²⁹I as well as excess
1208 fissionogenic isotopes (*e.g.*, ¹³⁶Xe) from decay of ²³⁸U and ²⁴⁴Pu (KUNZ et al., 1998;
1209 MOREIRA et al., 1998; STAUDACHER and ALLÈGRE, 1982, Fig. 14). The ¹²⁹Xe/¹³⁰Xe ratio of
1210 the upper-mantle is estimated to be 7.9 based on both MORB and CO₂-well gas
1211 measurements (HOLLAND and BALLENTINE, 2006; MOREIRA et al., 1998). An important
1212 parameter is the fraction of ¹³⁶Xe derived from ²⁴⁴Pu vs. ²³⁸U, which is difficult to
1213 estimate because the fission spectra of these two actinides are close. Kunz et al.
1214 (1998) estimated that 32±10 % of fissionogenic ¹³⁶Xe (*i.e.*, excess relative to air) was
1215 from ²⁴⁴Pu and that the rest was from ²³⁸U, similar within uncertainties to the
1216 decomposition obtained for plume-related magmas by Yokochi and Marty (2005).
1217 Assuming non-radiogenic mantle Xe to be U-Xe (a hypothetical component
1218 described in Sect. 5.2; PEPIN, 2000a) or solar wind-Xe, Pepin and Porcelli (2006)
1219 obtained a higher fraction of Pu-derived Xe of 63-75 %.

1220 The elemental compositions of the MORB source is compiled in Table 4 (MOREIRA
1221 et al., 1998). The inferred composition of the source of CO₂ well gases is identical to
1222 that of MORBs (HOLLAND and BALLENTINE, 2006). The ³He/²²Ne is not very far from
1223 the solar ratio; *i.e.*, 4.9 (MOREIRA et al., 1998) or 10.2 (Honda and McDougall 1998) vs
1224 2.65 for the solar composition. Yokochi and Marty (2004) showed that the source
1225 ³He/²²Ne ratio varied systematically between mantle reservoirs and that this ratio
1226 correlated with the time-integrated excess in nucleogenic ²¹Ne*, presumably
1227 reflecting mantle differentiation processes. Heavier noble gases ³⁶Ar, ⁸⁴Kr, and ¹³⁰Xe
1228 present an abundance pattern that is more akin to a meteoritic or a fractionated
1229 solar component. Yet, the non-radiogenic isotopic composition is dominantly
1230 atmospheric and distinct from meteorite values. Holland and Ballentine (2006)
1231 suggested that this pattern best matched the noble gas composition of seawater,
1232 implying that the heavy noble gas inventory of the mantle could have been derived
1233 from recycling. This conclusion was corroborated by subsequent studies that found
1234 seawater-derived noble gases in mantle wedge peridotites (Sumino et al. 2010) and
1235 subducted serpentinites (Kendrick et al. 2011). Thus, trapped noble gases may have
1236 had two sources. Light noble gases (*i.e.*, He and Ne) could have been derived from
1237 solar composition by ion implantation or dissolution in the magma ocean of nebular
1238 gases, while heavier noble gases could have been derived from recycling of air.

1239 In Table 4, we summarize our knowledge of the upper-mantle volatile
1240 composition based on MORB and CO₂ well gas measurements.

1241 5.1.2. Plumes

1242 Plume-derived magmas can have very high $^3\text{He}/^4\text{He}$ ratios (Fig. 10). The current
 1243 record holder is a sample from the Baffin Island with a R/R_A ratio of 49.5 (STUART et
 1244 al., 2003). These elevated $^3\text{He}/^4\text{He}$ ratios indicate that the samples originate from a
 1245 source region that is less degassed than the source of MORBs (see Anderson 1998
 1246 for an alternative view point). OIB samples from Loihi (Hawaii) as well as intrusive
 1247 samples from the Kola Peninsula (Russia) have provided a wealth of data on the
 1248 composition of plume-related sources. The $^{20}\text{Ne}/^{22}\text{Ne}$ ratio in samples from Kola is
 1249 close to solar (YOKOCHI and MARTY, 2004). The $^{21}\text{Ne}/^{22}\text{Ne}$ ratios of Loihi (HIYAGON et
 1250 al., 1992; HONDA et al., 1993; VALBRACHT et al., 1997b) and Kola (MARTY et al., 1998;
 1251 YOKOCHI and MARTY, 2004) are lower than MORBs, indicating that their mantle
 1252 sources are less degassed than the convective upper-mantle (Fig. 11). The $^{40}\text{Ar}/^{36}\text{Ar}$
 1253 ratio of the source of plume samples is around 4,500-8,000 (Farley and Craig 1994;
 1254 MARTY et al., 1998; VALBRACHT et al., 1997a; Tieloff et al. 2000, 2002), confirming
 1255 that their source mantles are not as efficiently degassed as the MORB mantle (Fig.
 1256 12). Krypton isotope ratios are indistinguishable from those in the atmosphere.
 1257 Stable Xe isotopes are again indistinguishable from the atmosphere. However,
 1258 excess ^{129}Xe and fissionogenic isotopes are found (Poreda and Farley 1992; TRIELOFF
 1259 et al., 2000; YOKOCHI and MARTY, 2004). The precision of Xe isotope measurements on
 1260 plume samples is insufficient to disentangle what results from decay of ^{244}Pu from
 1261 decay of ^{238}U . This decomposition is critical to establish the timescale of mantle
 1262 degassing as the two parent nuclides have considerably different half-lives. Yokochi
 1263 and Marty (2004) proposed an elegant method to estimate the relative
 1264 contributions of these two nuclides to Xe fission isotopes based on the $^{136}\text{Xe}^*/^4\text{He}^*$
 1265 ratio (Fig. 14). The rationale is that ^{244}Pu -decay produces a $^{136}\text{Xe}/^4\text{He}$ ratio that is
 1266 very different from that produced by decay of ^{238}U . They concluded that 33-60 % of
 1267 fission ^{136}Xe was from decay of ^{244}Pu while the rest was from decay of ^{238}U . This is
 1268 similar (within error bars) to the estimate of $\sim 32 \pm 10$ % of fission ^{136}Xe from ^{244}Pu
 1269 for MORBs (KUNZ et al., 1998).

1270
 1271

1272 5.2. Model age of atmosphere retention

1273 Wetherill (1975) calculated a model age of the atmosphere that has influenced all
 1274 discussions on Earth's early evolution. The atmosphere contains excess $^{129}\text{Xe}^*$ that
 1275 must come from the decay of ^{129}I . In the simplest case of a two-stage model,
 1276 radiogenic Xe is entirely lost to space until some retention time t_r , after which time it
 1277 is completely retained. Stated otherwise, the amount of $^{129}\text{Xe}^*$ found in the
 1278 atmosphere (6.8 ± 0.5 % of atmospheric ^{129}Xe , PEPIN, 2000a) should correspond to
 1279 the amount of ^{129}I that was in the crust when the atmosphere became retentive for
 1280 Xe. Accordingly, we have,

$$1281 \frac{^{129}\text{Xe}^*_{\text{atm}}}{^{127}\text{I}_{\text{crust}}} = \left(\frac{^{129}\text{I}}{^{127}\text{I}} \right)_{t_r} = e^{-\lambda_{129} t_r}. \quad (18)$$

1282 The amount of radiogenic ^{129}Xe in Earth's atmosphere is 2.8×10^{11} mol (PEPIN,
 1283 2000a). The ^{127}I content of the crust is 2.6×10^{17} mol (DÈRUELLE et al., 1992). These
 1284 surface inventories correspond to a retention time of ~ 100 Myr. Several studies
 1285 have refined this approach and have found similar closure times (*e.g.*, ZHANG, 1998).

1286 In the first 100 My, $1 - \exp(-\lambda_{129} \times 100) = 99\%$ of ^{129}I would have decayed and the
1287 corresponding inventory of ^{129}Xe is missing from the present Earth. This means that
1288 at least the same amount and possibly more of the initial inventory of Xe non-
1289 radiogenic isotopes on Earth was lost to space. This result is consistent with the
1290 large isotopic fractionation of Xe isotopes seen in the atmosphere, which could have
1291 been created by hydrodynamic escape of an H_2 -rich protoatmosphere (HUNTEN et al.,
1292 1987). A similar dating method could potentially be used based on fissionogenic Xe
1293 isotopes. This approach however faces an important difficulty. If one corrects
1294 atmospheric Xe for mass fractionation using light Xe isotopes, one obtains an
1295 isotopic composition that has less of some of the heavy isotopes of Xe than the solar
1296 composition (PEPIN, 2000a). This is an odd result as it is difficult to envision how a
1297 nebular component could be deficient in some isotopes compared to solar
1298 composition. Pepin and Phinney (1978, "Components of Xenon in the Solar System",
1299 unpublished preprint) speculated that such a component existed and named it U-Xe
1300 (here U does not mean uranium; it stands for "Ur", a German word for indigenous).
1301 This component is not found on Mars (martian Xe seems to be derived from solar
1302 Xe, SWINDLE and JONES, 1997) and was also not detected in any meteoritic component
1303 (BUSEMANN and EUGSTER, 2002). Cometary ice is one of the few noble gas reservoirs
1304 in the solar system that has not been documented yet and it might be the carrier of
1305 the elusive U-Xe. The amounts of fissionogenic Xe in Earth's atmosphere depends
1306 heavily on the assumed starting composition, which is not well defined. Therefore,
1307 the contributions of plutogenic and uraniumogenic Xe in Earth's atmosphere are
1308 uncertain.

1309
1310

1311 5.3. Model age of mantle degassing

1312 The radiogenic nuclides that could potentially be used to constrain the timescale
1313 of atmosphere formation are ^4He , ^{21}Ne , ^{40}Ar , ^{129}Xe , and fissionogenic Xe isotopes (e.g.,
1314 ^{136}Xe). ^4He is of limited use as it is continuously lost to space. ^{21}Ne is also of limited
1315 use as the atmospheric composition is near the mass fractionation line that runs
1316 through the solar composition, so the amount of nucleogenic ^{21}Ne in the atmosphere
1317 is highly uncertain. This leaves us with ^{40}Ar , ^{129}Xe , and ^{136}Xe . Because the different
1318 parent radionuclides to these isotopes have a range of half-lives from 15.7 My
1319 (^{129}Xe) to 4.47 Gy (^{238}U), noble gas isotopes can be used to investigate the degassing
1320 history of the Earth over different timescales. Models of mantle degassing often
1321 assume that this follows a first order rate, where the rate of degassing is
1322 proportional to the amount in the mantle. This can be understood if the volume of
1323 mantle tapped by melting is approximately constant and the mantle is well mixed.

1324 Early degassing is best investigated using Xe as it possess several parent
1325 radionuclides with short half-lives (KUNZ et al., 1998; YOKOCHI and MARTY, 2005).
1326 Mantle degassing timescales are plagued by the fact that the initial Xe isotopic
1327 composition is uncertain (i.e., "U"-Xe component, Sect. 5.2). However, Earth's mantle
1328 has excess fissionogenic Xe compared to air, which makes the decomposition into
1329 plutogenic and uraniumogenic components more robust (e.g., one can assume
1330 conservatively that the initial Xe isotopic composition of the mantle lies between U-
1331 Xe and air-Xe). The most refined model at the present time is that proposed by

1332 Yokochi and Marty (2005), who used their decomposition of ^{136}Xe into ^{238}U and
 1333 ^{244}Pu -derived components to constrain the degassing history of the Earth (also see
 1334 COLTICE et al., 2009). If no degassing had taken place after solar system formation,
 1335 then the ratio of $^{136}\text{Xe}_{\text{Pu}}/^{136}\text{Xe}_{\text{U}}$ should be identical to the chondritic ratio, *i.e.* 27. On
 1336 the other hand, if most degassing had taken place after ^{244}Pu decay, then mantle Xe
 1337 would have been dominated by ^{238}U -derived fission and the $^{136}\text{Xe}_{\text{Pu}}/^{136}\text{Xe}_{\text{U}}$ would be
 1338 close to zero. A similar reasoning can be applied to the ratio of $^{129}\text{Xe}^*/^{136}\text{Xe}_{\text{Pu}}$. The
 1339 fact that a significant fraction of mantle ^{136}Xe is derived from ^{244}Pu therefore
 1340 indicates that most Xe degassing took place while ^{244}Pu was live. A concordant age
 1341 for Pu-U and I-Pu cannot be obtained by using a single stage degassing history (KUNZ
 1342 et al., 1998; TOLSTIKHIN and HOFMANN, 2005; YOKOCHI and MARTY, 2005). A solution to
 1343 this problem is to consider a model where the degassing occurs over a period Δt
 1344 after solar system birth and to assume that the rate of degassing during that time
 1345 was proportional to the amount in the mantle,

$$\begin{aligned}
 \frac{d^{136}\text{Xe}^*}{dt} &= P(t)\lambda Y - \alpha^{136}\text{Xe}^*, \quad t < \Delta t \\
 \frac{d^{136}\text{Xe}^*}{dt} &= P(t)\lambda Y, \quad t > \Delta t
 \end{aligned}
 \tag{19}$$

1347 where $P(t)$ is the abundance of the parent nuclide, λ is its decay constant, Y is the
 1348 decay yield, and α is a degassing constant. Using the two ratios $^{136}\text{Xe}_{\text{Pu}}/^{136}\text{Xe}_{\text{U}}$ and
 1349 $^{129}\text{Xe}^*/^{136}\text{Xe}_{\text{Pu}}$, Yokochi and Marty (2005) were able to write down two equations
 1350 and solve the system for the two unknowns α and Δt . They obtained $\alpha \sim 1 \times 10^{-8}$ to
 1351 2×10^{-8} . According to this analysis, mantle Xe was degassed early with an e-folding
 1352 timescale of ~ 50 -100 My. By 100 My, 60-90 % of mantle Xe would have been
 1353 degassed. The degassing history of the Earth recorded by $^{40}\text{Ar}^*$ (OZIMA, 1975; Turner
 1354 1989; ZHANG and ZINDLER, 1989) also supports very early degassing of the mantle. A
 1355 more extensive discussion of the degassing history of the Earth is provided in
 1356 Chapter 2 of this volume (Zhang 2012). It is worth noting that the history recorded
 1357 by radiogenic isotopes could be largely decoupled from that of non-radiogenic
 1358 isotopes in the atmosphere. For examples, most noble gases in air could be derived
 1359 from a proto-atmosphere of trapped nebular gases with no relationship with the
 1360 degassing history of the mantle.

1361

1362

1363 **6. The origin of major volatile elements in Earth**

1364

1365 Laboratory analyses show a clear correlation between the water content in
 1366 meteorites and the heliocentric distance of the parent bodies from which the
 1367 meteorites are thought to come from (Fig. 15). Although there is the theoretical
 1368 possibility that water-rich planetesimals formed in the hot regions of the disk by
 1369 water-vapor absorption on silicate grains (Muralidharan et al., 2008; King et al.,
 1370 2010), empirical evidence suggests that the planetesimals in the terrestrial planet
 1371 region were extremely dry. In contrast, the Earth has a water content that, although
 1372 small, is non-negligible and definitely larger than what the above-mentioned
 1373 correlation would suggest for material condensed at 1 AU. In fact, the terrestrial

1374 water content is $\sim 7 \times 10^{-4}$ of Earth's mass (Table 1, Lecuyer et al., 1998). A larger
1375 quantity of water might have resided in the primitive Earth and might have been
1376 subsequently lost during core formation and impacts. Thus, the current Earth
1377 contains more water than enstatite chondrites and possibly the primitive Earth had
1378 water amounts comparable to, or larger than, ordinary chondrites. Where did this
1379 water come from, if the local planetesimals were dry? There are basically three
1380 possibilities for the origin of water on Earth, if water was not present in sufficient
1381 quantity in the local planetesimals.

1382 One model is that of the *nebular origin*. Ikoma and Genda (2006) assumed that, at
1383 the end of the Earth formation process, there was still some nebular hydrogen in the
1384 proto-planetary disk. In this condition, the Earth attracted nebular gas by gravity,
1385 forming an hydrogen-rich atmosphere, up to a mass of 10^{21} kg. Then, atmospheric
1386 hydrogen was oxidized by some oxides such as FeO in the magma ocean to produce
1387 water. However, in this model, the initial D/H ratio of the water would be solar.
1388 Increasing the D/H ratio by a factor of 6 by the process of hydrodynamic escape
1389 discussed in Genda and Ikoma (2008) would require unrealistically long timescales,
1390 *i.e.* the hydrodynamic escape of the primitive atmosphere should have been
1391 protracted over billions of years, while evidence from ^{129}I - ^{129}Xe indicates that this
1392 must have occurred in the first ~ 100 - 150 Myr of the solar system history (Sect. 5.2).
1393 Such a model would also not explain the relatively oxidized nature of Earth's mantle
1394 (oxygen fugacity at the FMQ buffer, 3.5 log unit above the IW buffer where metallic
1395 Fe is in equilibrium with FeO).

1396 A second possibility is that the water was brought to Earth by the
1397 bombardment of comets (Delsemme, 1992, 1999). A first problem with this model is
1398 that the D/H ratio in the water vapor released by long period comets from the Oort
1399 cloud is about twice that on Earth (Balsiger et al., 1995; Eberhardt et al., 1995; Meier
1400 et al., 1998; Bockelee-Morvan et al., 1998), and there are no known terrestrial
1401 processes that could *decrease* the D/H ratio of the original water on Earth. A similar
1402 constraint exists for the $^{15}\text{N}/^{14}\text{N}$ ratio (Jehin et al. 2009). Recently, the D/H ratio of a
1403 Jupiter-family comet originating from the Kuiper belt (103P/Hartley 2) was
1404 measured and the value ($1.61 \pm 0.24 \times 10^{-4}$) was found to be indistinguishable from
1405 terrestrial composition (Hartogh et al. 2011). This result came as a surprise as
1406 Kuiper belt comets are thought to have formed in a more external region of the solar
1407 system than Oort-cloud comets and a gradient in D/H ratio with heliocentric
1408 distance is expected (Drouart et al. 1999). Oort cloud comets are presently farther
1409 away from the Sun than Kuiper belt comets but they are thought to have formed in
1410 more internal regions (*i.e.*, between Uranus and Saturn) and have been
1411 subsequently ejected to their present location (Fernandez and Ip, 1981). The
1412 discovery of a comet with a terrestrial D/H ratio reopens the possibility that such
1413 objects delivered water to the Earth. However, the $^{15}\text{N}/^{14}\text{N}$ ratio of CN in comet
1414 103P/Hartley 2 was also measured and the value is twice that of Earth's atmosphere
1415 (Meech et al. 2011; Marty 2012) and is similar to $^{15}\text{N}/^{14}\text{N}$ ratios measured in other
1416 comets (Jehin et al. 2009). Furthermore, comets are probably rich in noble gases
1417 compared to Earth and delivery of major volatile elements by cold icy bodies would
1418 have completely obliterated the noble gas composition of the atmosphere (Dauphas
1419 2003). Therefore, geochemical evidence suggests that comets did not deliver Earth's

1420 oceans but further work is needed to characterize the elemental and isotopic
1421 compositions of H, N, and noble gases in comets from diverse regions. A second
1422 problem with a cometary origin of Earth's oceans is that the collision probability of
1423 comets with the Earth is very small. Of the planetesimals scattered by the giant
1424 planets from the proto-planetary disk, only 1 in a million would strike our planet
1425 (Morbidelli et al., 2000), which is far from enough for the following reasons. From
1426 studies on the range of radial migration that the giant planets should have suffered,
1427 due to their interaction with planetesimals after the disappearance of the disk of gas
1428 (Malhotra, 1995; Hahn and Malhotra, 1999; Gomes et al., 2004, 2005), it is expected
1429 that the total mass of the cometary disk was 35-50 Earth masses; moreover, from
1430 measurements of the ice/dust ratio in comets (Kuppers et al., 2005), it is now
1431 believed that less than half of the mass of a comet is in water-ice. Putting all these
1432 elements together, the mass of water delivered by comets to the Earth should have
1433 been $\sim 2.5 \times 10^{-5}$ Earth masses (neglecting impact losses), i.e. 10% of the crustal
1434 water. This corresponds to the upper-limit allowed by constraints on the D/H ratio
1435 on Oort-cloud comets (Dauphas et al. 2000).

1436 The third possibility and the one that we favor is that the Earth accreted water
1437 from primitive planetesimals and/or planetary embryos originally from the outer
1438 asteroid belt (Morbidelli et al., 2000; Raymond et al., 2004, 2005, 2006, 2007;
1439 O'Brien et al., 2006; Dauphas, 2003). The abundance pattern of major volatile
1440 elements as well as their isotopic compositions are very close to those observed in
1441 carbonaceous chondrites (Fig. 16). Major elements could have been delivered
1442 during the main stage of Earth's accretion by one or several partially hydrated
1443 embryos. An alternative possibility, however, is that H, C and N were delivered as
1444 part of a late veneer of volatile-rich asteroids, *i.e.* after formation of Earth's core.
1445 Evidence for a late veneer of the Earth-Moon system by extraterrestrial materials
1446 comes from measurements of highly siderophile elements in Earth's mantle, which
1447 abundances in Earth's mantle are too high to be explained by core-mantle
1448 equilibration and must have been supplied after Earth's core had formed (CHOU,
1449 1978; JAGOUTZ et al., 1979; MORGAN, 1986). It is thus estimated that 0.7×10^{22} to
1450 2.7×10^{22} kg of matter impacted the Earth after the completion of core formation.
1451 Using a CI chondrite composition of ~ 6 wt% H_2O , such a late veneer would have
1452 delivered 0.4×10^{21} to 1.6×10^{21} kg of water, which is comparable to the amount in
1453 the oceans of $\sim 1.4 \times 10^{21}$ kg. However, the highly siderophile abundance pattern of
1454 the mantle, is different from that of carbonaceous chondrites and all other chondrite
1455 groups (Fig. 17; BECKER et al., 2006; FISCHER-GÖDDE et al. 2010; WALKER, 2009),
1456 questioning the idea that the late veneer was chondritic or that the nature of the late
1457 veneer can be inferred from the pattern of highly siderophile elements in Earth's
1458 mantle. Furthermore, the fact that Earth's mantle plots on the correlation defined by
1459 chondrites for Mo and Ru suggests that the nature of the material accreted by the
1460 Earth did not change drastically before and after core formation (DAUPHAS et al.,
1461 2004a), so the late veneer was relatively dry (Fig. 17).

1462 A strong argument that water was delivered to Earth as part of its main
1463 accretion stage rather than as part of a later veneer comes from examination of the
1464 H_2O -Xe budgets (DAUPHAS, 2003). Accretion of the late veneer probably proceeded

1465 by impacts that had little erosive capability on the atmosphere. Indeed, even the
1466 giant moon forming impact that is thought to have punctuated the main stage of
1467 accretion of the Earth could only remove 10-30 % of the atmosphere (Genda and
1468 Abe, 2002, 2005). Subsequent smaller impacts would have induced lower ground
1469 motions resulting in little atmospheric loss. The H₂O/Xe of Earth is much higher
1470 than that of chondrites, including water-rich types such as CI (Fig. 18). Thus, if one
1471 were to deliver all water on Earth by a late veneer, too much Xe would have been
1472 delivered to the atmosphere compared to the present inventory. In addition,
1473 meteoritic Xe does not have the appropriate stable isotopic composition (Earth's Xe
1474 is fractionated isotopically by ~40 ‰/amu relative to solar and chondritic
1475 compositions). A solution to this conundrum is that water was delivered to the
1476 Earth at a time when impacts could deposit enough energy to remove some of the
1477 gases accumulated in the protoatmosphere. Water, which reacted with rocks and
1478 formed oceans was preferentially retained (Genda and Abe 2005). Xenon, which is
1479 chemically inert, accumulated in the atmosphere and was lost by impacts. Some C
1480 and N present in Earth's protoatmosphere might have been lost at that time. Late
1481 accretion of cometary volatiles delivered noble gases depleted in Xe, thus explaining
1482 the missing Xe problem. To summarize, from a geochemical point of view, it is likely
1483 that Earth's major volatile inventory was acquired during the main stage of
1484 planetary growth by accretion of water-rich embryos and planetesimals, otherwise
1485 too much Xe with inappropriate isotopic composition would have been delivered.

1486 Water was recently found in appreciable quantities in lunar rocks (Saal et al.
1487 2008; Boyce et al. 2010; McCubbin et al. 2010; Greenwood et al. 2011; Hauri et al.
1488 2011). This suggests that Earth accreted water before the Moon-forming impact.
1489 However, Greenwood et al. (2011) measured high water D/H ratios in lunar apatite
1490 crystals and argued that this was indicative of a cometary origin unrelated to Earth's
1491 oceans. Water-rich water glasses have D/H ratios that partially overlap with
1492 terrestrial values and the higher D/H ratios measured in some samples could reflect
1493 isotopic fractionation upon water loss (Hauri et al. 2010; Saal et al. 2011). The water
1494 content of the Moon can potentially provide important constraints on the timing and
1495 nature of water delivery to Earth but uncertainties in the D/H ratio of juvenile lunar
1496 water prevent a definitive conclusion to be reached.

1497 Albarède (2009) recently argued based on volatile element isotopic ratios
1498 (e.g., ⁶⁶Zn/⁶⁴Zn) that the Earth must have accreted dry and that volatile elements
1499 were delivered late in Earth's accretion history. However, Zn isotopes are poor
1500 tracers of the accretion history of water on our planet. The silicate Earth contains
1501 2.2×10²⁰ kg of Zn (55 ppm Zn, McDONOUGH and SUN, 1995b) with a δ⁶⁶Zn value of
1502 ~+0.25 ‰. To deliver Earth's oceans, 2.3×10²² kg of CI material would be needed,
1503 which would deliver 7.3×10¹⁸ kg of Zn (CI contain ~312 ppm Zn) with a δ⁶⁶Zn value
1504 of ~+0.45 ‰. Adding this amount to the Earth would deliver only ~3 % of the Zn
1505 inventory and would change its isotopic composition by only ~0.006 ‰, which is
1506 unresolvable. On the contrary, adding this amount would deliver ~3 times the Xe
1507 inventory of the atmosphere and would completely obliterate its isotopic
1508 composition. This shows that Zn isotopes are insensitive to the presence of water-
1509 bearing planetary bodies in the mix of material that made the Earth. Xenon isotopes

1510 and H₂O/Xe ratios provide much tighter constraints on the origin of Earth's oceans.
1511 Mann et al. (2009) and Wood et al. (2010) found evidence that the accretion of
1512 moderately volatile elements to the Earth occurred mostly before core formation
1513 was complete. Wood et al. (2010) noted that the relative abundance of elements
1514 in our planet is correlated not only with condensation temperature but also
1515 with chemical affinity. Highly siderophile volatile elements are more depleted in
1516 the mantle than moderately siderophile elements or lithophile elements with the
1517 *same* condensation temperature. This implies that these volatile elements saw the
1518 formation of the Earth's core.

1519 To address the question of the delivery of water by asteroids from a
1520 modeling point of view, we need to distinguish between the classical scenario, in
1521 which the outer belt is originally inhabited by primitive objects that are removed by
1522 mutual scattering and interactions with resonances with Jupiter, and the Grand Tack
1523 scenario. In the first case, as we have seen above, the amount of material accreted by
1524 the terrestrial planets from the asteroid belt depends on the eccentricity of the orbit
1525 of Jupiter. If Jupiter's orbit was almost circular, the terrestrial planets should have
1526 accreted 10-20 % of their mass from beyond 2.5 AU (O'Brien et al., 2006), most of
1527 which should have been of carbonaceous chondritic nature. Thus, the terrestrial
1528 planets should have been originally very water-rich, possibly even as much as
1529 envisioned by Abe et al. (2000), and should have lost most of their water by impacts.
1530 However, the amount of material accreted from the outer asteroid belt drops with
1531 increasing eccentricity of Jupiter. If Jupiter had an original orbit with an eccentricity
1532 comparable to, or larger than the current one, no material would have been accreted
1533 from the outer asteroid belt, and the terrestrial planets would have been dry
1534 (O'Brien et al., 2006; Raymond et al., 2009). In the Grand Tack scenario, the
1535 primitive asteroids have been implanted into the asteroid belt from in between the
1536 orbits of the giant planets and beyond. In the simulations carried out by Walsh et al.
1537 (2011), for every primitive planetesimal implanted in the outer asteroid belt, 10–30
1538 planetesimals end up on orbits that cross the terrestrial planet forming region, for a
1539 total of 3–11x10⁻² Earth masses. O'Brien et al. (2010) showed that, in this situation,
1540 the Earth could accrete about 0.5-2 % of its mass from these objects, enough to
1541 supply a few times the current amount of water on our planet (assuming that the
1542 primitive planetesimals were 5-10 % water by mass). Walsh et al. and O'Brien et al.
1543 did not consider primitive planetary embryos in their simulations, so in principle
1544 the total amount of primitive material supplied to the Earth could be somewhat
1545 larger than the reported estimate.

1546 A common feature of the classical and Grand Tack scenarios for the asteroidal
1547 delivery of water to the terrestrial planets is that the water is accreted *during* the
1548 formation of the planets and not in a *late veneer* fashion (*i.e.*, after core formation is
1549 complete), which is consistent with geochemical evidence (*i.e.*, Mo-Ru isotope
1550 anomalies and H₂O/Xe budgets). The accretion of water, though, is not uniform
1551 throughout the planet accretion history; instead it accelerates towards the end, as
1552 shown in Fig. 19. Although many issues have yet to be resolved, we are approaching
1553 a coherent and global view of the terrestrial planet formation history indicating that
1554 water was acquired by our planet very early in its history.

1555

1556 **7. The late heavy bombardment**

1557 The end of the terrestrial formation process was presumably characterized by a
1558 gradual decline of the bombardment rate, due to the decrease of the number of
1559 planetesimals still on planet-crossing orbits. Numerical simulations show that the
1560 number of planet-crossing planetesimals decays as $\exp[-t/T(t)]$, with $T(t)$ initially
1561 equal to ~ 10 My and then increasing up to ~ 100 My (Morbidelli et al., 2000b; Bottke
1562 et al., 2007). The abundance of highly siderophile elements in the Earth's mantle
1563 constrains that at most 1 % of an Earth mass was accreted during this declining
1564 bombardment, after the formation of the Earth's core. Presumably, the last episode
1565 of core-mantle (partial) re-equilibration on the Earth occurred during the last giant
1566 impact suffered by our planet, most likely associated with the formation of the
1567 Moon. This event is dated to have occurred about 4.5 Gy ago (TOUBOUL et al., 2007).
1568 The Moon, however, shows evidence of a surge in the bombardment rate,
1569 approximately 4 Gy ago, *i.e.* ~ 500 My after its formation (TERA et al., 1974). In fact,
1570 about 10-15 basins, *i.e.* impact structures larger than 300 km in diameter, formed in
1571 an interval of time ranging at most from 4.1 to 3.8 Gy ago, Nectaris basin being the
1572 oldest and Imbrium and Orientale the most recent ones (Wilhelms et al., 1987). The
1573 formation of so many basins in such a short time-range cannot be due to a
1574 bombardment declining since the onset of terrestrial planet formation (even
1575 assuming $T=100$ Myr; Bottke et al., 2007). The surge of the bombardment rate 4 Gyr
1576 ago is called the "Late Heavy Bombardment" (LHB). Several lines of evidence
1577 suggest that the LHB concerned all the objects in the inner solar system (including
1578 asteroid Vesta) and possibly even the satellites of the giant planets.

1579 From a modeling point of view, the origin of the LHB is most likely related to a
1580 sudden change in the orbits of the giant planets. We have seen above that, at the
1581 disappearance of the gas-disk, the giant planets should have had orbits different
1582 from the current ones: the orbital separation among the planets, the eccentricities
1583 and inclinations were significantly smaller; the planets were probably in resonance
1584 with each other. If this is true, the orbits of the giant planets must have changed at
1585 some point of the history of the solar system, so to achieve the current
1586 configuration. The so-called "Nice model" is probably the one that gives the most
1587 comprehensive description of how this happened (see Morbidelli, 2011 for an
1588 extensive review). According to this model, at the disappearance of the gas-disk, the
1589 giant planets were surrounded by a massive disk of planetesimals. This trans-
1590 planetary disk was the surviving part of the original icy planetesimal disk that did
1591 not participate in the construction of the giant planet themselves and was not
1592 depleted by the migration of the giant planets during the gas-disk phase (Gomes et
1593 al., 2005). The gravitational interaction between the planets and this disk slowly
1594 modified the orbits of the former until eventually the planets became unstable
1595 (Tsiganis et al., 2005; Morbidelli et al., 2007; Batygin and Brown, 2010). The planets
1596 started to have close encounters with each other. Their orbits became more
1597 eccentric and inclined. In particular, Uranus and Neptune acquired very eccentric
1598 orbits that started to penetrate through the planetesimal disk. The planetesimals got
1599 scattered away by these planets. In response, the dynamical dispersal of the disk
1600 damped the eccentricities and inclinations of the orbits of Uranus and Neptune,

1601 bringing these planets to orbits very similar to the current ones (Fig. 20). By this
1602 process, the current orbits of the giant planets can be remarkably well reproduced
1603 (Tsiganis et al., 2005; Batygin and Brown, 2010). Moreover, if the inner edge of the
1604 trans-planetary disk was located a few AU beyond the orbit of the last planet, the
1605 trigger of the giant planet instability generically occurs after several hundreds of
1606 millions of years of quiet evolution, so that the dispersal of the disk could occur at
1607 the LHB time (Gomes et al., 2005; Levison et al., 2011). The Nice model explains not
1608 only the dynamical transition of the giant planets from their primordial orbits to the
1609 current orbits, but also the origin and orbital distribution of three populations of
1610 small objects in the outer solar system: Jupiter's Trojans (Morbidelli et al., 2005),
1611 the irregular satellites of the giant planets (Nesvorny et al., 2007; Bottke et al., 2009)
1612 and the Kuiper belt (Levison et al., 2008; Batygin et al., 2011).

1613 In the framework of the Nice model, the LHB is caused by two populations of
1614 impactors. The first population is that of the icy planetesimals from the trans-
1615 planetary disk, that we can identify with "comets" given that this same disk
1616 generated also the Kuiper belt. When the disk was dispersed, most of the population
1617 was ultimately ejected onto hyperbolic orbit. About 1/3 of the population, though,
1618 passed temporarily through the inner solar system and about 10^{-6} of the objects
1619 entered in collisions with the Earth. Thus, given that the trans-planetary disk is
1620 estimated to have contained ~ 35 Earth masses in planetesimals, about 2×10^{23} g of
1621 cometary material should have hit the Earth at the LHB time. This, however, should
1622 be regarded as an upper estimate. In fact, it is well known that comets can disrupt
1623 on their way into the inner solar system. For instance, for the current population of
1624 Jupiter family comets, it is estimated that the physical lifetime as active comets is
1625 about 1/10 of the dynamical lifetime (Levison and Duncan, 1997). Notice, though,
1626 that many "dead comets" just survive as inactive objects that can still have physical
1627 collisions with the planets. Such comets would have delivered little of Earth's water
1628 inventory but could have modified its noble gas, in particular supplying Ar and Kr as
1629 explained in sect. 4.4 (Dauphas 2003, Marty and Meibom 2007).

1630 The second population of impactors is that of asteroids. Asteroids from the
1631 current main belt boundaries should have delivered to the Earth only $\sim 10^{22}$ g of
1632 material (Morbidelli et al., 2010). However, it is possible that before the LHB the
1633 asteroid belt extended further inwards, towards the orbit of Mars. The population
1634 situated between 1.8 AU and the current inner border of the asteroid belt (2.2 AU)
1635 would have been heavily decimated during the radial displacement of the orbits of
1636 Jupiter and Saturn and could have caused about 10 basins on the Moon and ~ 200 on
1637 the Earth (Bottke et al., 2011), delivering to our planet a total mass of about 2×10^{23}
1638 g. The left-over of this population are the asteroids in the Hungaria region. As said
1639 previously, the Hungaria asteroids are mostly E-type, which are probably linked to
1640 enstatite chondrites. Thus, the dominant asteroidal contribution would have been of
1641 enstatite nature and would not have contributed to the water inventory of the Earth.

1642

1643 **8. Conclusion: a not so rare Earth?**

1644

1645 Geochemical and dynamical approaches offer complementary perspectives on
1646 the origin of volatile elements on Earth. Hydrogen, carbon, and nitrogen are present
1647 in proportions that correspond approximately to those found in volatile-rich
1648 meteorites. In addition, they have similar D/H, $^{13}\text{C}/^{12}\text{C}$, and $^{15}\text{N}/^{14}\text{N}$ ratios. Both
1649 observations strongly support the view that they were derived from the accretion of
1650 volatile-rich bodies akin to carbonaceous chondrites. Little is known about the
1651 composition of comets and further work is warranted before a definitive conclusion
1652 can be reached on their contribution to Earth's volatile elements. Still, available
1653 evidence suggests that comets are unlikely water sources for the Earth. A
1654 remarkable feature of the Earth is that its $\text{H}_2\text{O}/\text{Xe}$ ratio is higher than all possible
1655 extraterrestrial sources. This is consistent with the idea that water was delivered
1656 during the main stage of planetary growth when erosive processes were still
1657 significant and inert Xe could be decoupled from reactive water. Dynamical
1658 modeling also supports this view that Earth's water was delivered by accretion of
1659 partially hydrated planetesimals and embryos during the main building stage of the
1660 Earth.

1661 Overall, the circumstances that prevailed to the delivery of water to the Earth
1662 are probably shared in many other planet-forming stellar systems (Raymond et al.,
1663 2007). However, numerical simulations show that the delivery of water from the
1664 outer planetesimal disk to the forming terrestrial planets can be inhibited in some
1665 giant planet orbital configurations and evolutions, particularly those involving large
1666 orbital eccentricities (Raymond et al., 2004). With improvements in observations,
1667 detection of oceans on extrasolar planets might be feasible by looking for specular
1668 reflection of starlight on the planet's ocean or detection of water vapor in their
1669 atmospheres. Such, observations of remote planetary systems may inform us on the
1670 evolution of the young Earth, for which we have limited geological record. Closer to
1671 us, significant progress in our understanding of water delivery to terrestrial planets
1672 could be achieved by studying in more detail solar system objects like comets and
1673 Venus.

1674
1675

1676 **Acknowledgements.** We thank R. Yokochi, I.N. Tolstikhin, F.J. Ciesla, B. Marty,
1677 K.J. Zahnle, B. Schmitt, E. Quirico, P. Beck, and U. Marboeuf for discussions. Insightful
1678 and thorough reviews by Chris Ballentine and John Chambers were greatly
1679 appreciated. I.N. Tolstikhin provided Fig. 8 and part of the caption that accompanies
1680 it. Part of this review was written during a sabbatical stay of N.D. at Institut de
1681 Planétologie et d'Astrophysique de Grenoble. Eric Quirico and Florence Lelong are
1682 thanked for their hospitality. This work was supported by a Packard fellowship and
1683 NASA through grant NNX09AG59G to N.D.

1684
1685
1686

1687 **Figure captions**

1688

1689 **Fig. 1.** Patterns of isotopic anomalies in bulk planetary materials (enstatite,
1690 carbonaceous, and ordinary chondrites). Note that all isotopic anomalies are
1691 normalized relative to the composition of the silicate Earth, which has a composition
1692 of 0 in this diagram (by convention). $\Delta^{17}\text{O}$ data are from Clayton et al. (1991),
1693 Clayton and Mayeda (1999, 1984); $\epsilon^{50}\text{Ti}$ from Trinquier et al. (2009); $\epsilon^{54}\text{Cr}$ from
1694 Trinquier et al. (2007), Qin et al. (2010); $\epsilon^{92}\text{Mo}$ from Dauphas et al. (2002a, c) ,
1695 Burkhardt et al. (2011). Other elements show isotopic anomalies at a bulk scale (e.g.,
1696 Ba and Ru) but the systematics of these elements is less developed. Only volatile-
1697 poor enstatite chondrites are a match to the terrestrial composition for all elements.

1698 **Fig. 2.** An illustration of the process of runaway growth. Each panel
1699 represents a snapshot of the system at a different time. The coordinates represent
1700 the semi major axis a and the eccentricity e of orbits of the objects in a portion of the
1701 disk centered at 1 AU. The size of the dots is proportional to the physical radius of
1702 the objects. Initially, the system is made of a planetesimal population, in which two
1703 objects are 2 times more massive than the others. These objects accrete
1704 planetesimals very fast, increasing exponentially their mass ratio relative to the
1705 individual planetesimals. They become planetary embryos. Notice how the
1706 eccentricity of the planetary embryos remain low, while the eccentricities of the
1707 planetesimals are excited with time. The embryos also separate from each other as
1708 they grow. At the end, the embryos have grown by a factor 200, whereas the mean
1709 mass of the planetesimals has grown only by a factor of 2. From Kokubo and Ida
1710 (1998).

1711

1712 **Fig. 3.** The growth of terrestrial planets from a disk of planetary embryos.
1713 Each panel shows the semi-major axis and eccentricity of the bodies in the system at
1714 a given time, reported on top of the panel. Embryos and protoplanets are
1715 represented with red dots, whose size is proportional to the cubic root of their
1716 mass. Planetesimals are represented in green. The big blue dot represents Jupiter. A
1717 system of 3 terrestrial planets, the most massive of which has approximately an
1718 Earth mass, is eventually formed inside of 2 AU, whereas only a small fraction of the
1719 original planetesimal population survives within the asteroid belt boundaries
1720 (sketched with dashed curves). From O'Brien et al. (2006).

1721

1722 **Fig. 4.** The orbits of embryos (green full dots) and planetesimals (red dots)
1723 at the end of the inward-then-outward migration of Jupiter, when the gas is fully
1724 removed. The dash curve in the right bottom corner marks the inner boundary of
1725 the asteroid belt. From this state, the system evolves naturally in a timescale of a
1726 few 10^7 y into two Earth-mass planets at ~ 0.7 and 1 AU and a small Mars at 1.5 AU.
1727 (see Fig. 4).

1728

1729 **Fig. 5.** The mass distribution of the synthetic terrestrial planets produced in
 1730 the Walsh et al. (2010) simulations. The open symbols represent the planets
 1731 produced in different runs starting from different initial conditions. The horizontal
 1732 lines denote the perihelion-aphelion excursion of the planets on their eccentric final
 1733 orbits. The black squares show the real planets of the solar system. The large mass
 1734 ratio between the Earth and Mars is statistically reproduced.

1735

1736 **Fig. 6.** Noble gas concentrations (Table 2) and isotopic compositions (Table 3)
 1737 in Mars, Earth, CI-chondrites, Comets, and Solar composition. The cometary
 1738 concentrations were derived from noble gas trapping experiments in amorphous ice
 1739 (calculated at 55 K). The composition of Venus' atmosphere is not plotted as it is
 1740 very uncertain. The concentrations (left panel) are normalized to solar composition
 1741 $\text{Log}(C/C_{\odot})$. The isotopic compositions are given using the fractionation factor
 1742 ($\text{\%}/\text{amu}$); $F_{\text{Ne}} = [(^{22}\text{Ce}/^{20}\text{Ne})_{\text{reservoir}} / (^{22}\text{Ce}/^{20}\text{Ne})_{\text{Solar}} - 1] \times 1000 / (22 - 20)$, $F_{\text{Ar}} =$
 1743 $[(^{38}\text{Ar}/^{36}\text{Ar})_{\text{reservoir}} / (^{38}\text{Ar}/^{36}\text{Ar})_{\text{Solar}} - 1] \times 1000 / (38 - 36)$, $F_{\text{Kr}} =$
 1744 $[(^{83}\text{Kr}/^{84}\text{Kr})_{\text{reservoir}} / (^{83}\text{Kr}/^{84}\text{Kr})_{\text{Solar}} - 1] \times 1000 / (83 - 84)$, $F_{\text{Xe}} =$
 1745 $[(^{128}\text{Xe}/^{130}\text{Xe})_{\text{reservoir}} / (^{128}\text{Xe}/^{130}\text{Xe})_{\text{Solar}} - 1] \times 1000 / (128 - 130)$. Mars and Earth have
 1746 different noble gas abundance patterns and isotopic compositions relative to
 1747 possible progenitors.

1748

1749 **Fig. 7.** Hydrodynamic escape-preferential Xe retention model of the origin of
 1750 Earth's noble gases (Pepin 1991, 1995). The isotopic compositions are given next to
 1751 the data points in $\text{\%}/\text{amu}$ relative to solar. The initial atmosphere (empty circles)
 1752 has solar isotopic composition ($F=0 \text{\%}/\text{amu}$) and near solar elemental abundances
 1753 except for a severe depletion in Ne. Hydrodynamic escape driven by one or several
 1754 giant impact leads to noble gas removal with preferential depletion and isotopic
 1755 fractionation of the lighter gases (red circles). The large isotopic fractionation is
 1756 established at this stage. Mantle noble gases with solar isotopic compositions
 1757 (dashed line) are degassed into the atmosphere where they are mixed with the
 1758 fractionated noble gases remaining from the escape episode (mixture shown with
 1759 green circles). During this stage, Xe is assumed to be retained in the mantle/core.
 1760 Most Kr in Earth's atmosphere is from mantle degassing. In a final stage, Ne is
 1761 partially lost to space and isotopically fractionated by hydrodynamic escape driven
 1762 by EUV-radiation from the young Sun. Heavier noble gases are unaffected. The final
 1763 modeled composition is shown in blue circles. A difficulty with this model is that no
 1764 mantle reservoir has been documented yet that could host the missing Xe.
 1765 Furthermore, this scenario cannot explain the measured Kr isotopic composition of
 1766 CO_2 well gases (HOLLAND et al., 2009).

1767

1768 **Fig. 8.** Hydrodynamic escape-solubility controlled degassing model of the origin
 1769 of Earth's noble gases (Tolstikhin & O'Nions, 1994). The isotopic compositions are
 1770 given next to the data points in $\text{\%}/\text{amu}$ relative to solar. Proto-terrestrial material
 1771 (thick black line) has Xe, Kr and Ar as in the South Oman E-chondrite (Pepin, 1991)
 1772 and has solar-wind-like $^3\text{He}/^{22}\text{Ne}$ ratio. All these gases in these materials are

1773 isotopically non-fractionated ($F=0$ ‰/amu). Stage 1 of the degassing-dissipation
1774 process: Xe has been lost from the atmosphere, mass fractionated and set in this
1775 reservoir; its amount is slightly below the present day value as a small portion is
1776 still retained in the mantle and is degassed later. All lighter noble gases have been
1777 lost from the atmosphere quantitatively, but their amounts in the mantle exceed the
1778 atmospheric values. Stage 2: Kr has been degassed, partially lost from the
1779 atmosphere, slightly fractionated and set in this reservoir; only a small amount of Kr
1780 still resides in the mantle, whereas amounts of the lighter gases still exceed those in
1781 the atmosphere. Stage 3: Ar has been degassed, partially lost from the atmosphere,
1782 fractionated and set in this reservoir. Ne abundance in the mantle still exceeds the
1783 air abundance and Ne degasses, releases from the atmosphere and fractionates later
1784 on. Helium isotopes dissipate from the atmosphere continuously, with a mean
1785 residence time of ~ 1 Myr, so that He concentration is negligibly small in the present
1786 day atmosphere. Solar He abundance in non-dissipated atmosphere is shown in this
1787 Figure. This model cannot explain the heavy Kr isotopic composition of Earth's
1788 mantle relative to the atmosphere (HOLLAND et al., 2009).

1789
1790 **Fig. 9.** Hydrodynamic escape-cometary input model of the origin of Earth's
1791 noble gases (Dauphas 2003). The isotopic compositions are given next to the data
1792 points in ‰/amu relative to solar. The initial atmosphere (empty circles) has solar
1793 isotopic composition ($F=0$ ‰/amu) and solar elemental abundances. Following an
1794 episode of hydrodynamic escape possibly driven by EUV radiation from the T-Tauri
1795 sun, noble gases are depleted and isotopically fractionated (red circles). The isotopic
1796 composition of Xe is established at that stage. Comets deliver noble gases trapped in
1797 amorphous ice that display a depletion in Xe relative to Kr (dashed line; Bar-Nun
1798 and Owen). This late cometary bombardment can contribute most of the inventories
1799 of Ar and Kr without affecting much the isotopic composition of Ne and Xe (blue
1800 circles). One difficulty with this model is that it relies on the composition of
1801 hypothetical comets based on trapping experiments that are not fully understood.

1802
1803 **Fig. 10.** Histograms of $^3\text{He}/^4\text{He}$ ratio (R/R_A) of arcs, MORBs, and intraplate
1804 magmatism. Most data are from a compilation published in 2006
1805 (<http://pubs.usgs.gov/ds/2006/202/>) updated with data published since then.
1806 MORBs have a narrow distribution of R/R_A values that peaks at a mode of 7.3. The
1807 mean of 8.9 is higher, which reflects the fact that the distribution has a tail towards
1808 high R/R_A values corresponding to an enriched source. Intraplate magmatism
1809 includes plume sources that are characterized by elevated $^3\text{He}/^4\text{He}$ ratios (i.e., less
1810 degassed than the MORB source).

1811
1812 **Fig. 11.** Neon isotope systematics of Earth's mantle. **A.** Mantle Ne is prone to
1813 contamination at Earth's surface by air. This produces linear mixing arrays in
1814 $^{20}\text{Ne}/^{22}\text{Ne}$ vs $^{21}\text{Ne}/^{22}\text{Ne}$ space between air and mantle end-members. The different
1815 mixing lines point to different end-members with elevated $^{20}\text{Ne}/^{22}\text{Ne}$ (i.e., towards
1816 solar composition) but characterized by various contributions of nucleogenic $^{21}\text{Ne}^*$.
1817 The more degassed samples (MORBs) have higher U/Ne ratios and therefore higher
1818 $^{21}\text{Ne}/^{22}\text{Ne}$ ratios compared to plume-related samples such as those from Loihi,

1819 Hawaii. The highest $^{20}\text{Ne}/^{22}\text{Ne}$ ratios in plumes are found in Kola peninsula and
1820 approach the solar ratio. Other samples have lower $^{20}\text{Ne}/^{22}\text{Ne}$ ratios and it is
1821 uncertain at present whether this reflects the presence of a non-solar end-member
1822 in the mantle ($^{20}\text{Ne}/^{22}\text{Ne} \sim 12.5$) or if this limit reflects residual air contamination.
1823 Data from <http://pubs.usgs.gov/ds/2006/202/> for most MORBs (light green
1824 circles), Moreira et al. (1998) for popping-rocks (large dark green triangles in the
1825 MORB field), Yokochi and Marty (2004) for Kola (large orange circles), Tieloff et al.
1826 (2000) for Hawaii and Iceland (large blue squares). MFL stands for mass
1827 fractionation line. **B.** Attempt to derive the Ne isotopic composition of the mantle
1828 (see Ballentine et al. 2005; Holland and Ballentine 2006 for details). CO_2 well gas
1829 samples define a mixing line between a mantle end-member and a mixture between
1830 crust and air. The depleted mantle end-member can be inferred by taking the
1831 intersection between the MORB line and that derived by CO_2 well gases. Using a
1832 more refined scheme, Holland and Ballentine (2006) obtained $^{20}\text{Ne}/^{22}\text{Ne}$ and
1833 $^{21}\text{Ne}/^{22}\text{Ne}$ ratios of 12.49 ± 0.04 and 0.0578 ± 0.0003 , respectively, for the depleted
1834 mantle.

1835

1836 **Fig. 12.** Radiogenic ^{40}Ar in the mantle. The $^{20}\text{Ne}/^{22}\text{Ne}$ ratio is a proxy of air
1837 contamination as there is a contrast between the Ne isotopic composition of air
1838 (~ 9.8) and that of the atmosphere (12.5-13.7). In this diagram, popping rocks and
1839 plume-related magmas (i.e., Loihi seamount, Kola peninsula, and Iceland) define
1840 correlations that point to different $^{40}\text{Ar}/^{36}\text{Ar}$ ratios end-members between the
1841 depleted upper-mantle (25,000-44,000) and the plume-source ($\sim 4,500$),
1842 corresponding to different extents of degassing. Data sources: Popping rocks
1843 (Moreira et al. 1998), Loihi, Hawaii (Valbracht et al. 1997; Tieloff et al. 2000);
1844 Iceland (Tieloff et al. 2000); Kola (Marty et al. 1998; Yokochi and Marty 2004,
1845 2005).

1846

1847 **Fig. 13.** Kr-Xe non-radiogenic isotopic compositions of CO_2 well-gases (data
1848 from Holland et al. 2009). The samples define a correlation corresponding to mixing
1849 between air and the mantle source. The black arrow shows the direction expected
1850 for mass fractionation. As shown, air cannot be derived from mantle gases by simple
1851 mass fractionation. Instead, the data can be explained if the atmosphere received a
1852 late addition of cometary materials that modified its heavy noble gas isotopic
1853 composition (Dauphas, 2003). Holland et al. (2009) argued that the mantle member
1854 of the mixing derives from a trapped meteoritic component. This end-member could
1855 also be nebular gases of a transient atmosphere fractionated by hydrodynamic
1856 escape while the Earth had not yet reached its full size.

1857

1858 **Fig. 14.** Radiogenic Xe isotope systematics in the mantle. **A, B.** Determination of
1859 the $^{129}\text{Xe}/^{130}\text{Xe}$ ratio of the source of MORBs (Moreira et al. 1998; Holland and
1860 Ballentine 2006). Popping rocks define a correlation corresponding to mixing
1861 between air and the mantle (A, Moreira et al. 1998). At a $^{20}\text{Ne}/^{22}\text{Ne}$ ratio of 12.5-
1862 13.7, the $^{129}\text{Xe}/^{130}\text{Xe}$ is estimated to be 7.6-8.2. CO_2 -well gases define a correlation
1863 corresponding to mixing between mantle and air+crustal gases (B, Holland and
1864 Ballentine 2006). It intersects the MORB correlation at a $^{129}\text{Xe}/^{130}\text{Xe}$ ratio of

1865 7.90±0.14. **C, D.** Decomposition of ^{136}Xe into ^{238}U and ^{244}Pu -fission derived
1866 components (Kunz et al. 1998; Yokochi and Marty 2005). ^{238}U -decay and ^{244}Pu
1867 decay produce ^{136}Xe and ^4He in different ratios. Yokochi and Marty (2005) used the
1868 $^{21}\text{Ne}^*/^4\text{He}^*$ ratio to correct for $^{136}\text{Xe}/^4\text{He}$ during degassing and concluded that 33-60
1869 % of total fission ^{136}Xe was from ^{244}Pu -decay (C). ^{244}Pu and ^{238}U -fission produce Xe
1870 isotopes with different spectra, which Kunz et al. (1998) used to conclude that
1871 32±10 % of total fission ^{136}Xe was from ^{244}Pu -decay (D).

1872 **Fig. 15.** CI and CM meteorites are the most rich in water; water amounts to
1873 about 5 to 10% of their total mass (Robert and Epstein, 1982; Kerridge, 1985). They
1874 are expected to come from C-type asteroids, predominantly in the asteroid belt and
1875 possibly accreted even further out (Walsh et al., 2010). Water in ordinary
1876 chondrites amounts for only 0.1% of the total weight (Robert, 1977; Robert et al.,
1877 1979; McNaughton et al. 1981), or a few times as much (Jaresewich 1966); they are
1878 spectroscopically linked to S-type asteroids, predominant between 2 and 2.5 AU.
1879 Finally, enstatite chondrites are very dry, with only 0.01% of their total mass in
1880 water (ref.); they are expected to come from E-type asteroids, which dominate the
1881 Hungaria region in the very inner asteroid belt at 1.8 AU.

1882

1883 **Fig. 16.** Major volatile element concentrations (Table 2) and isotopic
1884 compositions (Table 3) in Earth, CI-chondrites, Comets, and Solar composition. The
1885 concentrations (left panel) are normalized to solar composition $\text{Log}(C/C_{\odot})$. The
1886 isotopic compositions are given in δ -notation (‰); $\delta D = [(D/H)_{\text{reservoir}} / (D/H)_{\text{VSMOW}} - 1] \times 1000$,
1887 $\delta^{13}\text{C} = [(^{13}\text{C}/^{12}\text{C})_{\text{reservoir}} / (^{13}\text{C}/^{12}\text{C})_{\text{VPDB}} - 1] \times 1000$, and $\delta^{15}\text{N} = [(^{15}\text{N} / ^{14}\text{N})_{\text{reservoir}} / (^{15}\text{N} / ^{14}\text{N})_{\text{VPDB}} - 1] \times 1000$, where VSMOW (Vienne Standard Mean Ocean
1888 Water) and VPDB (Vienna Pee Dee belemnite) are two terrestrial reference
1889 materials stored in Vienna. Although at a lower concentration, Earth has the same
1890 abundance pattern as CI-chondrites. The isotopic compositions of the major volatile
1891 elements on Earth are also very close to CI-chondrites.
1892
1893

1894 **Fig. 17.** Constraints from moderately and highly siderophile elements on the
1895 nature of the late veneer. **A.** Highly siderophile element pattern of the terrestrial
1896 primitive mantle, EH, EL, O, and CV chondrites (Becker et al. 2006, Fischer-Gödde et
1897 al. 2011). The primitive mantle has approximately chondritic composition except for
1898 large excess in Ru. This excess could be due to accretion of a late veneer with non-
1899 chondritic composition (Puchtel et al. 2008) or mixing of a chondritic late-veneer
1900 with fractionated highly siderophile elements remaining in the mantle after core
1901 formation (Dauphas et al. 2002b). Walker (2009) recently provided a very detailed
1902 review of that question. **B.** Correlation between Mo and Ru isotopic anomalies in
1903 meteorites (Dauphas et al. 2004; Chen et al. 2010; Burkhardt et al. 2011). The
1904 dashed line corresponds to mixing between terrestrial and s-process end-members.
1905 Molybdenum is a moderately siderophile element and most of its inventory in
1906 Earth's mantle was delivered during the main stage of Earth's accretion. Ruthenium
1907 is a highly siderophile element and most of its inventory in Earth's mantle was
1908 delivered after completion of core formation, as part of the late veneer. The fact that

1909 Earth's mantle plots on the correlation defined by meteorites suggests that the
1910 nature of the material accreted by the Earth did not change drastically before and
1911 after core formation.

1912
1913 **Fig. 18.** H₂O/Xe constraints on the origin of Earth's atmosphere (data from
1914 Tables 1 and 2). Earth and presumably Mars have H₂O/Xe ratios that are much
1915 higher than those of chondrites and comets. If such objects had delivered Earth's
1916 oceans as part of a late veneer, they would have delivered too much Xe with the
1917 wrong isotopic composition compared to what is in the atmosphere. Most likely,
1918 water was delivered during the main stage of terrestrial growth when Xe could be
1919 lost from the protoatmosphere by impact erosion (and hydrodynamic escape) while
1920 reactive water was more efficiently retained.

1921
1922 **Fig. 19.** The fraction of the total mass of a terrestrial planet as a function of
1923 the said planet 's total mass, from a simulation of O'Brien et al. (2010). In this case,
1924 50 % of the water is accreted when the planet is at least 90 % of it's final mass.
1925 Assuming that the "wet material" is 5 % water by mass, consistent with CM
1926 carbonaceous chondrites, this planet would have at the end 4 times the amount of
1927 crustal water on Earth.

1928
1929 **Fig. 20.** The evolution of the giant planets in the Nice model. Here, each
1930 planet is represented by a pair of curves of distinctive color (Jupiter in blue, Saturn
1931 in red, Uranus in green and Neptune in magenta). The inner curve marks the
1932 perihelion distance and the outercuve the aphelion distance, as a function of time.
1933 Thus, when the two curves are very close, the planet's orbit is almost circular. When
1934 the two curves separate from each other, the eccentricity is large. In this simulaiton,
1935 the instability of the giant planets occurs at 762 My. From Levison et al. (2011)

1936
1937
1938
1939
1940

1941

1942

1943

1944 **References**

1945

- 1946 Abe, Y., Ohtani, E., Okuchi, T., Righter, K., Drake, M. (2000). Water in the Early Earth.
1947 Origin of the Earth and Moon 413-433.
- 1948 Adachi, I., Hayashi, C., and Nakazawa, K., 1976. Gas Drag Effect on Elliptic Motion of a
1949 Solid Body in Primordial Solar Nebula. *Progress of Theoretical Physics* **56**,
1950 1756-1771.
- 1951 Agnor, C.B., Canup, R.M., Levison, H.F. (1999). On the Character and Consequences of
1952 Large Impacts in the Late Stage of Terrestrial Planet Formation. *Icarus* 142,
1953 219-237.
- 1954 Albarede, F., 2009. Volatile accretion history of the terrestrial planets and dynamic
1955 implications. *Nature* **461**, 1227-1233.
- 1956 Alexander , R. (2008) From discs to planetesimals: evolution of gas and dust discs.
1957 *New. Astron. Rev.* 52, 60-77.
- 1958 Allegre, C.J., Manhès, G., Gopel, C. (1995). The age of the Earth. *Geochimica et*
1959 *Cosmochimica Acta* 59, 2445-1456.
- 1960 Allegre, C. J., Hofmann, A., and O'Nions, K., 1996. The argon constraints on mantle
1961 structure. *Geophys. Res. Lett.* **23**, 3555-3557.
- 1962 Anderson, D.L. (1998) The helium paradoxes. *Proceedings of the National Academy*
1963 *of Sciences* 95, 4822-4827.
- 1964 Ballentine, C.J. and Burnard P.G. 2002. Production, release and transport of noble
1965 gases in the continental crust. *Reviews in Mineralogy and Geochemistry* 47,
1966 481-538.
- 1967 Ballentine, C. J. and Holland, G., 2008. What CO₂ well gases tell us about the origin of
1968 noble gases in the mantle and their relationship to the atmosphere.
1969 *Philosophical Transactions of the Royal Society A: Mathematical, Physical and*
1970 *Engineering Sciences* **366**, 4183-4203.
- 1971 Ballentine, C. J., Marty, B., Sherwood Lollar, B., and Cassidy, M., 2005. Neon isotopes
1972 constrain convection and volatile origin in the Earth's mantle. *Nature* **433**, 33-
1973 38.
- 1974 Ballester, G. E., Sing, D. K., and Herbert, F., 2007. The signature of hot hydrogen in
1975 the atmosphere of the extrasolar planet HD 209458b. *Nature* **445**, 511-514.
- 1976 Balsiger H., Altwegg K. and Geiss J. (1995). D/H and ¹⁸O/¹⁶O ratio in hydronium ion
1977 and in neutral water from in situ ion measurements in Comet P/Halley. J.
1978 *Geophys. Res.*, 100, 5834-5840.
- 1979 Balsiger, H., Altwegg, K., Bochsler, P., Eberhardt, P., Fischer, J., Graf, S., Jäckel, A.,
1980 Kopp, E., Langer, U., Mildner, M., Müller, J., Riesen, T., Rubin, M., Scherer, S.,
1981 Wurz, P., Wüthrich, S., Arijs, E., Delanoye, S., Keyser, J., Neefs, E., Nevejans, D.,
1982 Rème, H., Aoustin, C., Mazelle, C., Médale, J. L., Sauvaud, J., Berthelier, J. J.,
1983 Bertaux, J. L., Duvet, L., Illiano, J. M., Fuselier, S., Ghielmetti, A., Magoncelli, T.,
1984 Shelley, E., Korth, A., Heerlein, K., Lauche, H., Livi, S., Loose, A., Mall, U., Wilken,
1985 B., Gliem, F., Fiethe, B., Gombosi, T., Block, B., Carignan, G., Fisk, L., Waite, J.,
1986 Young, D., and Wollnik, H., 2007. Rosina – Rosetta Orbiter Spectrometer for Ion
1987 and Neutral Analysis. *Space Science Reviews* **128**, 745-801.
- 1988 Bar-Nun, A., Kleinfeld, I., and Kochavi, E., 1988. Trapping of gas mixtures by
1989 amorphous water ice. *Physical Review B* **38**, 7749.

- 1990 Bar-Nun, A. and Owen, T., 1998. Trapping of gases in water ice and consequences to
1991 comets and the atmospheres of the inner planets. In: Schmitt, B. B., De Bergh,
1992 C., and Festou, M. Eds.), *Solar System Ices*. Kluwer, Dordrecht.
- 1993 Batygin, K., Brown, M.E. (2010). Early Dynamical Evolution of the Solar System:
1994 Pinning Down the Initial Conditions of the Nice Model. *The Astrophysical*
1995 *Journal* 716, 1323-1331.
- 1996 Batygin, K., Brown, M.E., Fraser, W.C. (2011). In-situ Formation of the Cold Classical
1997 Kuiper Belt. *ApJ*, submitted.
- 1998 Becker, H., Horan, M. F., Walker, R. J., Gao, S., Lorand, J. P., and Rudnick, R. L., 2006.
1999 Highly siderophile element composition of the Earth's primitive upper mantle:
2000 Constraints from new data on peridotite massifs and xenoliths. *Geochimica et*
2001 *Cosmochimica Acta* **70**, 4528-4550.
- 2002 Bianchi, D., Sarmiento, J. L., Gnanadesikan, A., Key, R. M., Schlosser, P., and Newton,
2003 R., 2010. Low helium flux from the mantle inferred from simulations of oceanic
2004 helium isotope data. *Earth and Planetary Science Letters* **297**, 379-386.
- 2005 Binzel, R.P., Bus, S.J., Burbine, T.H., Sunshine, J.M. (1996). Spectral Properties of
2006 Near-Earth Asteroids: Evidence for Sources of Ordinary Chondrite Meteorites.
2007 *Science* 273, 946-948.
- 2008 Bizzarro, M. and et al., 2005. Rapid Timescales for Accretion and Melting of
2009 Differentiated Planetesimals Inferred from ²⁶Al-²⁶Mg Chronometry. *The*
2010 *Astrophysical Journal Letters* **632**, L41.
- 2011 Blum, J. and Wurm, G., 2008. The growth mechanisms of macroscopic bodies in
2012 protoplanetary disks. *Annual Review of Astronomy and Astrophysics* **46**, 21-56.
- 2013 Bockelee-Morvan D., Gautier D., Lis D.C., Young K., Keene J., Phillips T., Owen T.,
2014 Crovisier J., Goldsmith P.F., Bergin E.A., Despois D. and Wooten A. (1988).
2015 Deuterated Water in Comet C/1996 B2 (Hyakutake) and its Implications for
2016 the Origin of Comets. *Icarus*, 193, 147-162.
- 2017 Bockelee-Morvan, D., Biver, N., Jehin, E., Cochran, A. L., Wiesemeyer, H., Manfroid, J.,
2018 Hutsemekers, D., Arpigny, C., Boissier, J., Cochran, W., Colom, P., Crovisier, J.,
2019 Milutinovic, N., Moreno, R., Prochaska, J. X., Ramirez, I., Schulz, R., and Zucconi,
2020 J. M., 2008. Large excess of heavy nitrogen in both hydrogen cyanide and
2021 cyanogen from comet 17P/Holmes. *Astrophysical Journal Letters* **679**, L49-L52.
- 2022 Bockelee-Morvan, D., Crovisier, J., Mumma, M. J., and Weaver, H. A., 2004. The
2023 composition of cometary volatiles. In: Festou, M. C., Keller, H. U., and Weaver,
2024 H. A. Eds.), *Comets II*. University of Arizona Press, Tucson.
- 2025 Bogard, D. D., Clayton, R. N., Marti, K., Owen, T., and Turner, G., 2001. Martian
2026 volatiles: isotopic composition, origin, and evolution. *Space Science Reviews* **96**,
2027 425-458.
- 2028 Bottke, W.F., Levison, H.F., Nesvorny, D., Dones, L. (2007). Can planetesimals left
2029 over from terrestrial planet formation produce the lunar Late Heavy
2030 Bombardment?. *Icarus* 190, 203-223.
- 2031 Bottke, W.F., Nesvorny, D., Vokrouhlicky, D., Morbidelli, A. (2010). The Irregular
2032 Satellites: The Most Collisionally Evolved Populations in the Solar System. *The*
2033 *Astronomical Journal* 139, 994-1014.

2034 Bottke, W.F., Vokrouhlicky, D., Minton, D., Nesvorny, D., Morbidelli, A., Brasser, R.,
2035 Simonson, B. (2011). The Great Archean Bombardment, or the Late Heavy
2036 Bombardment. *42nd Lunar and Planetary Science Conference, Abstract #2591*
2037 Boyce J.W., Liu Y., Rossman G.R., Guan Y., Eiler J.M. Stolper E.M., Taylor L.A. (2010)
2038 Lunar apatite with terrestrial volatile abundances. *Nature* 466, 466-469.
2039 Boyd, S. R., 2001. Nitrogen in future biosphere studies. *Chemical Geology* **176**, 1-30.
2040 Boynton, W. V., Ming, D. W., Kounaves, S. P., Young, S. M. M., Arvidson, R. E., Hecht, M.
2041 H., Hoffman, J., Niles, P. B., Hamara, D. K., Quinn, R. C., Smith, P. H., Sutter, B.,
2042 Catling, D. C., and Morris, R. V., 2009. Evidence for Calcium Carbonate at the
2043 Mars Phoenix Landing Site. *Science* **325**, 61-64.
2044 Bridges, J. C., Catling, D. C., Saxton, J. M., Swindle, T. D., Lyon, I. C., and Grady, M. M.,
2045 2001. Alteration assemblages in martian meteorites: Implications for near-
2046 surface processes. *Space Science Reviews* **96**, 365-392.
2047 Brock, D. S. and Schrobilgen, G. J., 2010. Synthesis of the missing oxide of xenon,
2048 XeO₂, and its implications for Earth's missing xenon. *Journal of the American*
2049 *Chemical Society* [dx.doi.org/10.1021/ja110618g](https://doi.org/10.1021/ja110618g).
2050 Bromley, B. C. and Kenyon, S. J., 2006. A hybrid N-body-coagulation code for planet
2051 formation. *Astronomical Journal* **131**, 2737-2748.
2052 Burbine, T.H., Binzel, R.P., Bus, S.J., Buchanan, P.C., Hinrichs, J.L., Hiroi, T., Meibom, A.,
2053 Sunshine, J.M. (2000). Forging Asteroid-Meteorite Relationships Through
2054 Reflectance Spectroscopy. Lunar and Planetary Institute Science Conference
2055 Abstracts 31, 1844.
2056 Burkhardt, C., Kleine, T., Oberli, F., Pack, A., Bourdon, B., Wieler, R., 2011.
2057 Nucleosynthetic Mo isotopic anomalies in planetary materials as tracers of
2058 circumstellar disk processes. Lunar and Planetary Science Conference 42,
2059 #2554.
2060 Burnard, P., Graham, D., and Turner, G., 1997. Vesicle-Specific Noble Gas Analyses of
2061 "Popping Rock": Implications for Primordial Noble Gases in Earth. *Science* **276**,
2062 568-571.
2063 Busemann, H. and Eugster, O., 2002. The trapped noble gas component in
2064 achondrites. *Meteoritics & Planetary Science* **37**, 1865-1891.
2065 Caffee, M. W., Hudson, G. B., Velsko, C., Huss, G. R., Alexander, E. C., and Chivas, A. R.,
2066 1999. Primordial Noble Gases from Earth's Mantle: Identification of a Primitive
2067 Volatile Component. *Science* **285**, 2115-2118.
2068 Campins, H., Hargrove, K., Pinilla-Alonso, N., Howell, E.S., Kelley, M.S., Licandro, J.,
2069 Mothe-Diniz, T., Fernandez, Y., Ziffer, J. (2010). Water ice and
2070 organics on the surface of the asteroid 24 Themis. *Nature* 464, 1320-1321.
2071 Canup, R.M., Esposito, L.W. (1996). Accretion of the Moon from an Impact-Generated
2072 Disk. *Icarus* 119, 427-446.
2073 Canup, R.M., Asphaug, E. (2001). Origin of the Moon in a giant impact near the end of
2074 the Earth's formation. *Nature* 412, 708-712.
2075 Canup, R.M., Ward, W.R. (2002). Formation of the Galilean Satellites: Conditions of
2076 Accretion. *The Astronomical Journal* 124, 3404-3423.
2077 Cartigny, P., Boyd, S. R., Harris, J. W., and Javoy, M., 1997. Nitrogen isotopes in
2078 peridotitic diamonds from Fuxian, China: the mantle signature. *Terra Nova* **9**,
2079 175-179.

2080 Cartigny P., Harris J.W., Javoy M. (2001) Diamond genesis, mantle fractionations and
2081 mantle nitrogen content: a study of d13C-N concentrations in diamonds. *Earth*
2082 *and Planetary Science Letters* 185, 85-98.

2083 Cartigny, P., Pineau, F., Aubaud, C., and Javoy, M., 2008. Towards a consistent mantle
2084 carbon flux estimate: Insights from volatile systematics (H₂O/Ce, dD, CO₂/Nb)
2085 in the North Atlantic mantle (14° N and 34° N) *Earth and Planetary Science*
2086 *Letters* **265**, 672-685.

2087 Cassen, P., 2001. Nebular thermal evolution and thermal properties of primitive
2088 planetary materials. *Meteoritics & Planetary Science* **36**, 671-700.

2089 Cates, N. L. and Mojzsis, S. J., 2007. Pre-3750†Ma supracrustal rocks from the
2090 Nuvvuagittuq supracrustal belt, northern QuÈbec. *Earth and Planetary Science*
2091 *Letters* **255**, 9-21.

2092 Chambers, J.E., Wetherill, G.W. (1998). Making the Terrestrial Planets: N-Body
2093 Integrations of Planetary Embryos in Three Dimensions. *Icarus* 136, 304-327.

2094 Chambers, J.E., Wetherill, G.W. (2001). Planets in the asteroid belt. *Meteoritics and*
2095 *Planetary Science* 36, 381-399.

2096 Chambers, J.E. (2010). Planetesimal formation by turbulent concentration. *Icarus*
2097 208, 505-517.

2098 Chen, J.H., Papanastassiou, D.A., Wasserburg, G.J. (2010) Ruthenium endemic isotope
2099 effects in chondrites and differentiated meteorites. *Geochimica et*
2100 *Cosmochimica Acta* 74, 3851-3862.

2101 Chou, C.-L., 1978. Fractionation of siderophile elements in the Earth's upper mantle.
2102 *Proceedings of the Lunar and Planetary Science Conference* **9**, 219-230.

2103 Christensen, P. R., 2006. Water at the poles and in permafrost regions of Mars.
2104 *Elements* **2**, 151-155.

2105 Chyba, C. F., 1991. Terrestrial mantle siderophiles and the lunar impact record.
2106 *Icarus* **92**, 217-233.

2107 Clayton, R.N., Mayeda, T.K. (1984) Oxygen isotopic compositions of enstatite
2108 chondrites and aubrites. *Journal of Geophysical Research (Supplement)*, C245-
2109 C249.

2110 Clayton, R.N., Mayeda, T.K., Goswami, J.N., Olsen, E.J. (1991) Oxygen isotope studies
2111 of ordinary chondrites. *Geochimica et Cosmochimica Acta* 55, 2317-2337.

2112 Clayton, R.N., Mayeda, T.K. (1999) Oxygen isotope studies of carbonaceous
2113 chondrites. *Geochimica et Cosmochimica Acta* 63, 2089-2104.

2114 Clayton, R. N., 1993. Oxygen isotopes in meteorites. *Annual Review of Earth and*
2115 *Planetary Sciences* **21**, 115-149.

2116 Coltice, N., Marty, B., and Yokochi, R., 2009. Xenon isotope constraints on the
2117 thermal evolution of the early Earth. *Chemical Geology* **266**, 4-9.

2118 Craig, H., Clarke, W. B., and Beg, M. A., 1975. Excess 3He in deep water on the East
2119 Pacific Rise. *Earth and Planetary Science Letters* **26**, 125-132.

2120 Craig, H. and Lupton, J. E., 1976. Primordial neon, helium, and hydrogen in oceanic
2121 basalts. *Earth and Planetary Science Letters* **31**, 369-385.

2122 Criss R.E., Farquhar J. 2008. Abundance, notation, and fractionation of light stable
2123 isotopes. *Reviews in Mineralogy & Geochemistry* 68, 15-30.

2124 Cuzzi, J.N., Hogan, R.C., Shariff, K. (2008). Toward Planetesimals: Dense Chondrule
2125 Clumps in the Protoplanetary Nebula. *The Astrophysical Journal* 687, 1432-
2126 1447.

2127 Cuzzi, J.N., Hogan, R.C., Bottke, W.F. (2010). Towards initial mass functions for
2128 asteroids and Kuiper Belt Objects. *Icarus* 208, 518-538.

2129 Dauphas, N., Marty, B. 1999. Heavy nitrogen in carbonatites of the Kola Peninsula: A
2130 possible signature of the deep mantle. *Science* 286, 2488-2490.

2131 Dauphas, N., 2003. The dual origin of the terrestrial atmosphere. *Icarus* **165**, 326-
2132 339.

2133 Dauphas, N., Cates, N. L., Mojzsis, S. J., and Busigny, V., 2007. Identification of
2134 chemical sedimentary protoliths using iron isotopes in the > 3750 Ma
2135 Nuvvuagittuq supracrustal belt, Canada. *Earth and Planetary Science Letters*
2136 **254**, 358-376.

2137 Dauphas, N. and Chaussidon, M., 2011. A perspective from extinct radionuclides on a
2138 young stellar object: The Sun and its accretion disk. *Annual Review of Earth and*
2139 *Planetary Sciences* **39**.

2140 Dauphas, N., Davis, A. M., Marty, B., and Reisberg, L., 2004a. The cosmic
2141 molybdenum-ruthenium isotope correlation. *Earth and Planetary Science*
2142 *Letters* **226**, 465-475.

2143 Dauphas, N. and Marty, B., 2002. Inference on the nature and the mass of Earth's late
2144 veneer from noble metals and gases. *J. Geophys. Res.* **107**, 5129.

2145 Dauphas, N., Marty, B., and Reisberg, L., 2002a. Inference on terrestrial genesis from
2146 molybdenum isotope systematics. *Geophysical Research Letters* **29**, -.

2147 Dauphas N., Reisberg L., Marty B. (2002b) An alternative explanation for the
2148 distribution of highly siderophile elements in the Earth. *Geochemical Journal*
2149 36, 409-419.

2150 Dauphas N., Marty B., Reisberg L., 2002c. Molybdenum evidence for inherited
2151 planetary scale isotope heterogeneity of the protosolar nebula. *The*
2152 *Astrophysical Journal* 565, 640-644.

2153 Dauphas, N. and Pourmand, A., 2011. Hf-W-Th evidence for rapid growth of Mars
2154 and clues on the birth of an oligarch. *Nature in press*.

2155 Dauphas, N., Robert, F., and Marty, B., 2000. The Late Asteroidal and Cometary
2156 Bombardment of Earth as Recorded in Water Deuterium to Protium Ratio.
2157 *Icarus* **148**, 508-512.

2158 Dauphas, N., van Zuilen, M., Wadhwa, M., Davis, A. M., Marty, B., and Janney, P. E.,
2159 2004b. Clues from Fe isotope variations on the origin of early Archean BIFs
2160 from Greenland. *Science* **306**, 2077-2080.

2161 de Bergh, C., Moroz, V. I., Taylor, F. W., Crisp, D., BÈzard, B., and Zasova, L. V., 2006.
2162 The composition of the atmosphere of Venus below 100†km altitude: An
2163 overview. *Planetary and Space Science* **54**, 1389-1397.

2164 Deines P. (1980) The carbon isotopic composition of diamonds: relationship to
2165 diamond shape, color, occurrence and vapor composition. *Geochimica et*
2166 *Cosmochimica Acta* 44, 943-961.

2167 Delsemme, A. H., 1988. The chemistry of comets. *Philosophical Transactions of the*
2168 *Royal Society, Series A* **325**, 509-523.

2169 Delsemme, A.H. (1992). Cometary origin of carbon and water on the terrestrial
2170 planets. *Advances in Space Research* 12, 5-12.

2171 Delsemme, A.H. (1999). The deuterium enrichment observed in recent comets is
2172 consistent with the cometary origin of seawater. *Planetary and Space Science*
2173 47, 125-131.

2174 DÈruelle, B., Dreibus, G., and Jambon, A., 1992. Iodine abundances in oceanic basalts:
2175 implications for Earth dynamics. *Earth and Planetary Science Letters* **108**, 217-
2176 227.

2177 Donahue, T. M. and Russell, C. T., 1997. The Venus atmosphere and ionosphere and
2178 their interaction with the solar wind: an overview. In: Bouger, S., Hunter, D. M.,
2179 and Phillips, R. J. Eds.), *Venus II*. University of Arizona Press.

2180 Graham, D.W. (2002) Noble gas isotope geochemistry of Mid-Ocean Ridge and Ocean
2181 Island Basalts: characterization of mantle source reservoirs. *Reviews in*
2182 *Mineralogy and Geochemistry* 47, 247-317.

2183 Eberhardt P., Reber M., Krankowski D. and Hodges R.R. (1995). The D/H and
2184 $^{18}\text{O}/^{16}\text{O}$ ratios in water from Comet P/Halley. *Astron. Astrophys.*, 302, 301—
2185 316.

2186

2187 Ehlmann, B. L., Mustard, J. F., Murchie, S. L., Poulet, F., Bishop, J. L., Brown, A. J.,
2188 Calvin, W. M., Clark, R. N., Marais, D. J. D., Milliken, R. E., Roach, L. H., Roush, T.
2189 L., Swayze, G. A., and Wray, J. J., 2008. Orbital Identification of Carbonate-
2190 Bearing Rocks on Mars. *Science* **322**, 1828-1832.

2191 Eugster, O., Eberhardt, P., and Geiss, J., 1967. The isotopic composition of krypton in
2192 unequilibrated and gas rich chondrites. *Earth and Planetary Science Letters* **2**,
2193 385-393.

2194 Farley K.A., Craig H. 1994. Atmospheric argon contamination of ocean island basalt
2195 olivine phenocrysts. *Geochimica et Cosmochimica Acta* 58. 2509-2517.

2196 Farley, K. A. and Neroda, E., 1998. NOBLE GASES IN THE EARTH'S MANTLE. *Annual*
2197 *Review of Earth and Planetary Sciences* **26**, 189-218.

2198 Fernandez J.A., Ip W.-H. (1981) Dynamical evolution of a cometary swarm in the
2199 outer planetary region. *Icarus* 47, 470-479.

2200 Fischer-Gâdde, M., Becker, H., and Wombacher, F., Rhodium, gold and other highly
2201 siderophile elements in orogenic peridotites and peridotite xenoliths. *Chemical*
2202 *Geology* **280**, 365-383.

2203 Fornasier, S., Migliorini, A., Dotto, E., Barucci, M.A. (2008). Visible and near infrared
2204 spectroscopic investigation of E-type asteroids, including 2867 Steins, a target
2205 of the Rosetta mission. *Icarus* 196, 119-134.

2206 Garrison, D. H. and Bogard, D. D., 1998. Isotopic composition of trapped and
2207 cosmogenic noble gases in several martian meteorites. *Meteoritics & Planetary*
2208 *Science* **33**, 721-736.

2209 Genda H., Abe Y. (2003) Survival of a proto-atmosphere through the stage of giant
2210 impacts: the mechanical aspects. *Icarus* 164, 149-162.

2211 Genda H., Abe Y. (2005) Enhanced atmospheric loss on protoplanets at the giant
2212 impact phase in the presence of oceans. *Nature* 433, 842-844.

2213 Genda, H., Ikoma, M. (2008). Origin of the ocean on the Earth: Early evolution of
2214 water D/H in a hydrogen-rich atmosphere. *Icarus* 194, 42-52.

- 2215 Gomes, R.S., Morbidelli, A., Levison, H.F. (2004). Planetary migration in a
 2216 planetesimal disk: why did Neptune stop at 30 AU?. *Icarus* 170, 492-507.
- 2217 Gomes, R., Levison, H.F., Tsiganis, K., Morbidelli, A. (2005). Origin of the cataclysmic
 2218 Late Heavy Bombardment period of the terrestrial planets. *Nature* 435, 466-
 2219 469.
- 2220 Gounelle, M., Morbidelli, A., Bland, P.A., Spurny, P., Young, E.D., Sephton, M. 2008.
 2221 Meteorites from the Outer Solar System?. *The Solar System Beyond Neptune*
 2222 525-541.
- 2223 Gradie, J., Tedesco, E. (1982). Compositional structure of the asteroid belt. *Science*
 2224 216, 1405-1407.
- 2225 Greenberg, R., Hartmann, W.K., Chapman, C.R., Wacker, J.F. (1978). Planetesimals to
 2226 planets - Numerical simulation of collisional evolution. *Icarus* 35, 1-26.
- 2227 Greenwood J.P., Itoh S., Sakamoto N., Warren P., Taylor L., Yurimoto H. (2011)
 2228 Hydrogen isotope ratios in lunar rocks indicate delivery of cometary water to
 2229 the moon. *Nature Geoscience* 4, 79-82.
- 2230 Greenzweig, Y., Lissauer, J.J. (1992). Accretion rates of protoplanets. II - Gaussian
 2231 distributions of planetesimal velocities. *Icarus* 100, 440-463.
- 2232 Grossman, L., 1972. Condensation in Primitive Solar Nebula. *Geochimica et*
 2233 *Cosmochimica Acta* 36, 597-&.
- 2234 Grossman, L. and Larimer, J. W., 1974. Early Chemical History of Solar-System.
 2235 *Reviews of Geophysics* 12, 71-101.
- 2236 Hahn, J.M., Malhotra, R. (1999). Orbital Evolution of Planets Embedded in a
 2237 Planetesimal Disk. *The Astronomical Journal* 117, 3041-3053.
- 2238 Halliday, A.N., Wanke, H., Birck, J.L., Clayton, R.N. (2001). The Accretion,
 2239 Composition and Early Differentiation of Mars. *Space Science Reviews* 96, 197-
 2240 230.
- 2241 Hansen, B.M.S. (2009). Formation of the Terrestrial Planets from a Narrow Annulus.
 2242 *The Astrophysical Journal* 703, 1131-1140.
- 2243 Harrison, T. M., 2009. The hadean crust: evidence from >4 Ga zircons. *Annual Review*
 2244 *of Earth and Planetary Sciences* 37, 479-505.
- 2245 Hauri E., Saal, A.E., Rutherford M.C., van Orman J.A. (2010) Hydrogen isotope
 2246 similarity of the Earth and Moon revealed by water in lunar volcanic glasses.
 2247 *Bulletin of the American Astronomical Society* 42, 987.
- 2248 Hauri E.H., Weinreich T., Saal, A.E., Rutherford M.C., van Orman J.A. (2011) High pre-
 2249 eruptive water contents preserved in lunar melt inclusions. *Science* 333, 213-
 2250 215.
- 2251 Heber, V. S., Wieler, R., Baur, H., Olinger, C., Friedmann, T. A., and Burnett, D. S., 2009.
 2252 Noble gas composition of the solar wind as collected by the Genesis mission.
 2253 *Geochimica et Cosmochimica Acta* 73, 7414-7432.
- 2254 Heimann, M. and Maier-Reimer, E., 1996. On the relations between the oceanic
 2255 uptake of CO₂ and its carbon isotopes. *Global Biogeochemical Cycles* 10, 89-
 2256 110.
- 2257 Hirth, G. and Kohlstedt, D. L., 1996. Water in the oceanic upper mantle: implications
 2258 for rheology, melt extraction and the evolution of the lithosphere. *Earth and*
 2259 *Planetary Science Letters* 144, 93-108.

- 2260 Hiyagon, H., Ozima, M., Marty, B., Zashu, S., and Sakai, H., 1992. Noble gases in
 2261 submarine glasses from mid-oceanic ridges and Loihi seamount: Constraints
 2262 on the early history of the Earth. *Geochimica et Cosmochimica Acta* **56**, 1301-
 2263 1316.
- 2264 Holland, G. and Ballentine, C. J., 2006. Seawater subduction controls the heavy noble
 2265 gas composition of the mantle. *Nature* **441**, 186-191.
- 2266 Holland, G., Cassidy, M., and Ballentine, C. J., 2009. Meteorite Kr in Earth,Àôs Mantle
 2267 Suggests a Late Accretionary Source for the Atmosphere. *Science* **326**, 1522-
 2268 1525.
- 2269 Hollenbach D.J., Yorke H.W., Johnstone D. 2000. Disk dispersal around young stars.
 2270 In *Protostars and Planets IV.* ed. Mannings W., Boss A.P., Russell S.S., pp. 401-
 2271 428. Tucson, AZ, Univ. Arizona Press.
- 2272 Honda, M., McDougall, I., Patterson, D.B., Doulgeris, A., Clague, D.A. (1991) Possible
 2273 solar noble-gas component in Hawaiian basalts. *Nature* **349**, 149-151.
- 2274 Honda, M., McDougall, I., Patterson, D. B., Doulgeris, A., and Clague, D. A., 1993. Noble
 2275 gases in submarine pillow basalt glasses from Loihi and Kilauea, Hawaii: A
 2276 solar component in the Earth. *Geochimica et Cosmochimica Acta* **57**, 859-874.
- 2277 Honda M., McDougall I. (1998) Primordial helium and neon in the Earth- a
 2278 speculation on early degassing. *Geophysical Research Letters* **25**, 1951-1954.
- 2279 Houlton, B. Z. and Bai, E., 2009. Imprint of denitrifying bacteria on the global
 2280 terrestrial biosphere. *Proceedings of the National Academy of Sciences* **106**,
 2281 21713-21716.
- 2282 Hsieh, H.H., Jewitt, D. (2006). A Population of Comets in the Main Asteroid Belt.
 2283 *Science* **312**, 561-563.
- 2284 Hunten, D. M., Pepin, R. O., and Walker, J. C. G., 1987. Mass fractionation in
 2285 hydrodynamic escape. *Icarus* **69**, 532-549.
- 2286 HutsemÈkers, D., Manfroid, J., Jehin, E., and Arpigny, C., 2009. New constraints on the
 2287 delivery of cometary water and nitrogen to Earth from the $^{15}\text{N}/^{14}\text{N}$ isotopic
 2288 ratio. *Icarus* **204**, 346-348.
- 2289 Ida, S., Makino, J. (1993). Scattering of planetesimals by a protoplanet - Slowing
 2290 down of runaway growth. *Icarus* **106**, 210.
- 2291 Ikoma, M., Genda, H. (2006). Constraints on the Mass of a Habitable Planet with
 2292 Water of Nebular Origin. *The Astrophysical Journal* **648**, 696-706.
- 2293 Jagoutz, E., Palme, H., Baddenhausen, H., Blum, K., Cendales, M., Dreibus, G., Spettel,
 2294 B., Lorenz, V., and Wanke, H., 1979. The abundances of major, minor and trace
 2295 elements in the earth's mantle as derived from primitive ultramafic nodules.
 2296 *Proc. Lunar Planet. Sci. Conf.* **10**, 2031-2050.
- 2297 Jaresewich, E. (1966). Chemical Analysis of Ten Stony Meteorites. *Geochimica et*
 2298 *Cosmochimica Acta*, **30**, 1261-1265
- 2299 Javoy, M., Kaminski, E., Guyot, F., Andrault, D., Sanloup, C., Moreira, M., Labrosse, S.,
 2300 Jambon, A., Agrinier, P., Davaille, A., and Jaupart, C., 2010. The chemical
 2301 composition of the Earth: Enstatite chondrite models. *Earth and Planetary*
 2302 *Science Letters* **293**, 259-268.
- 2303 Jehin, E., Manfroid, J., Hutsemekers, D., Arpigny, C., and Zucconi, J.-M., 2009. Isotopic
 2304 ratios in comets: status and perspectives. *Earth Moon and Planets*, 167-180.

2305 Jephcoat, A. P., 1998. Rare-gas solids in the Earth's deep interior. *Nature* **393**, 355-
2306 358.

2307 Jessberger, E. K., Christoforidis, A., and Kissel, J., 1988. Aspects of the major element
2308 composition of Halley's dust. *Nature* **332**, 691-695.

2309 Jewitt, D. C., Matthews, H. E., Owen, T., and Meier, R., 1997. Measurements of
2310 ¹²C/¹³C, ¹⁴N/¹⁵N, and ³²S/³⁴S Ratios in Comet Hale-Bopp (C/1995 O1).
2311 *Science* **278**, 90-93.

2312 Johansen, A., Oishi, J.S., Mac Low, M.M., Klahr, H., Henning, T., Youdin, A. (2007).
2313 Rapid planetesimal formation in turbulent circumstellar disks. *Nature* **448**,
2314 1022-1025.

2315 Johansen, A., Youdin, A., Mac Low, M.M. (2009). Particle Clumping and Planetesimal
2316 Formation Depend Strongly on Metallicity. *The Astrophysical Journal* **704**, L75-
2317 L79.

2318 Kendrick M.A., Scambelluri M., Honda M., Phillips D. (2011) High abundances of
2319 noble gas and chlorine delivered to the mantle by serpentinite subduction.
2320 *Nature Geoscience* **4**, 807-812.

2321 Kerridge, J. F., 1985. Carbon, hydrogen and nitrogen in carbonaceous chondrites:
2322 abundances and isotopic compositions in bulk samples. *Geochimica et*
2323 *Cosmochimica Acta* **49**, 1707-1714.

2324 King, H.E., Stimpfl, M., Deymier, P., Drake, M.J., Catlow, C.R.A., Putnis, A., de Leeuw,
2325 N.H. (2010). Computer simulations of water interactions with low-coordinated
2326 forsterite surface sites: Implications for the origin of water in the inner solar
2327 system. *Earth and Planetary Science Letters* **300**, 11-18.

2328 Kita, N. T., Huss, G. R., Tachibana, S., Amelin, Y., Nyquist, L. E., and Hutcheon, I. D.,
2329 2005. Constraints on the origin of chondrules and CAIs from short-lived and
2330 long-lived radionuclides. In: Krot, A. N., Scott, E. R. D., and Reipurth, B. Eds.),
2331 *Chondrites and the Protoplanetary Disk*. Astronomical Society of the Pacific, San
2332 Francisco.

2333 Kleine, T., Munker, C., Mezger, K., and Palme, H., 2002. Rapid accretion and early
2334 core formation on asteroids and the terrestrial planets from Hf-W
2335 chronometry. *Nature* **418**, 952-955.

2336 Kleine, T., Touboul, M., Bourdon, B., Nimmo, F., Mezger, K., Palme, H., Jacobsen, S.B.,
2337 Yin, Q.Z., Halliday, A.N. (2009). Hf-W chronology of the accretion and early
2338 evolution of asteroids and terrestrial planets. *Geochimica et Cosmochimica*
2339 *Acta* **73**, 5150-5188.

2340 Kokubo, E., Ida, S. (1998). Oligarchic Growth of Protoplanets. *Icarus* **131**, 171-178.

2341 Krasinsky, G.A., Pitjeva, E.V., Vasilyev, M.V., Yagudina, E.I. (2002). Hidden Mass in the
2342 Asteroid Belt. *Icarus* **158**, 98-105.

2343 Kunz, J., Staudacher, T., and Allègre, C. J., 1998. Plutonium-Fission Xenon Found in
2344 Earth's Mantle. *Science* **280**, 877-880.

2345 Koppers, M., and 40 colleagues 2005. A large dust/ice ratio in the nucleus of comet
2346 9P/Tempel 1. *Nature* **437**, 987-990.

2347 Kurz, M. D., Jenkins, W. J., and Hart, S. R., 1982. Helium isotopic systematics of
2348 oceanic islands and mantle heterogeneity. *Nature* **297**, 43-47.

2349 Lecuyer, C., Gillet, P., and Robert, F., 1998. The hydrogen isotope composition of
2350 seawater and the global water cycle. *Chemical Geology* **145**, 249-261.

- 2351 Lee, K. K. M. and Steinle-Neumann, G., 2006. High-pressure alloying of iron and
 2352 xenon: “Missing” Xe in the Earth's core? *J. Geophys. Res.* **111**,
 2353 B02202.
- 2354 Leshin Watson L., Hutcheon, I.D., Epstein S., Stolper E.M. (1994) Water on Mars:
 2355 clues from deuterium/hydrogen and water contents of hydrous phases in SNC
 2356 meteorites. *Science* 265, 86-90.
- 2357 Leshin L.A., Epstein S., Stolper E.M. (1996) Hydrogen isotope geochemistry of SNC
 2358 meteorites. *Geochimica et Cosmochimica Acta* 60, 2635-2650.
- 2359 Levison, H.F., Duncan, M.J. (1997). From the Kuiper Belt to Jupiter-Family Comets:
 2360 The Spatial Distribution of Ecliptic Comets. *Icarus* 127, 13-32.
- 2361 Levison, H.F., Morbidelli, A., Vanlaerhoven, C., Gomes, R., Tsiganis, K. (2008). Origin
 2362 of the structure of the Kuiper belt during a dynamical instability in the
 2363 orbits of Uranus and Neptune. *Icarus* 196, 258-273.
- 2364 Levison, H.F., Bottke, W.F., Gounelle, M., Morbidelli, A., Nesvorny, D., Tsiganis, K.
 2365 (2009). Contamination of the asteroid belt by primordial trans-Neptunian
 2366 objects. *Nature* 460, 364-366.
- 2367 Levison, H.F., Morbidelli, A., Tsiganis, K., Nesvorny, D., Gomes, R. (2011).
 2368 Reevaluating the Early Dynamical Evolution of the Outer Planets. in
 2369 preparation
- 2370 Lin, D.N.C., Papaloizou, J. (1986). On the tidal interaction between protoplanets and
 2371 the protoplanetary disk. III - Orbital migration of protoplanets. *The*
 2372 *Astrophysical Journal* 309, 846-857.
- 2373 Lissauer, J.J. (1987). Timescales for planetary accretion and the structure of the
 2374 protoplanetary disk. *Icarus* 69, 249-265.
- 2375 Lodders, K., 2010. Solar system abundances of the elements, *Principles and*
 2376 *Perspectives in Cosmochemistry*. Springer Berlin Heidelberg.
- 2377 Lupton, J. E., 1983. Terrestrial Inert Gases: Isotope Tracer Studies and Clues to
 2378 Primordial Components in the Mantle. *Annual Review of Earth and Planetary*
 2379 *Sciences* **11**, 371-414.
- 2380 Lupton, J. E. and Craig, H., 1981. A Major Helium-3 Source at 15°S on the East
 2381 Pacific Rise. *Science* **214**, 13-18.
- 2382 Lux, G., 1987. The behavior of noble gases in silicate liquids: Solution, diffusion,
 2383 bubbles and surface effects, with applications to natural samples. *Geochimica et*
 2384 *Cosmochimica Acta* **51**, 1549-1560.
- 2385 Lyra, W., Paardekooper, S.J., Mac Low, M.M. (2010). Orbital Migration of Low-mass
 2386 Planets in Evolutionary Radiative Models: Avoiding Catastrophic Infall. *The*
 2387 *Astrophysical Journal* 715, L68-L73.
- 2388 Mackenzie, F. T. and Lerman, A., 2006. *Carbon in the geobiosphere*. Springer,
 2389 Dordrecht.
- 2390 Malhotra, R. (1995). The Origin of Pluto's Orbit: Implications for the Solar System
 2391 Beyond Neptune. *The Astronomical Journal* 110, 420.
- 2392 Mann U., Frost D.J., Rubie D.C. (2009) Evidence for high-pressure core-mantle
 2393 differentiation from the metal-silicate partitioning of lithophile and weakly-
 2394 siderophile elements. *Geochimica et Cosmochimica Acta* 73, 7360-7386.

- 2395 Manning, C. V., McKay, C. P., and Zahnle, K. J., 2008. The nitrogen cycle on Mars:
 2396 Impact decomposition of near-surface nitrates as a source for a nitrogen
 2397 steady state. *Icarus* **197**, 60-64.
- 2398 Markowski, A., Leya, I., Quittè, G., Ammon, K., Halliday, A. N., and Wieler, R., 2006.
 2399 Correlated helium-3 and tungsten isotopes in iron meteorites: Quantitative
 2400 cosmogenic corrections and planetesimal formation times. *Earth and Planetary
 2401 Science Letters* **250**, 104-115.
- 2402 Marty, B., 1989. Neon and xenon isotopes in MORB: implications for the earth-
 2403 atmosphere evolution. *Earth and Planetary Science Letters* **94**, 45-56.
- 2404 Marty, B., 1995. Nitrogen content of the mantle inferred from N₂-Ar correlation in
 2405 oceanic basalts. *Nature* **377**, 326-329.
- 2406 Marty, B. 2012. The origins and concentrations of water, carbon, nitrogen and noble
 2407 gases on Earth. *Earth and Planetary Science Letters*, in press.
- 2408 Marty, B., Chaussidon, M., Wiens, R. C., Jurewicz, A. J. G., and Burnett, D. S., 2011. The
 2409 lowest ¹⁵N/¹⁴N end-member of the solar system is the Sun. *Lunar and
 2410 Planetary Science Conference* **42**, #1870.
- 2411 Marty, B. and Dauphas, N., 2002. Formation and early evolution of the atmosphere.
 2412 In: Fowler, C. M. R., Ebinger, C. J., and Hawkesworth, C. J. Eds.), *The Early Earth:
 2413 Physical, Chemical and Biological Development*.
- 2414 Marty, B. and Dauphas, N., 2003. The nitrogen record of crust-mantle interaction
 2415 and mantle convection from Archean to present. *Earth and Planetary Science
 2416 Letters* **206**, 397-410.
- 2417 Marty, B. and Meibom, A., 2007. Noble gas signature of the late heavy bombardment
 2418 in the Earth's atmosphere. *eEarth* **2**, 99-113.
- 2419 Marty, B., Palma, R. L., Pepin, R. O., Zimmermann, L., Schlutter, D. J., Burnard, P. G.,
 2420 Westphal, A. J., Snead, C. J., Bajt, S. a., Becker, R. H., and Simones, J. E., 2008.
 2421 Helium and Neon Abundances and Compositions in Cometary Matter. *Science*
 2422 **319**, 75-78.
- 2423 Marty, B., Tolstikhin, I., Kamensky, I. L., Nivin, E., Balaganskaya, E., and Zimmermann,
 2424 J. L., 1998. Plume-derived rare gases in 380 Ma carbonatites from the Kola
 2425 region (Russian) and the argon isotopic composition in the deep mantle. *Earth
 2426 and Planetary Science Letters* **164**, 179-192.
- 2427 Marty, B. and Yokochi, R., 2006. Water in the Early Earth. *Reviews in Mineralogy and
 2428 Geochemistry* **62**, 421-450.
- 2429 Marty, B. and Zimmerman, L., 1999. Volatiles (He, C, N, Ar) in mid-ocean ridge
 2430 basalts: assesment of shallow-level fractionation and characterization of
 2431 source composition. *Geochimica et Cosmochimica Acta* **63**, 3619-3633.
- 2432 Masset, F., Snellgrove, M. (2001). Reversing type II migration: resonance trapping of
 2433 a lighter giant protoplanet. *Monthly Notices of the Royal Astronomical Society*
 2434 **320**, L55-L59.
- 2435 Mazor, E., Heymann, D., and Anders, E., 1970. Noble gases in carbonaceous
 2436 chondrites. *Geochimica et Cosmochimica Acta* **34**, 781-824.
- 2437 McCubbin F.M., Steele A., Hauri E.H., Nekvasil H., Yamashita S., Hemley R.J, 2010,
 2438 Nominally hydrous magmatism on the Moon. *PNAS* **107**, 11223-11228.
- 2439 McDonough, W. F. and Sun, S. s., 1995b. The composition of the Earth. *Chemical
 2440 Geology* **120**, 223-253.

2441 McNaughton, N.J., Borthwick, J., Fallick, A.E., Pillinger, C.T. (1981).
 2442 Deuterium/hydrogen ratios in unequilibrated ordinary chondrites. *Nature*
 2443 294, 639-641.
 2444 Meech K.J. et al. (2011) EPOXI: Comet 103P/Hartley 2 observations from a
 2445 worldwide campaign. *The Astrophysical Journal Letters* 734, doi:1-
 2446 .1088/2041-8205/734/1/L1
 2447 Meier R., Owen T.C., Matthews H.E., Jewitt D.C., Bockelee-Morvan D., Biver N.,
 2448 Crovisier J. and Gautier D. (1998) A determination of the DHO/H₂O ratio in
 2449 Comet C/1995 O1 (Hale—Bopp). *Science*, 279, 842—844.
 2450 Meshik, A. P., Kehm, K., and Hohenberg, C. M., 2000. Anomalous xenon in zone 13
 2451 Okelobondo. *Geochimica et Cosmochimica Acta* **64**, 1651-1661.
 2452 Michael, P., 1995. Regionally distinctive sources of depleted MORB: evidence from
 2453 trace elements and H₂O. *Earth and Planetary Science Letters* **131**, 301-320.
 2454 Mojzsis, S. J., Harrison, T. M., and Pidgeon, R. T., 2001. Oxygen-isotope evidence from
 2455 ancient zircons for liquid water at the Earth's surface 4,300[thinsp]Myr ago.
 2456 *Nature* **409**, 178-181.
 2457 Montmessin, F., Fouchet, T., and Forget, F., 2005. Modeling the annual cycle of HDO
 2458 in the Martian atmosphere. *Journal of Geophysical Research* **110**,
 2459 doi:/10.1029/2004JE002357.
 2460 Moorbath, S., O'Nions, R. K., and Pankhurst, R. J., 1973. Early Archaean Age for the
 2461 Isua Iron Formation, West Greenland. *Nature* **245**, 138-139.
 2462 Morbidelli, A., Chambers, J., Lunine, J.I., Petit, J.M., Robert, F., Valsecchi, G.B., Cyr, K.E.
 2463 (2000). Source regions and time scales for the delivery of water to Earth.
 2464 *Meteoritics and Planetary Science* 35, 1309-1320.
 2465 Morbidelli, A., Petit, J.M., Gladman, B., Chambers, J. (2001). A plausible cause of the
 2466 late heavy bombardment. *Meteoritics and Planetary Science* 36, 371-380.
 2467 Morbidelli, A., Levison, H.F., Tsiganis, K., Gomes, R. (2005). Chaotic capture of
 2468 Jupiter's Trojan asteroids in the early Solar System. *Nature* 435, 462-465.
 2469 Morbidelli, A., Crida, A., Masset, F., Nelson, R.P. (2008). Building giant-planet cores at
 2470 a planet trap. *Astronomy and Astrophysics* 478, 929-937.
 2471 Morbidelli, A., Bottke, W.F., Nesvorny, D., Levison, H.F. (2009). Asteroids were born
 2472 big. *Icarus* 204, 558-573.
 2473 Morbidelli, A., Crida, A. (2007). The dynamics of Jupiter and Saturn in the gaseous
 2474 protoplanetary disk. *Icarus* 191, 158-171.
 2475 Morbidelli, A., Tsiganis, K., Crida, A., Levison, H.F., Gomes, R. (2007). Dynamics of the
 2476 Giant Planets of the Solar System in the Gaseous Protoplanetary Disk and Their
 2477 Relationship to the Current Orbital Architecture. *The Astronomical Journal*
 2478 134, 1790-1798.
 2479 Morbidelli, A., Brasser, R., Gomes, R., Levison, H.F., Tsiganis, K. (2010). Evidence
 2480 from the Asteroid Belt for a Violent Past Evolution of Jupiter's Orbit. *The*
 2481 *Astronomical Journal* 140, 1391-1401.
 2482 Morbidelli, A. (2010b). A coherent and comprehensive model of the evolution of the
 2483 outer Solar System. *Comptes Rendus Physique* 11, 651-659.
 2484 Moreira, M., Kunz, J., and All^v@gre, C., 1998. Rare Gas Systematics in Popping Rock:
 2485 Isotopic and Elemental Compositions in the Upper Mantle. *Science* **279**, 1178-
 2486 1181.

2487 Morgan, J. W., 1986. Ultramafic Xenoliths: Clues to Earth's Late Accretionary History.
2488 *J. Geophys. Res.* **91**, 12375-12387.

2489 Morishima, R., Stadel, J., Moore, B. (2010). From planetesimals to terrestrial planets:
2490 N-body simulations including the effects of nebular gas and giant planets.
2491 *Icarus* 207, 517-535.

2492 Morris, R. V., Ruff, S. W., Gellert, R., Ming, D. W., Arvidson, R. E., Clark, B. C., Golden, D.
2493 C., Siebach, K., Klingelhöfer, G. s., Schröder, C., Fleischer, I., Yen, A. S., and
2494 Squyres, S. W., 2010. Identification of Carbonate-Rich Outcrops on Mars by the
2495 Spirit Rover. *Science* **329**, 421-424.

2496 Mottl, M., Glazer, B. T., Kaiser, R. I., and Meech, K. J., 2007. Water and astrobiology.
2497 *Chemie Der Erde-Geochemistry* **67**, 253-282.

2498 Muralidharan, K., Deymier, P., Stimpfl, M., de Leeuw, N.H., Drake, M.J. (2008). Origin
2499 of water in the inner Solar System: A kinetic Monte Carlo study of water
2500 adsorption on forsterite. *Icarus* 198, 400-407.

2501 Muramatsu, Y. and Wedepohl, K. H., 1998. The distribution of iodine in the earth's
2502 crust. *Chemical Geology* **147**, 201-216.

2503 Nakamura, T., Noguchi, T., Tanaka, M., and al., 2011. Mineralogy and major element
2504 abundance of the dust particles recovered from Muses-C region on the asteroid
2505 Itokawa. *Lunar and Planetary Science Conference* **42**, 1766.

2506 Nesvorny, D., Vokrouhlicky, D., Morbidelli, A. (2007). Capture of Irregular Satellites
2507 during Planetary Encounters. *The Astronomical Journal* 133, 1962-1976.

2508 Nesvorny, D., Youdin, A.N., Richardson, D.C. (2010). Formation of Kuiper Belt
2509 Binaries by Gravitational Collapse. *The Astronomical Journal* 140, 785-793.

2510 Nesvorny, D., Jenniskens, P., Levison, H.F., Bottke, W.F., Vokrouhlicky, D., Gounelle,
2511 M. (2010b). Cometary Origin of the Zodiacal Cloud and Carbonaceous
2512 Micrometeorites. Implications for Hot Debris Disks. *The Astrophysical Journal*
2513 713, 816-836.

2514 Niles, P. B., Boynton, W. V., Hoffman, J. H., Ming, D. W., and Hamara, D., 2010. Stable
2515 isotope measurements of martian atmospheric CO₂ at the Phoenix landing site.
2516 *Science* **329**, 1334-1337.

2517 Notesco, G., Bar-Nun, A., and Owen, T., 2003. Gas trapping in water ice at very low
2518 deposition rates and implications for comets. *Icarus* **162**, 183-189.

2519 Notesco, G., Laufer, D., Bar-Nun, A., and Owen, T., 1999. An Experimental Study of the
2520 Isotopic Enrichment in Ar, Kr, and Xe When Trapped in Water Ice. *Icarus* **142**,
2521 298-300.

2522 Nutman, A. P., Mojzsis, S. J., and Friend, C. R. L., 1997. Recognition of >=3850 Ma
2523 water-lain sediments in West Greenland and their significance for the early
2524 Archaean Earth. *Geochimica et Cosmochimica Acta* **61**, 2475-2484.

2525 O'Brien, D.P., Morbidelli, A., Levison, H.F. (2006). Terrestrial planet formation with
2526 strong dynamical friction. *Icarus* 184, 39-58.

2527 O'Brien, D.P., Morbidelli, A., Bottke, W.F. (2007). The primordial excitation and
2528 clearing of the asteroid belt- Revisited. *Icarus* 191, 434-452.

2529 O'Brien, D.P., Walsh, K.J., Morbidelli, A., Raymond, S.N., Mandell, A.M., Bond, J.C.
2530 (2010). Early Giant Planet Migration in the Solar System: Geochemical and
2531 Cosmochemical Implications for Terrestrial Planet Formation. *Bulletin of the*
2532 *American Astronomical Society* 42, 948.

2533 O'Neil, J., Maurice, C., Stevenson, R. K., Larocque, J., Cloquet, C., David, J., Francis, D.,
2534 Martin J. van Kranendonk, R. H. S., and Vickie, C. B., 2007. Chapter 3.4 The
2535 Geology of the 3.8 Ga Nuvvuagittuq (Porpoise Cove) Greenstone Belt,
2536 Northeastern Superior Province, Canada, *Developments in Precambrian
2537 Geology*. Elsevier.

2538 Ott, U., 2002. Noble gases in meteorites - Trapped components. *Reviews in
2539 Mineralogy and Geochemistry* **47**, 71-100.

2540 Owen, T., Bar-Nun, A., and Kleinfeld, I., 1992. Possible cometary origin of heavy
2541 noble gases in the atmospheres of Venus, Earth and Mars. *Nature* **358**, 43-46.

2542 Owen, T., Biemann, K., Rushneck, D. R., Biller, J. E., Howarth, D. W., and Lafleur, A. L.,
2543 1977. The Composition of the Atmosphere at the Surface of Mars. *J. Geophys.
2544 Res.* **82**, 4635-4639.

2545 Ozima, M., 1975. Ar isotopes and Earth-atmosphere evolution models. *Geochimica et
2546 Cosmochimica Acta* **39**, 1127-1134.

2547 Ozima, M. and Podosek, F., 2001. *Noble Gas Geochemistry*. Cambridge University
2548 Press, Cambridge.

2549 Pepin, R., 2000a. On the Isotopic Composition of Primordial Xenon in Terrestrial
2550 Planet Atmospheres. *Space Science Reviews* **92**, 371-395.

2551 Pepin, R. O., 1991. On the origin and early evolution of terrestrial planet
2552 atmospheres and meteoritic volatiles. *Icarus* **92**, 2-79.

2553 Pepin, R. O., 1997. Evolution of Earth's Noble Gases: Consequences of Assuming
2554 Hydrodynamic Loss Driven by Giant Impact. *Icarus* **126**, 148-156.

2555 Pepin, R. O., 2000b. On the isotopic composition of primordial xenon in terrestrial
2556 planet atmospheres. *Space Science Reviews* **92**, 371-395.

2557 Pepin, R. O., 2006. Atmospheres on the terrestrial planets: Clues to origin and
2558 evolution. *Earth and Planetary Science Letters* **252**, 1-14.

2559 Pepin, R. O., Becker, R. H., and Rider, P. E., 1995. Xenon and krypton isotopes in
2560 extraterrestrial regolith solis and in the solar wind. *Geochimica et
2561 Cosmochimica Acta* **59**, 4997-5022.

2562 Petit, J.M., Morbidelli, A., Chambers, J. (2001). The Primordial Excitation and Clearing
2563 of the Asteroid Belt. *Icarus* **153**, 338-347.

2564 Pierens, A., Nelson, R.P. 2008. Constraints on resonant-trapping for two planets
2565 embedded in a protoplanetary disc. *Astronomy and Astrophysics* **482**, 333-
2566 340.

2567 Pineau F., Javoy M. (1983) Carbon isotopes and concentrations in mid-oceanic ridge
2568 basalts. *Earth and Planetary Science Letters* **62**, 239-257.

2569 Pollack, J. B., Kasting, J. F., Richardson, S. M., and Poliakov, K., 1987. The case for a
2570 wet, warm climate on early Earth. *Icarus* **71**, 203-224.

2571 Poreda R.J., Farley K.A. (1992) Rare gases in Samoan xenoliths. *Earth and Planetary
2572 Science Letters* **113**, 129-144,

2573 Puchtel I.S., Walker, R.J., James, O.B., Kring, D.A., 2008. Osmium isotope and highly
2574 siderophile element systematics of lunar impact melt breccias: implications for
2575 the late accretion history of the Moon and Earth. *Geochimica et Cosmochimica
2576 Acta* **72**, 3022-3042.

2577 Pujol M., Marty B., Burgess R. (2011) Chondritic-like xenon trapped in Archean
2578 rocks: a possible signature of the ancient atmosphere. *Earth and Planetary*
2579 *Science Letters* 308, 298-306.

2580 Qin, L. P., Dauphas, N., Wadhwa, M., Masarik, J., and Janney, P. E., 2008. Rapid
2581 accretion and differentiation of iron meteorite parent bodies inferred from Hf-
2582 182-W-182 chronometry and thermal modeling. *Earth and Planetary Science*
2583 *Letters* **273**, 94-104. Qin, L., Alexander, C.M.O.'D., Carlson, R.W., Horan, M.F.,
2584 Yokoyama, T. (2010) Contributors to chromium isotope variation of
2585 meteorites. *Geochimica et Cosmochimica Acta* 74, 1122-1145.

2586

2587 Rao, M. N., Bogard, D. D., Nyquist, L. E., McKay, D. S., and Masarik, J., 2002. Neutron
2588 capture isotopes in the martian regolith and implication for martian
2589 atmospheric noble gases. *Icarus* **156**, 352-372.

2590 Raquin, A. and Moreira, M., 2009. Atmospheric $^{38}\text{Ar}/^{36}\text{Ar}$ in the mantle:
2591 Implications for the nature of the terrestrial parent bodies. *Earth and Planetary*
2592 *Science Letters* **287**, 551-558.

2593 Raymond, S.N., Quinn, T., Lunine, J.I. (2004). Making other earths: dynamical
2594 simulations of terrestrial planet formation and water delivery. *Icarus* 168, 1-
2595 17.

2596 Raymond, S.N., Quinn, T., Lunine, J.I. (2005). Terrestrial Planet Formation in Disks
2597 with Varying Surface Density Profiles. *The Astrophysical Journal* 632, 670-676.

2598 Raymond, S.N., Quinn, T., Lunine, J.I. (2006). High-resolution simulations of the final
2599 assembly of Earth-like planets I. Terrestrial accretion and dynamics. *Icarus*
2600 183, 265-282.

2601 Raymond, S.N., Quinn, T., Lunine, J.I. (2007). High-Resolution Simulations of The
2602 Final Assembly of Earth-Like Planets. 2. Water Delivery And Planetary
2603 Habitability. *Astrobiology* 7, 66-84.

2604 Raymond, S.N., O'Brien, D.P., Morbidelli, A., Kaib, N.A. (2009). Building the
2605 terrestrial planets: Constrained accretion in the inner Solar System. *Icarus* 203, 644-
2606 662.

2607 Raymond, S. N., 2010. Formation of terrestrial planets. In: Barnes, R. (Ed.),
2608 *Formation and Evolution of Exoplanets*. Wiley, Weinheim, Germany.

2609 Richards, M. A., Yang, W.-S., Baumgardner, J. R., and Bunge, H.-P., 2001. Role of a low-
2610 viscosity zone in stabilizing plate tectonics: implications for comparative
2611 terrestrial planetology. *Geochemistry Geophysics Geosystems* **2**, 2000GC000115.

2612 Rivkin, A.S., Emery, J.P. (2010). Detection of ice and organics on an asteroidal
2613 surface. *Nature* 464, 1322-1323.

2614 Robert, F., Merlivat, L., Javoy, M. (1977). Water and Deuterium Content in Eight
2615 Condrites. *Meteoritics* 12, 349-356.

2616 Robert, F., Merlivat, L., Javoy, M. (1979). Deuterium concentration in the early solar
2617 system - Hydrogen and oxygen isotope study. *Nature* 282, 785-789.

2618 Robert F. and Epstein S. (1982). The concentration of isotopic compositions of
2619 hydrogen carbon and nitrogen in carbonaceous chondrites. *Geochim.*
2620 *Cosmochim. Acta*, 16, 81-95

2621 Robert, F. (2003). The D/H Ratio in Chondrites. *Space Science Reviews* 106, 87-101.

- 2622 Robert, F., Gautier, D., and Dubrulle, B., 2000. The solar system D/H ratio:
2623 observations and theories. *Space Science Reviews* **92**, 201-224.
- 2624 Robinson, T. D., Meadows, V. S., and Crisp, D., 2010. Detecting oceans on extrasolar
2625 planets using the glint effect. *The Astrophysical Journal Letters* **721**, L67-L71.
- 2626 Rudnick, R. L. and Gao, S., 2003. Composition of the continental crust. In: Holland, H.
2627 D. and Turekian, K. K. Eds.), *Treatise on Geochemistry*. Elsevier.
- 2628 Saal, A. E., Hauri, E. H., Langmuir, C. H., and Perfit, M. R., 2002. Vapour
2629 undersaturation in primitive mid-ocean-ridge basalt and the volatile content of
2630 Earth's upper mantle. *Nature* **419**, 451-455.
- 2631 Saal, A.E., Hauri E.H., Cascio M.L., Van Orman J.A. (2008) Volatile content of lunar
2632 volcanic glasses and the presence of water in the Moon's interior. *Nature* **454**,
2633 192-195.
- 2634 Saal A.E., Hauri E.H., Rutherford M.J., van Orman J. (2011) The volatile content and
2635 D/H ratios of the lunar picritic glasses, Wet vs Dry Moon conference, abstract
2636 #6034.
- 2637 Sandor, Z., Lyra, W., Dullemond, C.P. 2011. Formation of Planetary Cores at Type I
2638 Migration Traps. *The Astrophysical Journal* **728**, L9.
- 2639
- 2640 Sanloup, C. l., Schmidt, B. C., Perez, E. M. C., Jambon, A., Gregoryanz, E., and Mezouar,
2641 M., 2005. Retention of Xenon in Quartz and Earth's Missing Xenon. *Science* **310**,
2642 1174-1177.
- 2643 Sarda, P., Staudacher, T., and Allègre, C. J., 1988. Neon isotopes in submarine basalts.
2644 *Earth and Planetary Science Letters* **91**, 73-88.
- 2645 Sasaki, S. and Nakazawa, K., 1988. Origin of isotopic fractionation of terrestrial Xe:
2646 hydrodynamic fractionation during escape of the primordial H₂He
2647 atmosphere. *Earth and Planetary Science Letters* **89**, 323-334.
- 2648 Schoenberg, R., Kamber, B. S., Collerson, K. D., and Eugster, O., 2002. New W-isotope
2649 evidence for rapid terrestrial accretion and very early core formation.
2650 *Geochimica et Cosmochimica Acta* **66**, 3151-3160.
- 2651 Scott, E.R.D. (2006). Meteoritical and dynamical constraints on the growth
2652 mechanisms and formation times of asteroids and Jupiter. *Icarus* **185**, 72-82.
- 2653 Scott, P. C., Asplund, M., Grevesse, N., and Sauval, A. J., 2006. Line formation in solar
2654 granulation. VII. CO lines and the solar C and O isotopic abundances. *Astronomy
& Astrophysics* **456**, 675-688.
- 2655
- 2656 Shukolyukov, Y. A., Jessberger, E. K., Meshik, A. P., Vu Minh, D., and Jordan, J. L., 1994.
2657 Chemically fractionated fission-xenon in meteorites and on the earth.
2658 *Geochimica et Cosmochimica Acta* **58**, 3075-3092.
- 2659 Simon, S. B., Joswiak, D. J., Ishii, H. A., Bradley, J. P., Chi, M., Grossman, L., AlÉon, J.,
2660 Brownlee, D. E., Fallon, S., Hutcheon, I. D., Matrajt, G., and McKeegan, K. D.,
2661 2008. A refractory inclusion returned by Stardust from comet 81P/Wild 2.
2662 *Meteoritics & Planetary Science* **43**, 1861-1877.
- 2663 Sotin, C., Mitri, G., Rappaport, N., Schubert, G., Stevenson, D. (2010). Titan's Interior
2664 Structure. Titan from Cassini-Huygens 61-73.
- 2665 Staudacher, T. and Allègre, C. J., 1982. Terrestrial xenology. *Earth and Planetary
2666 Science Letters* **60**, 389-406.

2667 Stracke, A., Bizimis, M., and Salters, J. M., 2003. Recycling oceanic crust: Quantitative
2668 constraints. *Geochemistry Geophysics Geosystems* **4**,
2669 doi:10.1029/2001GC000223.

2670 Stuart, F. M., Lass-Evans, S., Godfrey Fitton, J., and Ellam, R. M., 2003. High $^3\text{He}/^4\text{He}$
2671 ratios in picritic basalts from Baffin Island and the role of a mixed reservoir in
2672 mantle plumes. *Nature* **424**, 57-59.

2673 Sumino H., Burgess R., Mizukami T., Wallis S.R., Holland G., Ballentine C.J. (2010)
2674 Seawater-derived noble gases and halogens in exhumed mantle wedge
2675 peridotite. *Earth and Planetary Science Letters* **294**, 163-172.

2676 Sundquist, E. T. and Visser, K., 2003. The geologic history of the carbon cycle. In:
2677 Holland, H. D. and Turekian, K. K. Eds.), *Treatise on Geochemistry*. Elsevier.

2678 Sunshine, J.M., and 22 colleagues (2006). Exposed Water Ice Deposits on the Surface
2679 of Comet 9P/Tempel 1. *Science* **311**, 1453-1455.

2680 Swindle, T. D., Caffee, M. W., and Hohenberg, C. M., 1986. Xenon and other noble
2681 gases in Shergottites. *Geochimica et Cosmochimica Acta* **50**, 1001-1015.

2682 Swindle, T. D. and Jones, J. H., 1997. The xenon isotopic composition of the
2683 primordial Martian atmosphere: Contributions from solar and fission
2684 components. *J. Geophys. Res.* **102**, 1671-1678.

2685 Tera, F., Papanastassiou, D. A., and Wasserburg, G. J., 1974. Isotopic evidence for a
2686 terminal lunar cataclysm. *Earth and Planetary Science Letters* **22**, 1-21.

2687 Tian, F., Toon, O. B., Pavlov, A. A., and De Sterck, H., 2005. Transonic hydrodynamic
2688 escape of hydrogen from extrasolar planetary atmospheres. *The Astrophysical*
2689 *Journal* **621**, 1049-1060.

2690 Tolstikhin, I. and Hofmann, A. W., 2005. Early crust on top of the Earth's core.
2691 *Physics of The Earth and Planetary Interiors* **148**, 109-130.

2692 Tolstikhin, I. and Kramers, J., 2008. *The evolution of matter: from the big bang to the*
2693 *present day*. Cambridge University Press, Cambridge.

2694 Tolstikhin, I. N. and O'Nions, R. K., 1994. The Earth's missing xenon: A combination
2695 of early degassing and of rare gas loss from the atmosphere. *Chemical Geology*
2696 **115**, 1-6.

2697 Touboul, M., Kleine, T., Bourdon, B., Palme, H., and Wieler, R., 2007. Late formation
2698 and prolonged differentiation of the Moon inferred from W isotopes in lunar
2699 metals. *Nature* **450**, 1206-1209.

2700 Trieloff, M., Kunz, J., Clague, D. A., Harrison, D., and Allègre, C. J., 2000. The Nature
2701 of Pristine Noble Gases in Mantle Plumes. *Science* **288**, 1036-1038.

2702 Trieloff M., Kunz J., Allegre C.J. (2002) Noble gas systematics of the Reunion mantle
2703 plume source and the origin of primordial noble gases in Earth's mantle. *Earth*
2704 *and Planetary Science Letters* **200**, 297-313.

2705 Trinquier, A., Birck, J.-L., and Allegre, C. J., 2007. Widespread ^{54}Cr heterogeneity in
2706 the inner solar system. *The Astrophysical Journal* **655**, 1179-1185.

2707 Trinquier, A., Elliott, T., Ulfbeck, D., Coath, C., Krot, A. N., and Bizzarro, M., 2009.
2708 Origin of Nucleosynthetic Isotope Heterogeneity in the Solar Protoplanetary
2709 Disk. *Science* **324**, 374-376.

2710 Tsiganis, K., Gomes, R., Morbidelli, A., Levison, H.F. (2005). Origin of the orbital
2711 architecture of the giant planets of the Solar System. *Nature* **435**, 459-461.

2712 Turner, G. (1989) The outgassing history of the Earth's atmosphere. *Journal of the*
2713 *Geological Society* **146**, 147-154.

2714 Valbracht, P. J., Staudacher, A., Malahoff, A., and Allegre, C. J., 1997a. Noble gas
2715 systematics of deep rift zone glasses from Loihi Seamount, Hawaii. *Earth and*
2716 *Planetary Science Letters* **150**, 399-411.

2717 Valbracht, P. J., Staudacher, T., Malahoff, A., and Allegre, C. J., 1997b. Noble gas
2718 systematics of deep rift zone glasses from Loihi Seamount, Hawaii. *Earth and*
2719 *Planetary Science Letters* **150**, 399-411.

2720 Vidal-Madjar, A., des Etangs, A. L., Desert, J. M., Ballester, G. E., Ferlet, R., Hebrard, G.,
2721 and Mayor, M., 2003. An extended upper atmosphere around the extrasolar
2722 planet HD209458b. *Nature* **422**, 143-146.

2723 Villeneuve, J., Chaussidon, M., and Libourel, G., 2009. Homogeneous Distribution of
2724 ²⁶Al in the Solar System from the Mg Isotopic Composition of Chondrules.
2725 *Science* **325**, 985-988.

2726 Von Zahn, U., Kumar, S., Niemann, H., and Prinn, R., 1983. Composition of the Venus
2727 atmosphere. In: Hunten, D. M., Colin, L., Donahue, T. M., and Moroz, V. I. Eds.),
2728 *Venus*. University of Arizona Press, Tucson, AZ.

2729 Walker, R. J., 2009. Highly siderophile elements in the Earth, Moon and Mars: Update
2730 and implications for planetary accretion and differentiation. *Chemie der Erde -*
2731 *Geochemistry* **69**, 101-125.

2732 Walsh, K.J., Morbidelli, A., Raymond, S.N., O'brien, D.P., Mandell, A.M. (2011)
2733 Sculpting of the inner Solar System by gas-driven orbital migration of Jupiter.
2734 *Nature*, in press.

2735 Ward, W.R. (1997). Protoplanet Migration by Nebula Tides. *Icarus* **126**, 261-281.

2736 Weidenschilling, S.J. (1977). Aerodynamics of solid bodies in the solar nebula.
2737 *Monthly Notices of the Royal Astronomical Society* **180**, 57-70.

2738

2739

2740 Wetherill, G. W., 1975. Radiometric Chronology of the Early Solar System. *Annual*
2741 *Review of Nuclear Science* **25**, 283-328.

2742 Wetherill, G.W. (1989). Origin of the asteroid belt. *Asteroids II* 661-680.

2743 Wieler, R., 2002. Noble gases in the solar system. *Reviews in Mineralogy and*
2744 *Geochemistry* **47**, 2-70.

2745 Wilde, S. A., Valley, J. W., Peck, W. H., and Graham, C. M., 2001. Evidence from detrital
2746 zircons for the existence of continental crust and oceans on the Earth
2747 4.4[thinsp]Gyr ago. *Nature* **409**, 175-178.

2748 Wilhelms D.L., McCannley J.F. and Trask N.J. (1987) The geologic history of the
2749 Moon. U.S. Geological survey professional paper, 1348.

2750 Williams, D. M. and Gaidos, E., 2008. Detecting the glint of starlight on the oceans of
2751 distant planets. *Icarus* **195**, 927-937.

2752 Wood B.J., Halliday A.N., Rehkamper M. (2010) Volatile accretion history of the
2753 Earth. *Nature* **467**, E6-E7.

2754 Workman, R. K. and Hart, S. R., 2005a. Major and trace element composition of the
2755 depleted MORB mantle (DMM). *Earth and Planetary Science Letters* **231**, 53-72.

2756 Workman, R. K. and Hart, S. R., 2005b. Major and trace element composition of the
2757 depleted MORB mantle (DMM). *Earth and Planetary Science Letters* **231**, 53-72.

2758 Yatsevich, I. and Honda, M., 1997. Production of nucleogenic neon in the Earth from
2759 natural radioactive decay. *J. Geophys. Res.* **102**, 10291-10298.
2760 Yin, Q., Jacobsen, S. B., Yamashita, K., Blichert-Toft, J., Telouk, P., and Albarede, F.,
2761 2002. A short timescale for terrestrial planet formation from Hf-W
2762 chronometry of meteorites. *Nature* **418**, 949-952.
2763 Yokochi, R. and Marty, B., 2004. A determination of the neon isotopic composition of
2764 the deep mantle. *Earth and Planetary Science Letters* **225**, 77-88.
2765 Yokochi, R. and Marty, B., 2005. Geochemical constraints on mantle dynamics in the
2766 Hadean. *Earth and Planetary Science Letters* **238**, 17-30.
2767 Zahnle, K. J. and Kasting, J. F., 1986. Mass fractionation during transonic escape and
2768 implications for loss of water from Mars and Venus. *Icarus* **68**, 462-480.
2769 Zahnle, K. J. and Walker, J. C. G., 1982. The evolution of solar ultraviolet luminosity.
2770 *Rev. Geophys.* **20**, 280-292.
2771 Zahnle, K.J. (2000) Hydrodynamic escape of ionized xenon from ancient
2772 atmospheres. American Astronomical Society DPS Meeting #32, Buletin of the
2773 American Astronomical Society 32, 1044.
2774 Zhang, Y., 1998. The young age of Earth. *Geochimica et Cosmochimica Acta* **62**, 3185-
2775 3189.
2776 Zhang, Y. and Zindler, A., 1989. Noble Gas Constraints on the Evolution of the Earth's
2777 Atmosphere. *J. Geophys. Res.* **94**, 13719-13737.
2778 Zolensky, M.E., and 74 colleagues (2006). Mineralogy and Petrology of Comet
2779 81P/Wild 2 Nucleus Samples. *Science* 314, 1735-1739.
2780

Table 1. Major volatile element abundances and isotopic ratios in Earth (excluding the core)

	H (mol)	δD_{VSMOW} (‰)	D/H	C (mol)	$\delta^{13}C_{VPDB}$ (‰)	$^{13}C/^{12}C$	N (mol)	$\delta^{15}N_{air}$ (‰)	$^{15}N/^{14}N$
Atmosphere (5.1×10^{18} kg)				6.60 (16)	-8	0.01115	2.82 (20)	0	0.003677
Hydrosphere (1.6×10^{21} kg)	1.80 (23)	-6	0.000155	3.20 (18)	0	0.01124	1.47 (18)	6	0.003699
Biosphere (1.6×10^{18} kg)	1.51 (20)	-100	0.000140	6.06 (16)	-25	0.01096	7.50 (14)	0	0.003677
Crust (2.8×10^{22} kg)	3.43 (22)	-75	0.000144	6.78 (21)	-4	0.01119	7.14 (19)	6	0.003699
Surface reservoirs (A+H+B+C)	2.15 (23)	-17	0.000153	6.78 (21)	-4	0.01119	3.55 (20)	1	0.003681
Mantle (4.0×10^{24} kg)	3.05 (23)	-80	0.000143	2.70 (22)	-5	0.01118	3.15 (20)	3	0.003688
Total Earth (5.97×10^{24} kg)	5.20 (23)	-54	0.000147	3.38 (22)	-5	0.01118	6.70 (20)	2	0.003684

Notes. Powers of ten multipliers in parentheses. See text for details and references.

$\delta D_{VSMOW} = [(D/H)/(D/H)_{VSMOW} - 1] \times 1000$; $\delta^{13}C_{VPDB} = [(^{13}C/^{12}C)/(^{13}C/^{12}C)_{VPDB} - 1] \times 1000$; $\delta^{15}N_{air} = [(^{15}N/^{14}N)/(^{15}N/^{14}N)_{air} - 1] \times 1000$.

Table 2. Abundances of H, C, N, and noble gases in solar and selected planetary reservoirs (in mol/g).

	¹ H	¹² C	¹⁴ N		²⁰ Ne	³⁶ Ar	⁸⁴ Kr	¹³⁰ Xe
Solar	7.112 (-01)	1.95 (-04)	5.80 (-05)		8.40 (-05)	2.15 (-06)	8.72 (-10)	6.42 (-12)
Venus (surface)	1.4 (-10)	2.2 (-06)	1.6 (-07)		1.6 (-11)	6.8 (-11)	6.10 (-14)	<3.7 (-15)
Earth	8.70 (-05)	5.60 (-06)	1.12 (-07)		4.87 (-13)	9.29 (-13)	1.92 (-14)	1.05 (-16)
Mars (surface)	9 (-07)	8.6 (-10)	4.8 (-11)		7.9 (-16)	8.10 (-15)	1.80 (-16)	1.30 (-18)
CI chondrites	6.7 (-03)	3.1 (-03)	1.1 (-04)		1.64 (-11)	4.33 (-11)	4.78 (-13)	6.47 (-14)
Comets	6.7 (-02)	1.4 (-02)	2.9 (-03)	From trapping 30 K	1.68 (-05)	1.30 (-04)	5.25 (-08)	3.87 (-10)
				experiments 35	<1.68 (-05)	4.60 (-05)	1.07 (-07)	4.76 (-10)
				40	<1.68 (-05)	1.71 (-05)	1.35 (-07)	4.14 (-10)
				45	<1.68 (-05)	6.21 (-06)	8.33 (-08)	2.33 (-10)
				50	<3.34 (-08)	2.25 (-06)	5.13 (-08)	1.28 (-10)
				55	<3.34 (-08)	8.19 (-07)	3.89 (-08)	7.54 (-11)
				60	<3.34 (-08)	2.97 (-07)	4.47 (-08)	7.37 (-11)
				65	<3.34 (-08)	1.10 (-07)	2.40 (-08)	8.27 (-11)
				70	<3.34 (-08)	4.01 (-08)	1.29 (-08)	9.28 (-11)

Notes. Powers of ten multipliers in parentheses. See text for details and references.

Solar in mol/g-Solar composition; Venus, Earth, and Mars in mol/g-Planet; CI chondrites in mol/g-Meteorite; Comets in mol/g-Comet (ice+dust).

Table 3. Isotopic compositions of major volatile elements and nobles gases in planetary reservoirs.

Major volatile elements, neon, and argon												
	D/H	δD (‰)	$^{13}C/^{12}C$	$\delta^{13}C$ (‰)	$^{15}N/^{14}N$	$\delta^{15}N$ (‰)	$^{20}Ne/^{22}Ne$	$^{21}Ne/^{22}Ne$	F_{Ne} (‰/amu)	$^{38}Ar/^{36}Ar$	$^{40}Ar/^{36}Ar$	F_{Ar} (‰/amu)
Solar (4.56 Ga)	0.000025	-839	0.0115	25	0.00218	-408	13.78	0.0329	0	0.1828	0.000284	0
Venus (surface)	0.024454	156000	0.0113	8	0.00366	-4	11.8		84	0.180	1.1	-8
Earth	0.000147	-54	0.01118	-5	0.003684	2	9.80	0.0290	203	0.1880	295.5	14
Mars (surface)	0.001012	5500	0.01121	-2.5	0.00596	620	7		484	0.26	1800	201
CI chondrites	0.000181	161	0.01112	-10	0.003831	42	9.0	0.03	266	0.185	<0.12	6
Comets Oort-cloud	0.000308	977	0.0107	-48	0.0068	850	solar?			solar?		
Comets Kuiper-belt	0.000161	34	0.0105	-63	0.00645	755	solar?			solar?		
Krypton												
	^{78}Kr	^{80}Kr	^{82}Kr	^{83}Kr	^{84}Kr	^{86}Kr	F_{Kr} (‰/amu)					
Solar	0.6365	4.088	20.482	20.291	100	30.24	0					
Earth	0.6087	3.9599	20.217	20.136	100	30.524	8					
Mars		4.32	20.99	20.58	100	29.75	-14					
CI chondrites	0.5962	3.919	20.149	20.141	100	30.95	7					
Comets	solar?											
Xenon												
	^{124}Xe	^{126}Xe	^{128}Xe	^{129}Xe	^{130}Xe	^{131}Xe	^{132}Xe	^{134}Xe	^{136}Xe	F_{Xe} (‰/amu)		
Solar	2.939	2.549	51.02	627.3	100	498	602.0	220.68	179.71	0		
Earth	2.337	2.180	47.15	649.6	100	521.3	660.7	256.3	217.6	38		
Mars	2.5	2.2	47.6	1555	100	513.9	648.1	259.7	227.7	33		
CI chondrites	2.851	2.512	50.73	654.2	100	504.3	615.0	235.9	198.8	3		
Comets	solar/fractionated?											

Notes. Powers of ten multipliers in parentheses. See text for details and references.

$\delta D_{VSMOW} = [(D/H)/(D/H)_{VSMOW} - 1] \times 1000$; $\delta^{13}C_{VPDB} = [(^{13}C/^{12}C)/(^{13}C/^{12}C)_{VPDB} - 1] \times 1000$; $\delta^{15}N_{air} = [(^{15}N/^{14}N)/(^{15}N/^{14}N)_{air} - 1] \times 1000$.

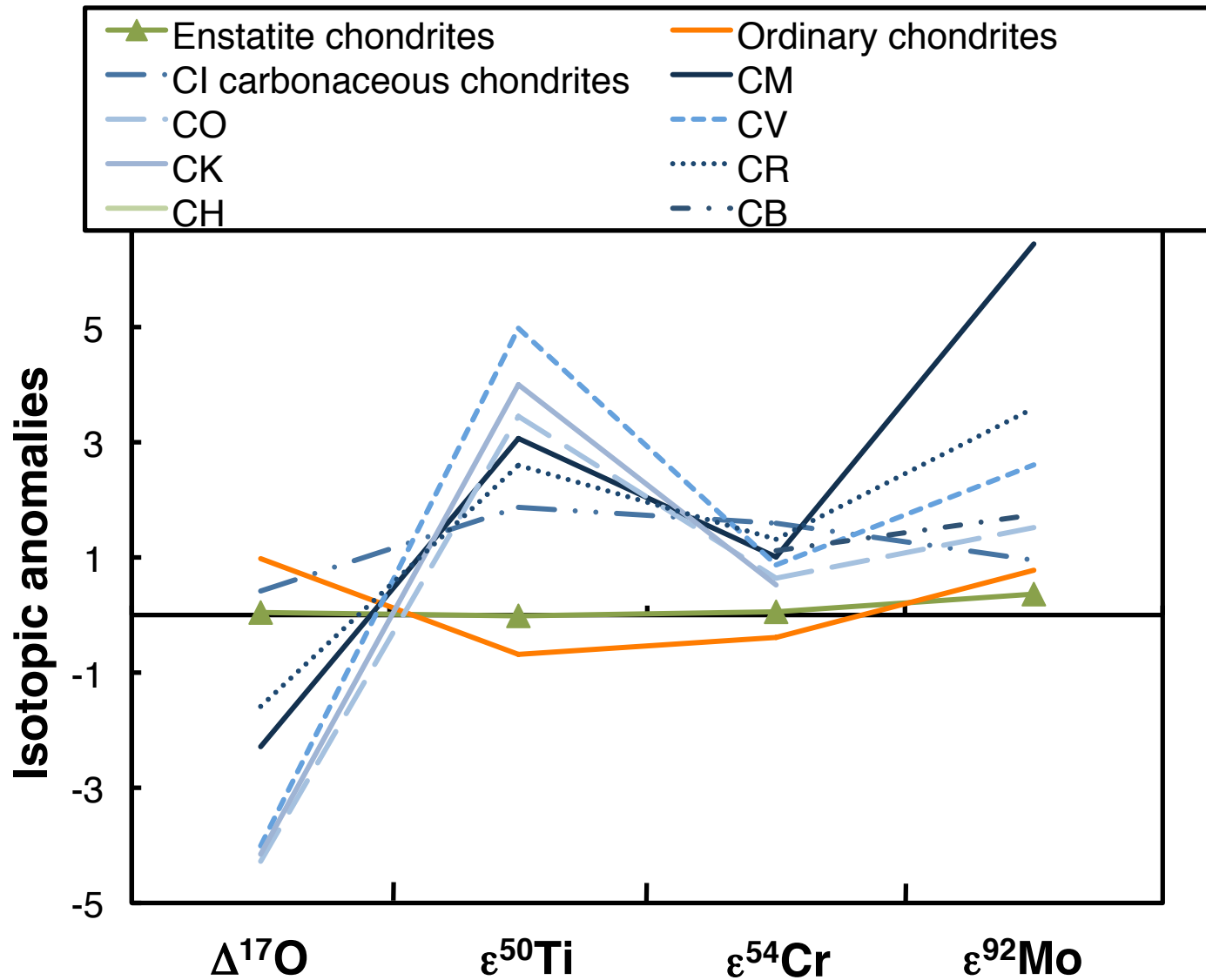
$F_E = [(^{i,j}E)_{reservoir}/(^{i,j}E)_{solar} - 1] \times 1000$, where (i,j)=(22,20) for Ne; (38,36) for Ar; (83,84) for Kr; (128,130) for Xe.

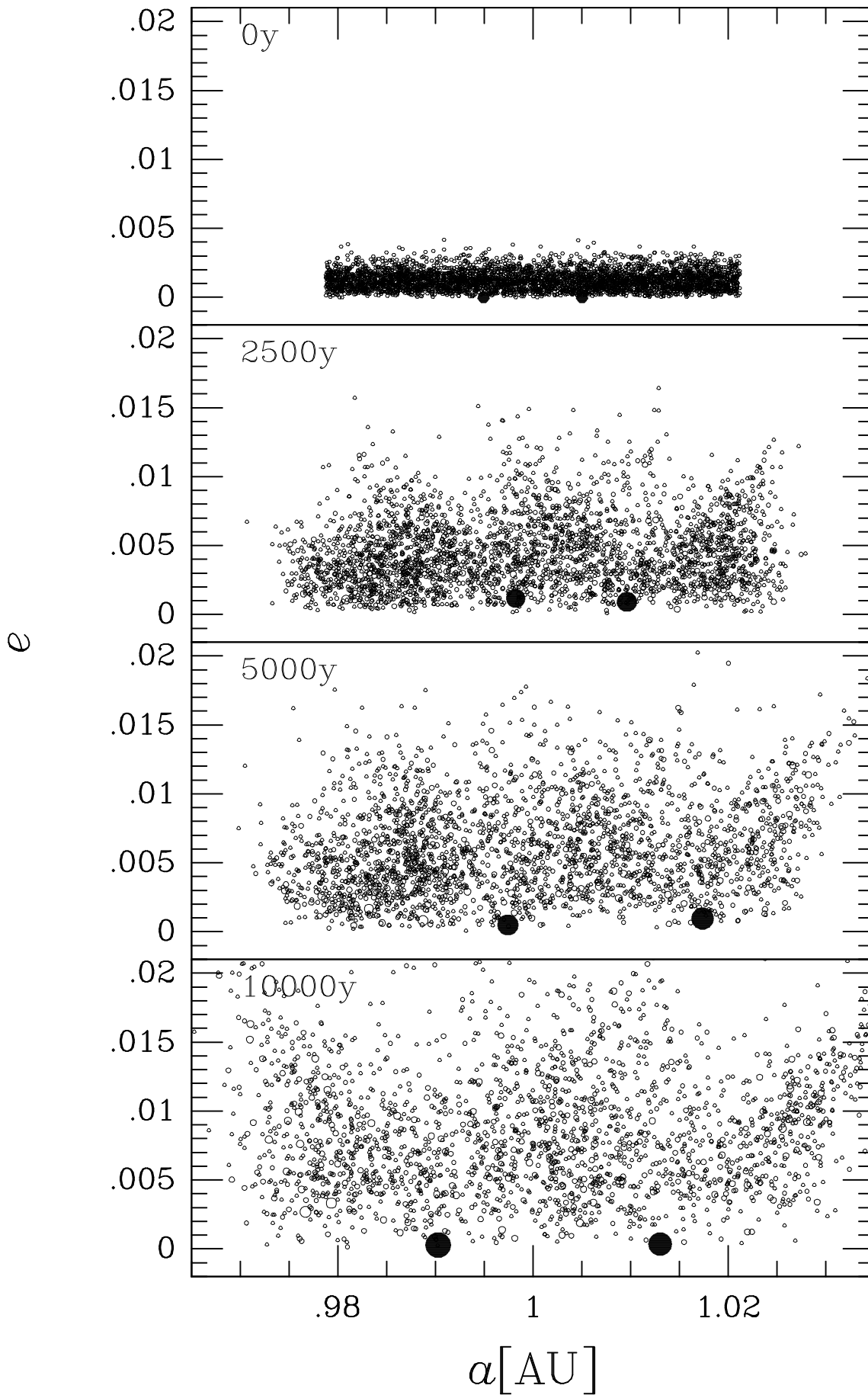
Table 4. Proposed volatile element composition of the depleted mantle

^1H	^{12}C	^{14}N	^3He	^{20}Ne	^{36}Ar	^{84}Kr	^{130}Xe
1.2 (-5)	1.8 (-6)	6.9 (-9)	8.4 (-16)	2.1 (-15)	2.1 (-15)	6.0 (-17)	1.1 (-18)
D/H	$^{13}\text{C}/^{12}\text{C}$	$^{15}\text{N}/^{14}\text{N}$	$^4\text{He}/^3\text{He}$	$^{20}\text{Ne}/^{22}\text{Ne}$	$^{21}\text{Ne}/^{22}\text{Ne}$	$^{38}\text{Ar}/^{36}\text{Ar}$	$^{40}\text{Ar}/^{36}\text{Ar}$
0.000143	0.01118	0.003659	99,000	12.49	0.0578	0.188	25,000
$^{78}\text{Kr}/^{84}\text{Kr}$	$^{80}\text{Kr}/^{84}\text{Kr}$	$^{82}\text{Kr}/^{84}\text{Kr}$	$^{83}\text{Kr}/^{84}\text{Kr}$	$^{86}\text{Kr}/^{84}\text{Kr}$			
0.00595	0.03901	0.2007	0.2006	0.3075			
$^{124}\text{Xe}/^{130}\text{Xe}$	$^{126}\text{Xe}/^{130}\text{Xe}$	$^{128}\text{Xe}/^{130}\text{Xe}$	$^{129}\text{Xe}/^{130}\text{Xe}$	$^{131}\text{Xe}/^{130}\text{Xe}$	$^{132}\text{Xe}/^{130}\text{Xe}$	$^{134}\text{Xe}/^{130}\text{Xe}$	$^{136}\text{Xe}/^{130}\text{Xe}$
0.02452	0.0225	0.479	7.6	5.37	6.99	2.79	2.55

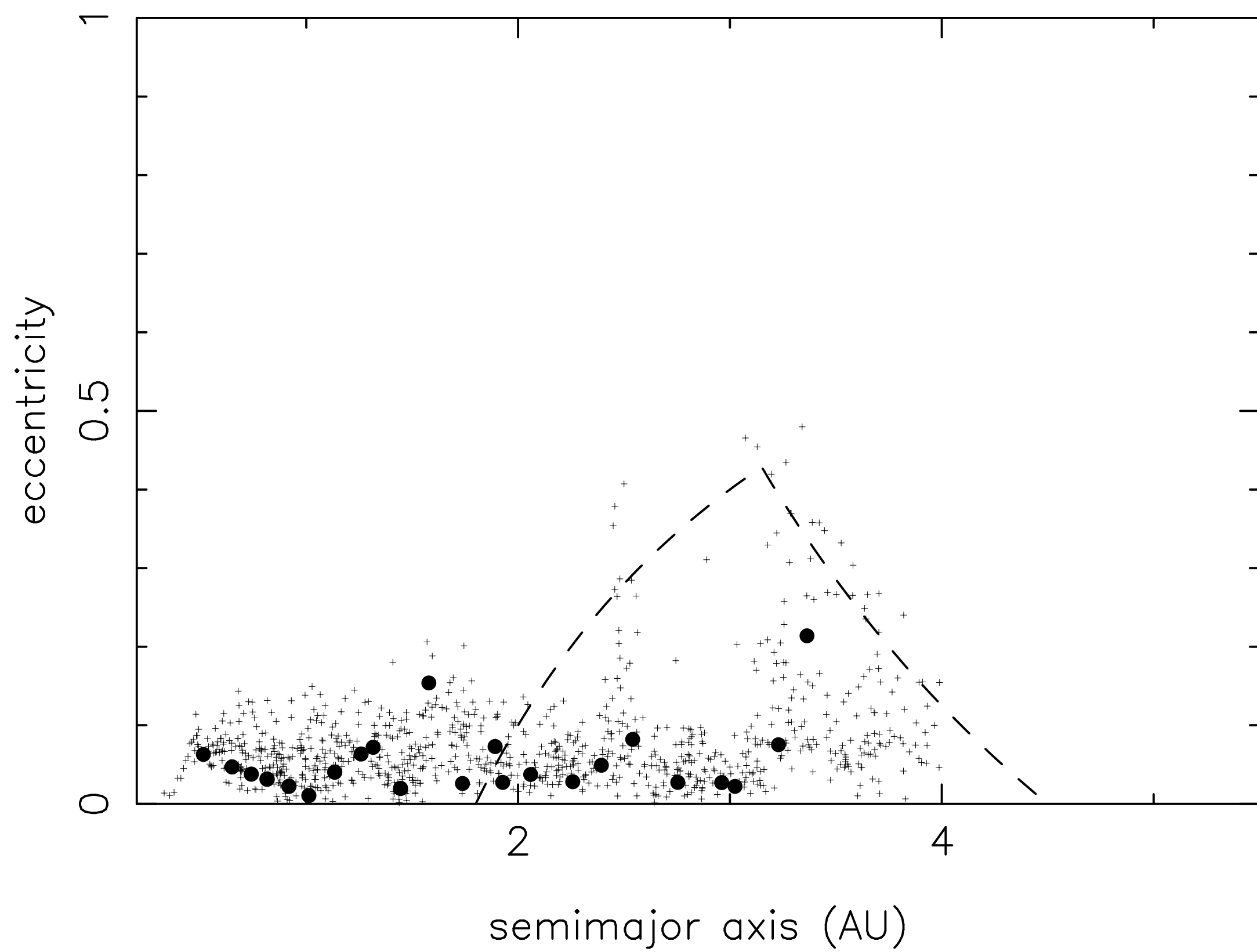
The concentrations are in mol/g of rock. The ^3He concentration was calculated by using the ^3He flux at ridges (Bianchi et al. 2010), 21 km³/year MORB production and 10 % partial melting. The $^4\text{He}/^3\text{He}$ ratio corresponds to the mode in the distribution of MORB values (7.3 R_A).

The Ne isotopic composition is from Holland and Ballentine (2006). ^{20}Ne , ^{36}Ar , ^{84}Kr , ^{130}Xe concentrations as well as $^{40}\text{Ar}/^{36}\text{Ar}$ and $^{129}\text{Xe}/^{130}\text{Xe}$ ratios are from Moreira et al. (1998) assuming a $^{20}\text{Ne}/^{22}\text{Ne}$ ratio of ~12.5. Major volatile element concentrations and isotopic compositions are from Sect. 3.1 (i.e., 110 ppm H₂O, 79 ppm CO₂, 0.1 ppm N₂). The $^{38}\text{Ar}/^{36}\text{Ar}$ ratio is the air value. The fissionogenic Xe isotopes ^{131}Xe , ^{132}Xe , ^{134}Xe , and ^{136}Xe are obtained from correlations with $^{129}\text{Xe}/^{130}\text{Xe}$ (the later ratio is taken to be 7.6), see Kunz et al. 1998. The $^{128}\text{Xe}/^{130}\text{Xe}$ ratio is obtained by regressing the CO₂ well gas data (Caffee et al. 1999, Holland and Ballentine 2006) to a $^{129}\text{Xe}/^{130}\text{Xe}$ ratio of 7.6. The $^{124}\text{Xe}/^{130}\text{Xe}$ and $^{126}\text{Xe}/^{130}\text{Xe}$ ratios are calculated assuming similar isotopic fractionation as $^{128}\text{Xe}/^{130}\text{Xe}$ relative to air. The $^{82}\text{Kr}/^{84}\text{Kr}$ ratio is obtained by regressing the data to a $^{128}\text{Xe}/^{130}\text{Xe}$ of 0.479 (Holland et al. 2009) and the inferred isotopic fractionation is applied to other Kr isotopes using an exponential law.

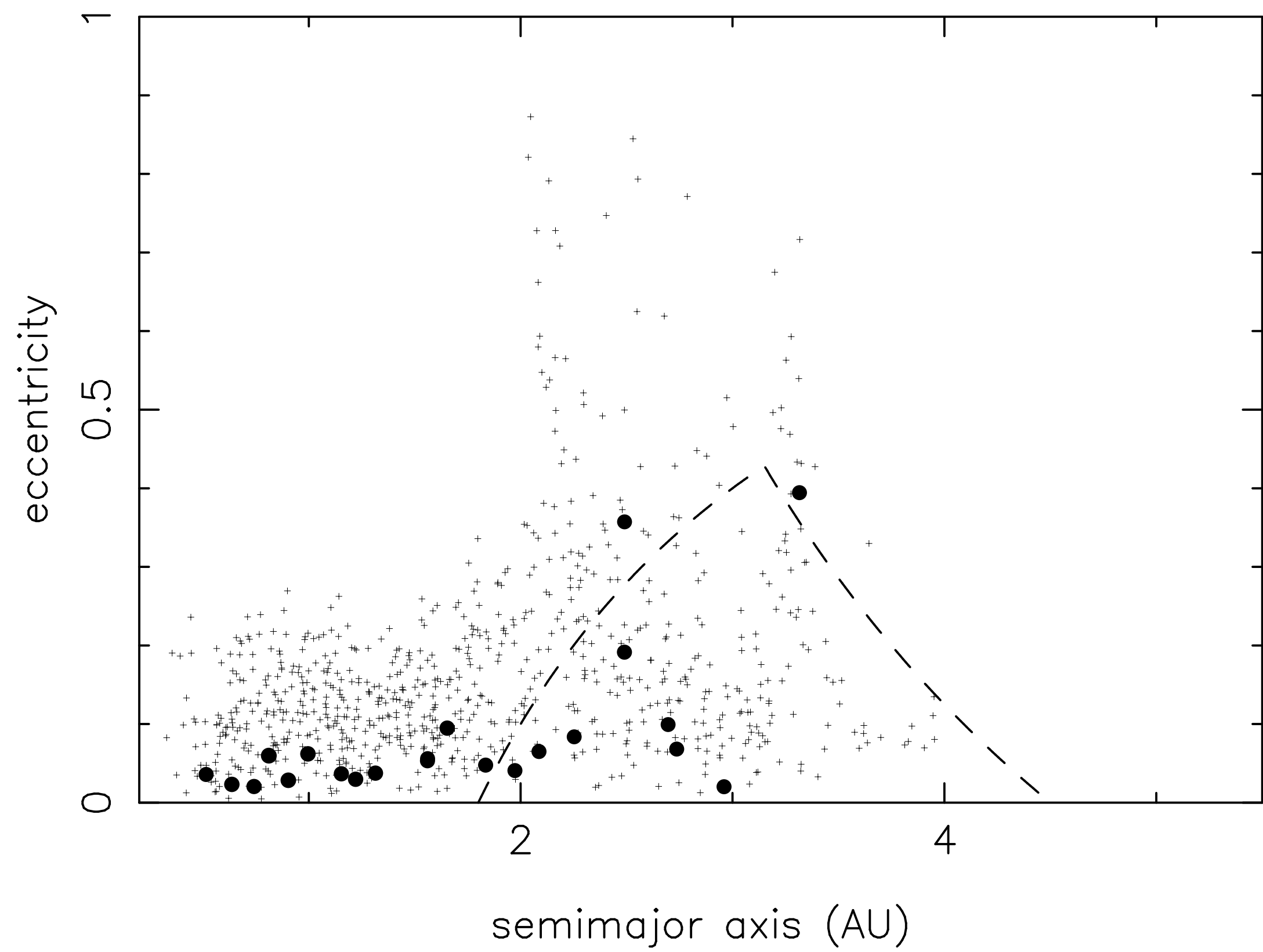




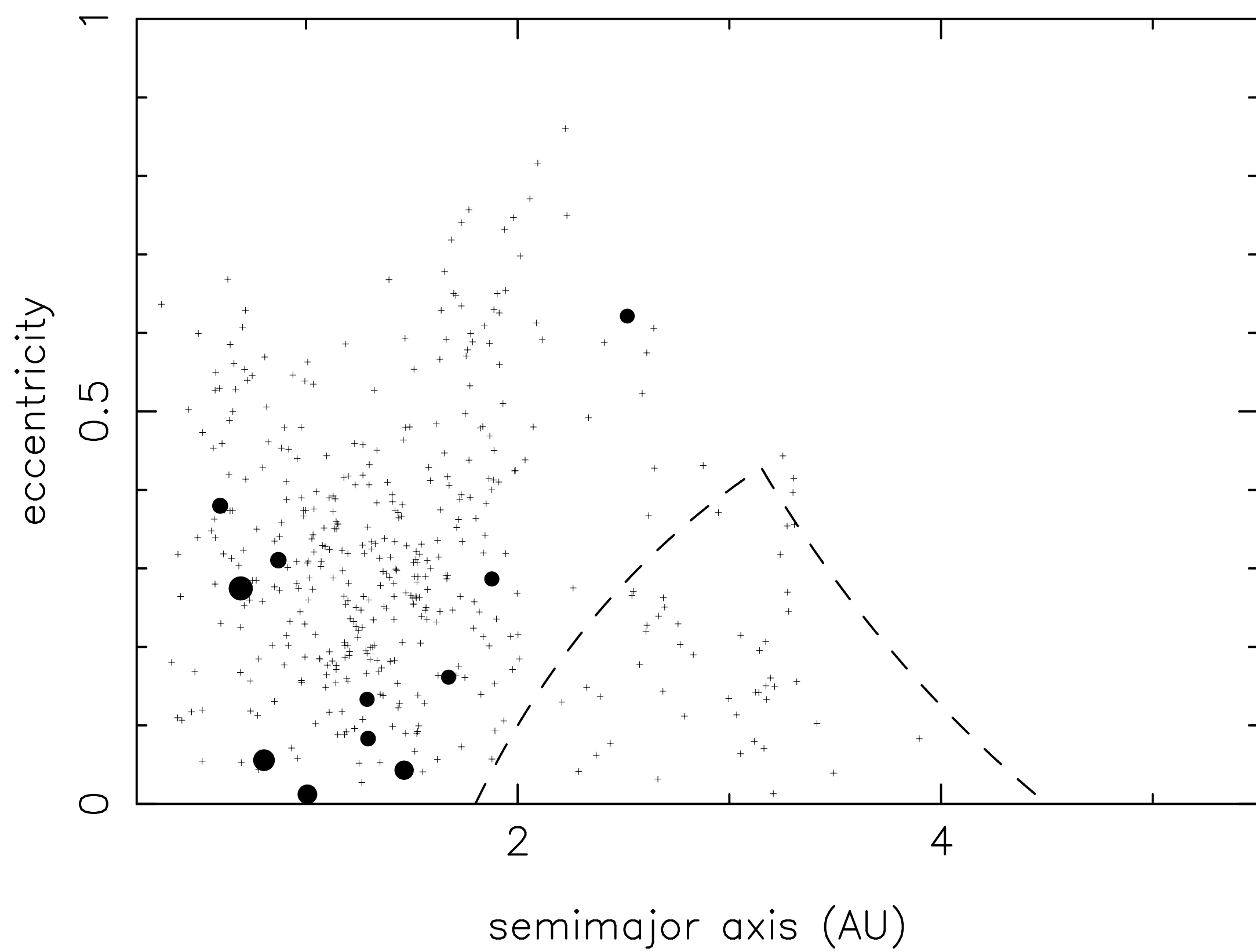
T= 0.1 My



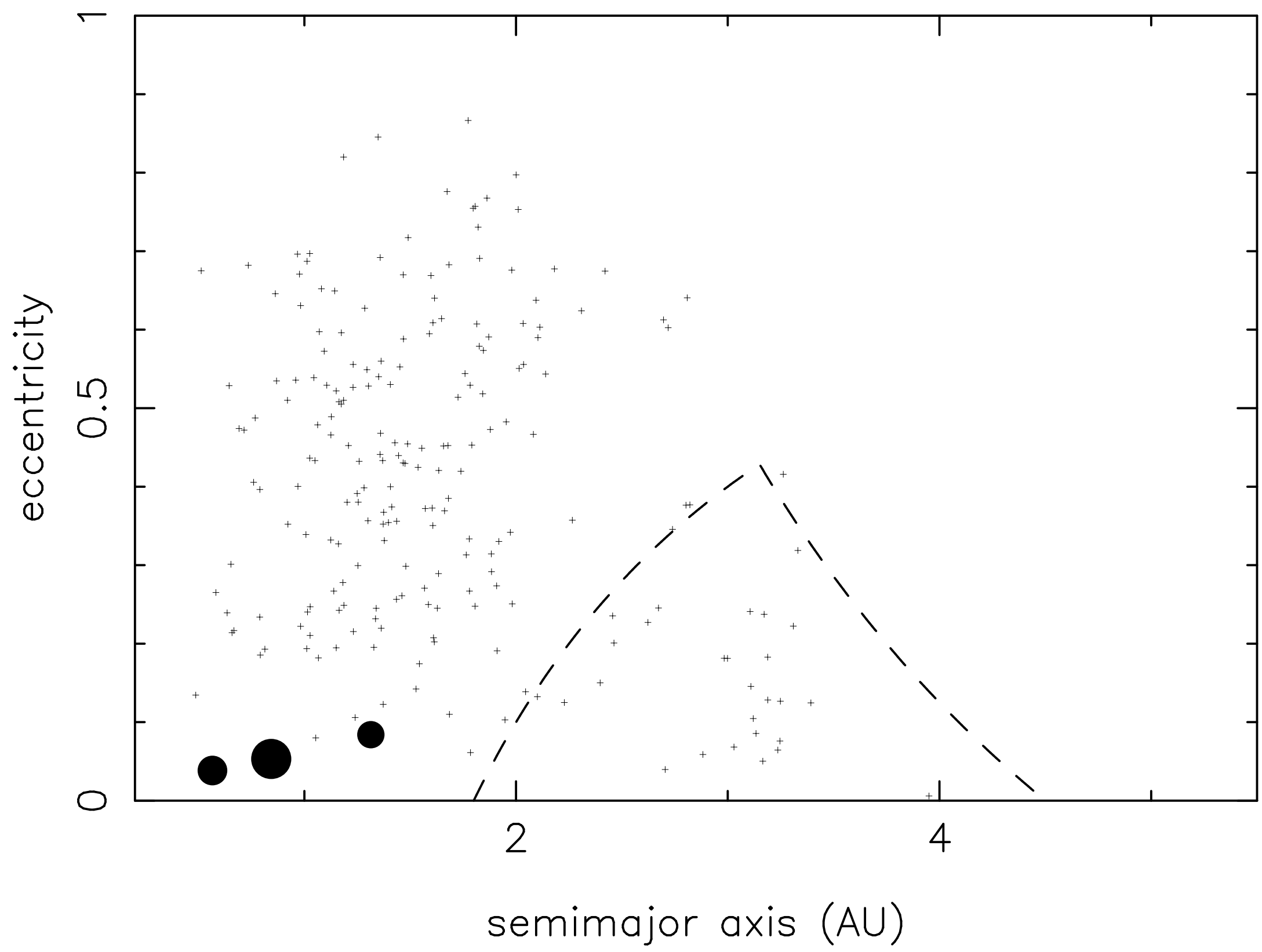
T= 1.0 My



T= 10.0 My



T= 40.0 My



T= 0.600 My

